

ESCOLA DE MEDICINA
PROGRAMA DE PÓS-GRADUAÇÃO EM MEDICINA E CIÊNCIAS DA SAÚDE

GIORDANO RAFAEL TRONCO ALVES

**SINAL DO HALO EM TOMOGRAFIA COMPUTADORIZADA DE TÓRAX: VALOR
DIAGNÓSTICO EM PACIENTES IMUNOCOMPETENTES E IMUNOCOMPROMETIDOS**

Porto Alegre
2018

PÓS-GRADUAÇÃO - *STRICTO SENSU*



Pontifícia Universidade Católica
do Rio Grande do Sul

GIORDANO RAFAEL TRONCO ALVES

**SINAL DO HALO EM TOMOGRAFIA COMPUTADORIZADA DE TÓRAX:
VALOR DIAGNÓSTICO EM PACIENTES IMUNOCOMPETENTES E
IMUNOCOMPROMETIDOS**

Tese apresentada como requisito para a obtenção do grau de Doutor pelo Programa de Pós-Graduação em Medicina e Ciências da Saúde da Pontifícia Universidade Católica do Rio Grande do Sul.

Orientador: Dr. Bruno Hochegger

PORTO ALEGRE

2018

Ficha Catalográfica

A474s Alves, Giordano Rafael Tronco

Sinal do Halo em Tomografia Computadorizada de Tórax : Valor Diagnóstico em Pacientes Imunocompetentes e Imunocomprometidos / Giordano Rafael Tronco Alves . – 2018.

67.

Tese (Doutorado) – Programa de Pós-Graduação em Medicina e Ciências da Saúde, PUCRS.

Orientador: Prof. Dr. Bruno Hochhegger.

1. Tomografia Computadorizada. 2. Nódulo Pulmonar. 3. Sinal do Halo.
I. Hochhegger, Bruno. II. Título.

Elaborada pelo Sistema de Geração Automática de Ficha Catalográfica da PUCRS
com os dados fornecidos pelo(a) autor(a).

Bibliotecária responsável: Salete Maria Sartori CRB-10/1363

RESUMO

Introdução: O sinal do halo consiste em uma área de opacidade em vidro-fosco ao redor de lesões pulmonares em imagens de tomografia computadorizada (TC) de tórax. Diferentes doenças já foram descritas como causadoras deste achado, porém uma análise maior e mais objetiva deste sinal ainda não foi conduzida.

Materiais e métodos: Os autores compararam imagens tomográficas de pacientes imunocompetentes e imunocomprometidos quanto a características do sinal do halo, a fim de identificar as de maior valor diagnóstico. Realizou-se um estudo observacional de exames realizados entre janeiro de 2011 e maio de 2015. Após busca inicial em banco de dados com palavras-chave, dois radiologistas torácicos analisaram os exames para determinar o número de lesões e sua distribuição, tamanho e contorno, bem como a espessura do halo e outros achados associados. O estudo obteve aprovação do comitê de ética institucional. Os testes de Qui-quadrado, t de Student e U de Mann-Whitney foram adotados de acordo com características amostrais, com um nível de significância de 0,05 bilateral.

Resultados: Um total de 85 pacientes (46 homens, 54%), foram avaliados, sendo 53 (62%) imunocompetentes e 32 (38%) imunocomprometidos. O principal diagnóstico entre os imunocompetentes foi o de neoplasia pulmonar (n=32, 64%), enquanto a aspergilose foi a principal condição entre imunocomprometidos (n=25, 78%). Lesões múltiplas e de distribuição randômica foram mais frequentes no grupo imunocomprometido ($p < 0,001$), sendo a espessura do halo também maior neste grupo ($p < 0,05$).

Conclusões: Conclui-se que as causas de sinal do halo diferem significativamente de acordo com o estado imunológico, sendo a espessura do halo, o número e a distribuição das lesões os dados de maior valor diagnóstico.

Palavras-chave: Tomografia computadorizada. Nódulo pulmonar. Sinal do halo.

ABSTRACT

Introduction: The halo sign consists of an area of ground-glass opacity surrounding pulmonary lesions on chest computed tomography (CT) scans. Different diseases have already been described as causing this finding, though a larger and more objective analysis of this sign has not been conducted yet.

Materials and methods: The authors compared CT images of immunocompetent and immunosuppressed patients in terms of halo sign features and seek to identify those of greatest diagnostic value. An observational study of exams performed between January of 2011 and May of 2015 was carried out. After initial database search with keywords, two thoracic radiologists reviewed the scans in order to determine the number of lesions, as well as their distribution, size, and contour, together with halo thickness and any other associated findings. The study obtained approval by the institutional ethics committee. The chi-squared test, Student t test and Mann-Whitney U test were adopted according to sample characteristics, with a bilateral level of significance of 0.05.

Results: A total of 85 patients (46 male, 54%) were evaluated, with 53 (62%) immunocompetent and 32 (38%) immunosuppressed. The main diagnosis among immunocompetents was lung cancer (n=32, 64%), whereas aspergillosis was the main condition in immunosuppressed patients (n=25, 78%). Multiple and randomly distributed lesions were more frequent in the immunosuppressed group ($p < 0.001$), with halo thickness also greater in this group ($p < 0.05$).

Conclusions: We concluded that the causes of the halo sign differ significantly according to immune status, and that halo thickness, the number and the distribution of lesions are the data with greatest diagnostic value.

Keywords: Computed tomography. Pulmonary nodule. Halo sign.

SUMÁRIO

| | |
|---|----|
| 1. INTRODUÇÃO | 7 |
| 1.1 SINAL DO HALO | 7 |
| 1.2 DOENÇAS INFECCIOSAS | 7 |
| 1.3 NEOPLASIAS | 8 |
| 1.4 OUTRAS CONDIÇÕES | 9 |
| 1.5 JUSTIFICATIVA | 9 |
| 1.6 OBJETIVOS | 9 |
| 2. METODOLOGIA | 10 |
| 2.1 DESENHO DO ESTUDO | 10 |
| 2.2 CRITÉRIOS DE INCLUSÃO E EXCLUSÃO | 10 |
| 2.3 IMAGENS | 11 |
| 2.4 ANÁLISE ESTATÍSTICA | 12 |
| 2.5 ASPECTOS ÉTICOS | 12 |
| 3. DESENVOLVIMENTO | 13 |
| 3.1 ARTIGO PRINCIPAL PUBLICADO | 13 |
| 4. REFERÊNCIAS | 14 |
| 5. ANEXOS | 16 |
| ANEXO A - DOCUMENTO DE APROVAÇÃO DO COMITÊ DE ÉTICA | 16 |
| ANEXO B - OUTROS ARTIGOS PRODUZIDOS NO PERÍODO | 17 |

1. INTRODUÇÃO

1.1 SINAL DO HALO

O sinal do halo tomográfico consiste em uma área de opacidade em vidro-fosco ao redor de um nódulo ou massa pulmonar [1]. O sinal do halo foi descrito pela primeira vez em 1985 por Kuhlman et al., que analisaram imagens de TC de tórax de nove pacientes com leucemia aguda que apresentaram aspergilose pulmonar invasiva [2].

Desde então - e apesar de sua infreqüência - o sinal do halo já foi relacionado com diversas doenças. Sua fisiopatologia geralmente envolve um dos seguintes mecanismos: hemorragia, inflamação ou crescimento neoplásico [3-5].

1.2 DOENÇAS INFECCIOSAS

Um número variado e extenso de doenças infecciosas pode produzir, em estudos tomográficos dos pulmões, nódulos cercados por hemorragia, infiltrados de células inflamatórias ou ambos, o que pode determinar a presença de sinal do halo [6]. Entre as possíveis condições infecciosas, a aspergilose, em sua forma angioinvasiva, é reconhecidamente a principal causa de sinal do halo em pacientes imunocomprometidos [7]. Patologicamente, caracteriza-se por focos de infarto rodeados por áreas de hemorragia alveolar. Os infartos são causados por invasão vascular direta do *Aspergillus*, com consequente trombose de vasos de pequeno e médio calibre, determinando necrose e hemorragia pulmonar adjacente. Assim, a área central de necrose corresponde, na tomografia, ao nódulo, enquanto a hemorragia periférica é representada pelo halo de atenuação em vidro-fosco [8]. A freqüência do sinal do halo tomográfico nos estágios iniciais da aspergilose angioinvasiva em pacientes neutropênicos febris é alta, chegando a 96% no dia 0 até 19% no dia 14 (curso natural da doença) [6]. Portanto, nestes pacientes, o sinal do halo indica precocemente a presença de infecção, mesmo antes de outros testes laboratoriais e/ou sorológicos.

Nódulos hemorrágicos cursando com sinal do halo tomográfico podem também ser observados em outras doenças fúngicas invasivas, como a mucormicose. Esta é uma grave e potencialmente fatal infecção fúngica oportunista, mais frequente em pacientes imunocomprometidos por doença renal crônica e diabetes. Contudo, sua descrição é esporádica, sendo relatada apenas em pequenas séries de casos na literatura [4]. Outras

micoses invasivas podem causar, ainda mais incomumente o sinal do halo, como a coccidioidomicose e a candidíase pulmonar [5,9].

Outras doenças infecciosas podem produzir sinal do halo tomográfico, sendo este secundário a infiltrado inflamatório perilesional. A lista inclui exemplos como a criptococose, a pneumonia herpética e citomegalovirose pulmonar. Nessas situações, o vidro-fosco observado é decorrente de processo inflamatório granulomatoso ao exame histológico. Entretanto, a ocorrência do sinal do halo nestas doenças é também esporádica, com apenas relatos de casos na literatura médica até a presente data [10,11].

Finalmente, um terceiro grupo de condições infecciosas podem potencialmente cursar com sinal do halo tomográfico, porém o mecanismo patológico permanece incerto. Os exemplos incluem infecção por *Coxiella burnetti*, mixovírus e o complexo *Mycobacterium avium*. Neste último, contudo, assim como nas micobacterioses em geral, acredita-se que o sinal do halo seja produzido por hemorragia perilesional, sendo esta decorrente de rupturas arteriais na forma de micropseudoaneurismas [4,6,11].

1.3 NEOPLASIAS

Metástases pulmonares de tumores hipervasculares, como angiossarcoma, coriocarcinoma, osteossarcoma e melanoma podem se manifestar com halo de atenuação em vidro-fosco, sendo este presumivelmente decorrente de hemorragia peritumoral, tendo em vista a fragilidade parietal do tecido neovascularizado. Outros tumores não metastáticos, como o sarcoma de Kaposi e o carcinoma pulmonar de células escamosas, também são descritos como possíveis causas de sinal do halo com mecanismo fisiopatológico semelhante às metástases supramencionadas [3,4,8].

O halo em vidro-fosco acompanhando nódulos tumorais pode também decorrer de infiltrado celular neoplásico, como ocorre no adenocarcinoma pulmonar de crescimento lepidico (anteriormente carcinoma bronquíolo-alveolar). Em uma série com 22 pacientes com este subtipo de neoplasia pulmonar primária, o sinal do halo foi descrito em 2 pacientes, sendo esta condição possível causa de sinal do halo tomográfico em pacientes sem imunossupressão [6]. Patologicamente, o halo em vidro-fosco é representado por invasão tumoral insidiosa para espaços aéreos distais, utilizando os próprios septos alveolares para progressão.

Finalmente, em metástases pulmonares de tumores não hipervasculares, o halo em vidro-fosco pode também ser causado por infiltração celular. Em uma série com 65

pacientes, com metástases pulmonares de adenocarcinomas extrapulmonares, o sinal do halo esteve presente em 2 casos (adenocarcinoma gastrointestinal) [12].

1.4 OUTRAS CONDIÇÕES

O sinal do halo tomográfico causado por hemorragia pode ainda ser observado em doenças não-infecciosas e não-neoplásicas, como granulomatose de Wegener, endometriose pulmonar (hemorragia catamenial) e mola hidatiforme [3]. Doenças pulmonares eosinofílicas, como infestação por parasitas ou eosinofilia pulmonar (síndrome de Loeffler) podem também cursar com infiltrado inflamatório e/ou hemorrágico perilesional, determinando o sinal do halo tomográfico [6,8]. Embora represente a causa clássica do sinal do halo invertido [13], a pneumonia em organização criptogênica pode também cursar com sinal do halo, com áreas centrais de abscessos neutrofilicos, com graus variáveis de exsudato inflamatório e alterações fibróticas periféricas.

Por fim, até mesmo causas iatrogênicas já foram descritas como causadoras do sinal do halo tomográfico, como cateterização de artéria pulmonar e biópsias transbrônquicas. Nessas situações, o achado de opacidade em vidro-fosco é relacionado a um estágio intermediário de reabsorção de hemorragia alveolar focal [1,3].

1.5 JUSTIFICATIVA

A maioria das informações disponíveis sobre o sinal do halo é derivada de pacientes com doenças pré-existentes [1-4]. No entanto, há dados limitados sobre sua possível utilidade em prever o diagnóstico final (ou grupo diagnóstico, por exemplo, infecção ou doença maligna). Ademais, os dados envolvendo as principais causas de sinal do halo em pacientes imunocompetentes ou imunocomprometidos advêm de estudos descritivos, usualmente com número limitado de indivíduos analisados [5].

1.6 OBJETIVOS

Objetivo geral:

- Determinar o valor diagnóstico do sinal do halo por meio da análise de relações entre medidas tomográficas e estado imunológico;

Objetivos específicos:

- Observar diferenças entre os principais diagnósticos em pacientes imunocompetentes e imunocomprometidos;
- Verificar eventuais associações entre a espessura do halo com algum subgrupo amostral;
- Avaliar diferenças entre o número de lesões, bem como sua distribuição, de acordo com o status imune.

2. METODOLOGIA

2.1 DESENHO DO ESTUDO

Realizou-se um estudo observacional de imagens de TC obtidas em pacientes de centro terciário no sul do Brasil (Centro de Diagnóstico por Imagem, Hospital São Lucas - PUCRS), de Janeiro de 2011 a Maio de 2015, onde doenças granulomatosas são endêmicas.

2.2 CRITÉRIOS DE INCLUSÃO E EXCLUSÃO

Os exames foram selecionados por meio de buscas nos sistemas de arquivamento e distribuição de imagens (PACSs, do inglês *picture archiving and communication systems*) com os termos:

- "halo "
- "sinal do halo "

Além das seguintes combinações de termos:

- "vidro-fosco " + "nódulo ";
- "nódulo " + "periferia";
- "vidro-fosco " + "periferia ".

Um radiologista geral analisou os arquivos selecionados dos PACSs, a fim de confirmar a presença do sinal do halo.

Os prontuários médicos foram então analisados para determinar o estado imunológico dos pacientes. Foram incluídos no grupo imunocomprometidos:

- pacientes com síndrome da imunodeficiência adquirida (SIDA);
- qualquer forma de imunodeficiência congênita;

- história recente (≤ 2 meses) de quimioterapia e/ou radioterapia;
- registro de linfopenia (contagem absoluta de linfócitos $\leq 1,0 \times 10^9$ l) ou neutropenia (contagem absoluta de neutrófilos $\leq 1,5 \times 10^9$ l) [14,15].

Os demais pacientes foram considerados imunocompetentes.

Caso o diagnóstico final não houvesse sido estabelecido até o momento da análise dos prontuários médicos, os pacientes eram acompanhados até o diagnóstico definitivo, com confirmação sorológica, histológica ou microbiológica [10,16].

2.3 IMAGENS

Todas as tomografias seguiram protocolo padrão, sendo realizadas com tomógrafos com no mínimo 16 fileiras de detectores (*multi-slice computed tomography*), com os seguintes parâmetros de aquisição:

- espessura dos cortes tomográficos, $\leq 1,25$ mm;
- tempo de rotação, 0,5 s;
- voltagem, 120 kV;
- corrente elétrica, 150-400 mA.

Para cada exame, foram registrados o número de lesões, bem como seu contorno (regular ou irregular), tamanho e distribuição, além de quaisquer outros achados associados. Os critérios para os achados tomográficos seguiram os definidos no Glossário de Termos da Sociedade Fleischner [1]. A definição de nódulo foi uma opacidade arredondada ou irregular, bem ou mal definida, com diâmetro ≤ 3 cm. A definição de cavidade foi a de um espaço com gás, visto como uma transparência ou área de baixa atenuação dentro de uma consolidação, massa ou nódulo pulmonar. O padrão de árvore em brotamento referiu-se a estruturas ramificadas centrolobulares, que se assemelham a uma árvore brotando [1]. A definição de opacidades em vidro-fosco envolveu áreas de aspecto nebuloso, de aumento de opacidade ou atenuação, sem obscurecimento dos vasos subjacentes, ao passo que a definição de consolidação denotou a opacificação homogênea do parênquima com obscurecimento dos vasos subjacentes [1]. As anormalidades foram também caracterizadas quanto à sua distribuição, qual seja nos lobos superiores, nos lobos inferiores e anormalidades distribuídas aleatoriamente [5,6].

As imagens de TC foram analisadas independentemente, em ordem aleatória, por dois radiologistas torácicos com mais de 10 anos de experiência e alheios às informações clínicas sobre os pacientes. Em eventuais discrepâncias, os dois radiologistas supracitados

e um terceiro radiologista torácico (este com mais de 40 anos de experiência) analisaram juntos as imagens, a fim de tomar uma decisão consensual final. Os nódulos e respectivos halos foram medidos em seu maior diâmetro em imagens de TC axial com janela para o pulmão [8].

2.4 ANÁLISE ESTATÍSTICA

O cálculo de tamanho amostral foi baseado no software estatístico BioEstat 5.0 (BIOESTAT 5.0, 2009), com poder estatístico de 0,8 (80%) e erro-alfa de 0,05. O resultado foi de uma amostra mínima de 60 indivíduos, divididos conforme o status imunológico (variável independente).

Para o armazenamento de dados e análise descritiva, utilizou-se o programa Microsoft Excel; para subseqüentes análises de correlações, o programa *Statistical Package for the Social Sciences*, versão 14.0 (SPSS Inc., Chicago, IL, EUA). O teste do qui-quadrado foi usado para as variáveis qualitativas.

O teste de Kolmogorov-Smirnov foi aplicado para determinar se os dados quantitativos apresentavam distribuição normal ou não. Para as variáveis paramétricas, o teste t de Student foi selecionado. Para as variáveis não paramétricas, adotou-se o teste U de Mann-Whitney. Todos os testes foram bilaterais, com nível de significância de 0,05.

2.5 ASPECTOS ÉTICOS

O presente estudo recebeu aprovação do Comitê de Ética institucional (Anexo A). O trabalho envolveu consultas em bancos de dados de pacientes, quais sejam os exames de tomografia computadorizada para as diversas medidas em lesões com sinal do halo, além de consulta em prontuário eletrônico para determinação do estado imunológico no período de realização do exame tomográfico.

Os potenciais riscos da pesquisa incluíram a eventual visualização de informações pessoais dos pacientes, pelos pesquisadores, durante a consulta de prontuário, externas ao escopo do estudo. A exposição à radiação x, intrínseca à tomografia, não foi determinada pela investigação científica em si, uma vez que os exames foram solicitados pelas equipes assistentes de acordo com indicações clínicas específicas.

Os benefícios desta pesquisa incluíram a caracterização objetiva do sinal do halo tomográfico, o que eleva seu valor diagnóstico em orientar decisões diagnósticas e

terapêuticas em grupos específicos, quais sejam imunocompetentes ou imunocomprometidos. Ademais, em âmbito institucional, o projeto fomentou melhoramentos nas ferramentas de busca nos bancos de imagens para futuras investigações científicas.

Dada a sua natureza, a obtenção de assinatura de consentimento livre e esclarecido não foi realizada. O termo de compromisso de utilização de dados foi assinado pelos pesquisadores envolvidos, garantindo proteção à identidade dos pacientes incluídos nas análises, conforme preconizado na Declaração de Helsinque.

3. DESENVOLVIMENTO

3.1 ARTIGO PRINCIPAL PUBLICADO



The halo sign: HRCT findings in 85 patients

Giordano Rafael Tronco Alves¹, Edson Marchiori¹, Klaus Irion²,
Carlos Schuler Nin³, Guilherme Watte³, Alessandro Comarú Pasqualotto³,
Luiz Carlos Severo³, Bruno Hochhegger^{1,3}

1. Programa de Pós-Graduação em Medicina (Radiologia), Universidade Federal do Rio de Janeiro, Rio de Janeiro (RJ) Brasil.
2. Radiology Department, Liverpool Heart and Chest Hospital, Liverpool, United Kingdom.
3. Universidade Federal de Ciências da Saúde de Porto Alegre, Porto Alegre (RS) Brasil.

Submitted: 28 February 2016.

Accepted: 21 July 2016.

Study carried out at the Irmandade da Santa Casa de Misericórdia de Porto Alegre, Porto Alegre (RS) Brasil.

ABSTRACT

Objective: The halo sign consists of an area of ground-glass opacity surrounding pulmonary lesions on chest CT scans. We compared immunocompetent and immunosuppressed patients in terms of halo sign features and sought to identify those of greatest diagnostic value. **Methods:** This was a retrospective study of CT scans performed at any of seven centers between January of 2011 and May of 2015. Patients were classified according to their immune status. Two thoracic radiologists reviewed the scans in order to determine the number of lesions, as well as their distribution, size, and contour, together with halo thickness and any other associated findings. **Results:** Of the 85 patients evaluated, 53 were immunocompetent and 32 were immunosuppressed. Of the 53 immunocompetent patients, 34 (64%) were diagnosed with primary neoplasm. Of the 32 immunosuppressed patients, 25 (78%) were diagnosed with aspergillosis. Multiple and randomly distributed lesions were more common in the immunosuppressed patients than in the immunocompetent patients ($p < 0.001$ for both). Halo thickness was found to be greater in the immunosuppressed patients ($p < 0.05$). **Conclusions:** Etiologies of the halo sign differ markedly between immunocompetent and immunosuppressed patients. Although thicker halos are more likely to occur in patients with infectious diseases, the number and distribution of lesions should also be taken into account when evaluating patients presenting with the halo sign.

Keywords: Tomography, X-ray computed; Aspergillosis; Lung neoplasms.

INTRODUCTION

The CT halo sign consists of an area of ground-glass opacity surrounding a pulmonary nodule or mass.⁽¹⁾ The halo sign was first described in 1985 by Kuhlman et al., who reviewed chest CT scans of nine patients with acute leukemia who developed invasive pulmonary aspergillosis.⁽²⁾ Since then—and despite its infrequency—the halo sign has been reported in association with a variety of conditions.^(3,4) Its pathophysiology usually involves one of three mechanisms: hemorrhage, inflammation, or neoplastic growth.⁽⁵⁾

Most of the available information about the halo sign has been derived from patients with pre-existing conditions. However, there are limited data on its potential usefulness in predicting the final diagnosis (or diagnostic group, e.g., infection or malignancy). Therefore, the objective of the present study was to determine the diagnostic value of the halo sign by exploring associations between CT measurements and immunological status in a cohort of patients presenting with the CT halo sign.

METHODS

This was a multicenter retrospective study of CT images obtained between January of 2010 and May of 2014 from patients presenting at any of seven tertiary care centers in southern Brazil, which is an endemic

area for granulomatous diseases. Scans were selected by searching the picture archiving and communication systems (PACSs) of all participating institutions using the terms “halo” and “halo sign”, as well as the following combinations of terms: “ground-glass” + “nodule”; “nodule” + “surround”; “nodule” + “periphery”; and “ground-glass” + “periphery”. The research protocol was approved by the local research ethics committee (Protocol no. 243.155). Given the retrospective nature of the study, informed consent was waived.

A general radiologist reviewed the files retrieved from the PACSs in order to confirm the presence of the halo sign. Medical records were reviewed in order to determine patient immune status. For the purpose of the present study, patients were considered immunosuppressed in the presence of AIDS; any form of congenital immunodeficiency; or a recent (\leq two-month) history of chemotherapy, radiation therapy, or decreased white blood cell count (lymphopenia [absolute lymphocyte count $\leq 1.0 \times 10^9$ L] or neutropenia [absolute neutrophil count $\leq 1.5 \times 10^9$ L]).^(6,7) All other patients were considered to be immunocompetent. If a final diagnosis had not been reached by the time of medical record review, patients were followed until a definitive diagnosis was made, with serological, histological, or microbiological confirmation. Histological sampling varied across the participating institutions, including transthoracic needle biopsy,

Correspondence to:

Giordano Rafael Tronco Alves. Avenida Roraima, 1000, CEP 97105-900, Santa Maria, RS, Brasil.
Tel.: 55 55 9729-1990. E-mail: grtalves@gmail.com
Financial support: None.

video-assisted thoracotomy, and open thoracotomy. Although serological and microbiological tests were performed in accordance with the corresponding (updated) guidelines, their performance was dependent on patient clinical background.

All CT scans were performed with multidetector scanners with at least 16 rows of detectors, the acquisition parameters being as follows: slice thickness, ≤ 1.25 mm; rotation time, 0.5 s; voltage, 120 kV; and electric current, 150-400 mA. Automatic exposure control was enabled. No contrast medium was used.

For each examination, the number of lesions, as well as their outline (regular vs. irregular), size, and distribution, together with any other associated findings, were recorded. The criteria for CT findings were those defined in the Fleischner Society Glossary of Terms.⁽¹⁾ A nodule was defined as a rounded or irregular opacity that was well or poorly defined and ≤ 3 cm in diameter. Mediastinal and hilar lymph nodes range in size from sub-CT resolution to 10 mm. A cavity was defined as a gas-filled space, seen as a lucency or low-attenuation area within a pulmonary consolidation, mass, or nodule. The tree-in-bud pattern refers to centrilobular branching structures that resemble a budding tree. Ground-glass opacities were defined as hazy areas of increased opacity or attenuation with no obscuration of the underlying vessels. Consolidation was defined as homogeneous opacification of the parenchyma with obscuration of the underlying vessels. Abnormalities were classified as being located in the upper lobes, located in the lower lobes, or randomly distributed.

The CT scans were independently reviewed in random order by two chest radiologists who had more than 10 years of experience and who were blinded to patient clinical information. Subsequently, the two aforementioned radiologists and a third chest radiologist (with more than 40 years of experience) together reviewed the scans in order to make a final consensus decision. The diameters of the nodules and halos were measured at their widest points on axial CT scans with lung window settings.

Microsoft Excel was used for data storage and descriptive analysis, and the Statistical Package for the Social Sciences, version 14.0 (SPSS Inc., Chicago, IL, USA), was used for correlations. The chi-square test was used for qualitative variables. The Kolmogorov-Smirnov test was used in order to determine whether quantitative data were normally distributed. For parametric variables, the Student's t-test was used. For nonparametric variables, the Mann-Whitney U test was used. All tests were two-tailed, and a significance level of 0.05 was used throughout.

RESULTS

Of the 20,210 CT examinations retrieved from the PACSs of the participating centers, 85 cases (0.42%) were selected for inclusion in the present study. Of those 85 patients, 46 were male. In addition, 32 were classified as being immunosuppressed at the time of

CT examination, and 53 were immunocompetent. Of those, 34 (64%) were diagnosed with a primary malignancy; of those, 24 had histopathologically confirmed adenocarcinoma. Of the 32 patients who were classified as being immunosuppressed, 25 (78%) had findings suggestive of invasive aspergillosis (positive results on direct mycological examination or histological findings). All but one of the immunosuppressed patients presenting with invasive aspergillosis were found to have neutropenia. In addition, 7 of those 25 were diagnosed with proven invasive fungal disease (on the basis of specimen culture results and radiological findings), and 18 were diagnosed with probable invasive aspergillosis (on the basis of positive microbiological studies and radiological findings).⁽⁸⁾ Other causes of the CT halo sign included metastases, lymphoproliferative diseases, tuberculosis, plasmacytoma, staphylococcal pneumonia, actinomycosis, cryptococcosis, and histiocytosis. Table 1 and Figure 1 show the frequencies of these diagnoses in the two study groups.

The number and distribution of lesions on CT scans were found to vary significantly according to patient immune status, with immunosuppressed patients tending to exhibit multiple and randomly distributed lesions (Table 2). In cases of multiple lesions, halo thickness tended to be greater (≥ 9 mm) in immunosuppressed patients ($p < 0.05$; Figure 2); the same was not true for single lesions ($p = 0.299$).

DISCUSSION

The present retrospective study revealed ten different etiologies of the CT halo sign in 85 individuals. Pathological findings of tumor cells, inflammatory infiltrates, and, most commonly, alveolar hemorrhage have been reported to account for the ground-glass opacities surrounding pulmonary lesions on CT

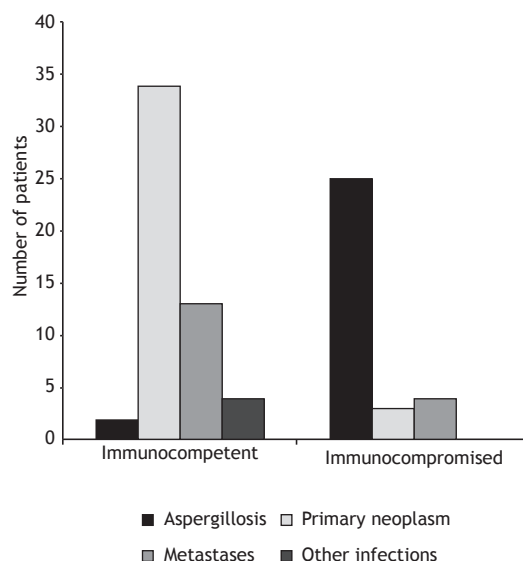


Figure 1. Bar chart showing final diagnosis in immunocompetent and immunocompromised patients presenting with the CT halo sign.

Table 1. Etiology of the CT halo sign, by patient immune status.^a

| Variable | Immunocompetent patients (n = 53) | Immunocompromised patients (n = 32) |
|------------------------------|--------------------------------------|--|
| Primary neoplasm | 34 (64) | - |
| Invasive aspergillosis | - | 25 (78) |
| Metastases | 13 (25.0) | 2 (6.3) |
| Lymphoproliferative diseases | - | 3 (9.4) |
| Tuberculosis | 2 (3.8) | - |
| Plasmacytoma | - | 2 (6.3) |
| Staphylococcal pneumonia | 1 (1.8) | - |
| Actinomycosis | 1 (1.8) | - |
| Cryptococcosis | 1 (1.8) | - |
| Histiocytosis | 1 (1.8) | - |

^aData presented as n (%).**Table 2.** Demographic data and CT findings, by patient immune status.^a

| | Total | Immunocompetent patients (n = 53) | Immunocompromised patients (n = 32) | p |
|--|----------|--------------------------------------|--|---------|
| Demographic data | | | | |
| Male gender ^b | 46 (54) | 29 (55) | 17 (53) | 0.887 |
| Age, years | 53 ± 17 | 55 ± 14 | 48 ± 21 | 0.135 |
| CT findings | | | | |
| Number of nodules ^c | 3 (1-16) | 2 (1-15) | 5 (1-16) | < 0.001 |
| 1 ^b | 41 (48) | 38 (72) | 3 (9) | < 0.001 |
| > 1 ^b | 44 (52) | 15 (28) | 29 (91) | |
| Nodule outline ^{b,*} | | | | |
| Regular | 46 (54) | 31 (58) | 15 (47) | 0.298 |
| Irregular | 39 (46) | 22 (42) | 17 (53) | |
| Nodule size, mm [†] | | | | |
| Solitary nodule | 25 ± 13 | 26 ± 14 | 16 ± 9 | 0.231 |
| Largest nodule | 16 ± 8 | 12 ± 8 | 19 ± 7 | 0.805 |
| Smallest nodule | 6 ± 3 | 6 ± 4 | 5 ± 2 | 0.007 |
| Halo thickness, mm [†] | | | | |
| Solitary nodule | 7 ± 3 | 7 ± 3 | 5 ± 1 | 0.299 |
| Largest nodule | 8 ± 4 | 5 ± 2 | 9 ± 4 | 0.001 |
| Smallest nodule | 5 ± 1 | 3 ± 1 | 5 ± 1 | 0.002 |
| Lesion distribution ^b | | | | |
| Random | 47 (55) | 15 (28) | 28 (91) | < 0.001 |
| Upper lobe | 23 (27) | 23 (44) | 1 (3) | < 0.001 |
| Lower lobe | 15 (18) | 15 (28) | 2 (6) | 0.003 |
| Associated findings ^b | | | | |
| Consolidation | 5 (63) | - | 5 (100) | 0.016 |
| Tree-in-bud pattern | 2 (25) | 2 (67) | - | |
| Cavitated nodules | 1 (12) | 1 (33) | - | |
| Diagnostic confirmation (n = 105) ^{b,†} | | | | |
| Serological | 30 (30) | 4 (7) | 26 (53) | < 0.001 |
| Microbiological | 22 (20) | 2 (4) | 20 (41) | < 0.001 |
| Histological | 53 (50) | 50 (89) | 3 (6) | < 0.001 |

^aData presented as mean ± SD, except where otherwise indicated. ^bData presented as n (%). ^cData presented as median (range). *For nodules presenting with a peripheral halo sign. [†]For patients with multiple lesions, data for the largest and smallest lesions are displayed separately. [‡]The number of diagnostic confirmations exceeds the number of cases because some diagnoses were confirmed by more than one method.

scans. (4,9) Although the halo sign has been causally associated with numerous other conditions, its presence is generally more helpful than challenging.(9) Studies involving immunocompromised patients have confirmed

the diagnostic value of the halo sign, demonstrating that its specificity increases as patient immune status deteriorates.(10,11) However, most available evidence consists of descriptive data. To our knowledge, the

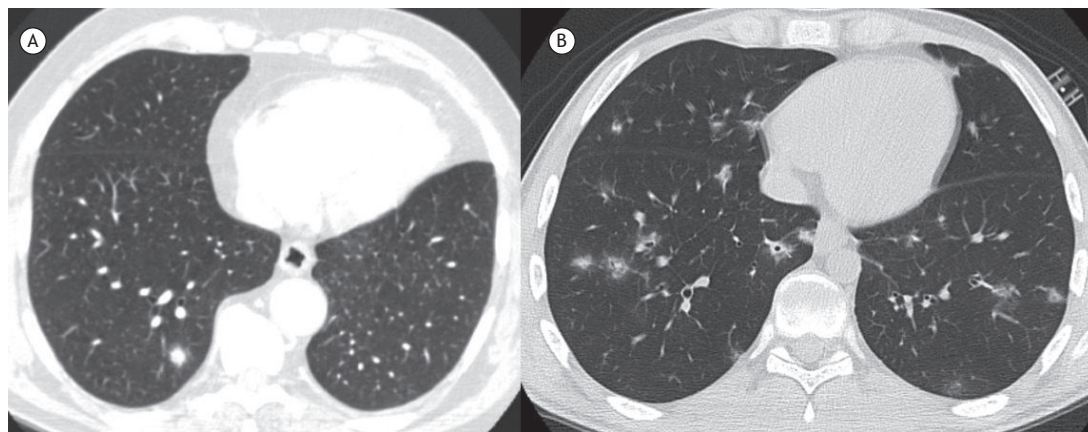


Figure 2. In A, axial CT scan of the chest of an asymptomatic, immunocompetent 54-year-old male patient, showing a right lower lobe pulmonary nodule surrounded by areas of ground-glass opacity (the CT halo sign); the final diagnosis was primary adenocarcinoma. In B, axial CT scan of the chest of an immunosuppressed 19-year-old male patient, showing multiple, randomly distributed pulmonary nodules surrounded by ground-glass opacities (the CT halo sign); the final diagnosis was aspergillosis.

present study was the first to address the correlations between the halo sign and patient immune status. In addition, our study demonstrated that thicker halos are associated with infectious diseases, whereas thinner halos are associated with neoplastic diseases. In agreement with the results of previous studies, the results of the present study showed that adenocarcinoma and pulmonary aspergillosis were the conditions that were most commonly associated with the halo sign in immunocompetent and immunosuppressed patients, respectively.^(4,12) In cases of multiple pulmonary nodules, halo thickness tended to be greater in immunocompromised patients than in immunocompetent patients. This finding is consistent with those of a study investigating characteristics of the reversed halo sign, in which greater rim thickness was associated with invasive fungal infection.⁽¹³⁾ The same cannot be concluded for solitary nodules, and this is possibly due to a statistically insufficient number of single lesions among the immunosuppressed patients (i.e., only three).

According to Gao et al., the relationships between ground-glass lung nodules and adjacent blood vessels can aid in establishing a final diagnosis based on the presence and degree of vascular distortion.⁽¹⁴⁾ This is particularly relevant for immunocompetent patients presenting with the CT halo sign. In the present study, a neoplastic etiology was found to be more common in the immunocompetent patients than in the immunosuppressed patients. However, given the reduced halo thickness in the former and the variety of possible pathophysiological mechanisms underlying the halo sign, further studies are needed in order to

determine whether this correlation can be extrapolated to smaller areas of ground-glass opacities.

Our study has some limitations. First, the retrospective nature of the study increases the likelihood that medical record inaccuracies affected our results. Second, the relatively small sample size did not allow us to perform an analysis of covariance in order to determine the combined contribution of halo sign features in predicting the final diagnosis. Third, dynamic changes observed in the long-term evaluation of the appearance of the halo sign, particularly in cases of infectious disease, might have affected some of our results. Finally, the definition of immunosuppression used in our study might be in disagreement with the constant improvements in the toxicity of chemotherapy and radiation therapy; however, that definition was adopted for research purposes only, and many other clinical parameters should be taken into account in a more practical scenario.

In summary, our findings are consistent with available data on the etiologies of the CT halo sign in immunocompetent and immunosuppressed patients. Given the differences in radiological presentation between these two groups of patients, appropriate assessment of halo sign features can be useful in clinical investigation. A diagnosis of primary neoplasm appears to be common among immunocompetent patients, as does a diagnosis of invasive aspergillosis among immunosuppressed patients. Thicker halos are associated with infectious diseases, whereas thinner halos are associated with neoplastic diseases; the number and distribution of lesions should also be taken into account, given that they can predict the final diagnosis.

REFERENCES

1. Hansell DM, Bankier AA, MacMahon H, McLoud TC, Müller NL, Remy J. Fleischner Society: glossary of terms for thoracic imaging. *Radiology*. 2008;246(3):697-722. <http://dx.doi.org/10.1148/radiol.2462070712>
2. Kuhlman JE, Fishman EK, Siegelman SS. Invasive pulmonary aspergillosis in acute leukemia: characteristic findings on CT, the CT halo sign, and the role of CT in early diagnosis. *Radiology*. 1985;157(3):611-4. <http://dx.doi.org/10.1148/>

- radiology.157.3.3864189
3. Lee YR, Choi YW, Lee KJ, Jeon SC, Park CK, Heo JN. CT halo sign: the spectrum of pulmonary diseases. *Br J Radiol.* 2005;78(933):862-5. <http://dx.doi.org/10.1259/bjr/77712845>
 4. Kim Y, Lee KS, Jung KJ, Han J, Kim JS, Suh JS. Halo sign on high resolution CT: findings in spectrum of pulmonary diseases with pathologic correlation. *J Comput Assist Tomogr.* 1999;23(4):622-6.
 5. Parrón M, Torres I, Pardo M, Morales C, Navarro M, Martínez-Schmizcraft M. The halo sign in computed tomography images: differential diagnosis and correlation with pathology findings [Article in Spanish]. *Arch Bronconeumol.* 2008;44(7):386-92. [http://dx.doi.org/10.1016/S0300-2896\(08\)70453-8](http://dx.doi.org/10.1016/S0300-2896(08)70453-8)
 6. Ng WL, Chu CM, Wu AK, Cheng VC, Yuen KY. Lymphopenia at presentation is associated with increased risk of infections in patients with systemic lupus erythematosus. *QJM.* 2006;99(1):37-47. <http://dx.doi.org/10.1093/qjmed/hci155>
 7. Valent P. Low blood counts: immune mediated, idiopathic, or myelodysplasia. *Hematology Am Soc Hematol Educ Program.* 2012;2012:485-91. <http://dx.doi.org/10.1182/asheducation-2012.1.485>
 8. De Pauw B, Walsh TJ, Donnelly JP, Stevens DA, Edwards JE, Calandra T, et al. Revised definitions of invasive fungal disease from the European Organization for Research and Treatment of Cancer/Invasive Fungal Infections Cooperative Group and the National Institute of Allergy and Infectious Diseases Mycoses Study Group (EORTC/MSG) Consensus Group. *Clin Infect Dis.* 2008;46(12):1813-21. <http://dx.doi.org/10.1086/588660>
 9. Pinto PS. The CT Halo Sign. *Radiology.* 2004;230(1):109-10. <http://dx.doi.org/10.1148/radiol.2301020649>
 10. Escuissato DL, Gasparetto EL, Marchiori E, Rocha Gde M, Inoue C, Pasquini R, et al. Pulmonary infections after bone marrow transplantation: high-resolution CT findings in 111 patients. *AJR Am J Roentgenol.* 2005;185(3):608-15. <http://dx.doi.org/10.2214/ajr.185.3.01850608>
 11. Blum U, Windfuhr M, Buitrago-Tellez C, Sigmund G, Herbst EW, Langer M. Invasive pulmonary aspergillosis. MRI, CT, and plain radiographic findings and their contribution for early diagnosis. *Chest.* 1994;106(4):1156-61. <http://dx.doi.org/10.1378/chest.106.4.1156>
 12. Gaeta M, Blandino A, Scribano E, Minutoli F, Volta S, Pandolfo I. Computed tomography halo sign in pulmonary nodules: frequency and diagnostic value. *J Thorac Imaging.* 1999;14(2):109-13.
 13. Marchiori E, Marom EM, Zanetti G, Hochegger B, Irion KL, Godoy MC. Reversed halo sign in invasive fungal infections: criteria for differentiation from organizing pneumonia. *Chest.* 2012;142(6):1469-73. <http://dx.doi.org/10.1378/chest.12-0114>
 14. Gao F, Li M, Ge X, Zheng X, Ren Q, Chen Y, et al. Multi-detector spiral CT study of the relationships between pulmonary ground-glass nodules and blood vessels. *Eur Radiol.* 2013;23(12):3271-7. <http://dx.doi.org/10.1007/s00330-013-2954-3>

4. REFERÊNCIAS

1. Hansell DM, Bankier AA, MacMahon H, McLoud TC, Müller NL, Remy J. Fleischner Society: glossary of terms for thoracic imaging. *Radiology*. 2008;246(3):697-722.
2. Kuhlman JE, Fishman EK, Siegelman SS. Invasive pulmonary aspergillosis in acute leukemia: characteristic findings on CT, the CT halo sign, and the role of CT in early diagnosis. *Radiology*. 1985;157(3):611-4.
3. Lee YR, Choi YW, Lee KJ, Jeon SC, Park CK, Heo JN. CT halo sign: the spectrum of pulmonary diseases. *Br J Radiol*. 2005;78(933):862-5.
4. Kim Y, Lee KS, Jung KJ, Han J, Kim JS, Suh JS. Halo sign on high resolution CT: findings in spectrum of pulmonary diseases with pathologic correlation. *J Comput Assist Tomogr*. 1999;23(4):622-6.
5. Gaeta M, Blandino A, Scribano E, Minutoli F, Volta S, Pandolfo I. Computed tomography halo sign in pulmonary nodules: frequency and diagnostic value. *J Thorac Imaging*. 1999;14(2):109-13.
6. Pinto PS. The CT Halo Sign. *Radiology*. 2004;230(1):109-10.
7. Blum U, Windfuhr M, Buitrago-Tellez C, Sigmund G, Herbst EW, Langer M. Invasive pulmonary aspergillosis. MRI, CT, and plain radiographic findings and their contribution for early diagnosis. *Chest*. 1994;106(4):1156-61.
8. Parrón M, Torres I, Pardo M, Morales C, Navarro M, Martínez-Schmizcraft M. The halo sign in computed tomography images: differential diagnosis and correlation with pathology findings. *Arch Bronconeumol*. 2008;44(7):386-92.
9. Escuissato DL, Gasparetto EL, Marchiori E, et al. Pulmonary infections after bone marrow transplantation: high-resolution CT findings in 111 patients. *AJR Am J Roentgenol*. 2005;185(3):608-15.
10. Zinck SE, Leung AN, Frost M, Berry GJ, Muller NL. Pulmonary cryptococcosis: CT and pathologic findings. *J Comput Assist Tomogr* 2002;26(3):330-4.

11. Primack SL, Hartman TE, Lee KS, Muller NL. Pulmonary nodules and the CT halo sign. *Radiology* 1994;190(2):513–5.
12. Gaeta M, Volta S, Scribano E, Loria G, Vallone A, Pandolfo I. Air-space pattern in lung metastasis from adenocarcinoma of the GI tract. *J Comput Assist Tomogr* 1996;20(2):300–4.
13. Marchiori E, Marom EM, Zanetti G, Hochegger B, Irion KL, Godoy MC. Reversed halo sign in invasive fungal infections: criteria for differentiation from organizing pneumonia. *Chest*. 2012;142(6):1469-73.
14. Ng WL, Chu CM, Wu AK, Cheng VC, Yuen KY. Lymphopenia at presentation is associated with increased risk of infections in patients with systemic lupus erythematosus. *QJM*. 2006;99(1):37-47.
15. Valent P. Low blood counts: immune mediated, idiopathic, or myelodysplasia. *Hematology Am Soc Hematol Educ Program*. 2012;2012:485-91.
16. De Pauw B, Walsh TJ, Donnelly JP, et al. Revised definitions of invasive fungal disease from the European Organization for Research and Treatment of Cancer/Invasive Fungal Infections Cooperative Group and the National Institute of Allergy and Infectious Diseases Mycoses Study Group (EORTC/MSG) Consensus Group. *Clin Infect Dis*. 2008;46(12):1813-21.

5. ANEXOS

ANEXO A - DOCUMENTO DE APROVAÇÃO DO COMITÊ DE ÉTICA

PARECER CONSUBSTANCIADO DO CEP

DADOS DO PROJETO DE PESQUISA

Título da Pesquisa: SINAL DO HALO EM TOMOGRAFIA DE TÓRAX DE ALTA RESOLUÇÃO: VALOR DIAGNÓSTICO EM PACIENTES IMUNOCOMPETENTES E

Pesquisador: Bruno Hochhegger

Área Temática:

Versão: 2

CAAE: 88508218.9.0000.5336

Instituição Proponente: UNIÃO BRASILEIRA DE EDUCAÇÃO E ASSISTENCIA

Patrocinador Principal: Financiamento Próprio

DADOS DO PARECER

Número do Parecer: 2.665.053

Apresentação do Projeto:

O sinal do halo consiste em uma área de opacidade em vidro fosco ao redor de lesões pulmonares em imagens de tomografia computadorizada (TC) de tórax. Diferentes patologias já foram descritas como causadores deste achado, porém uma análise maior e mais objetiva deste sinal ainda não foi conduzida. Propõe-se comparar pacientes imunocompetentes e imunodeprimidos quanto a características do sinal do halo a fim de identificar as de maior valor diagnóstico. Pretende-se realizar um estudo retrospectivo de tomografias realizadas entre janeiro de 2010 e novembro de 2017. Os pacientes serão classificados de acordo com seu estado imunológico. Dois radiologistas torácicos analisarão os exames a fim de determinar o número de lesões e sua distribuição, tamanho e contorno, bem como a espessura do halo e quaisquer outros achados associados.

Objetivo da Pesquisa:

Objetivo Primário:

O objetivo do presente estudo é determinar o valor diagnóstico do sinal do halo por meio da análise de relações entre medidas tomográficas e estado imunológico em uma coorte histórica de pacientes com o sinal do halo tomográfico.

Avaliação dos Riscos e Benefícios:

riscos e benefícios descritos

Endereço: Av. Ipiranga, 6681, prédio 50, sala 703

Bairro: Partenon

CEP: 90.619-900

UF: RS

Município: PORTO ALEGRE

Telefone: (51)3320-3345

Fax: (51)3320-3345

E-mail: cep@puhrs.br

Continuação do Parecer: 2.665.053

Riscos:

O presente projeto não acarreta quaisquer riscos à amostra em estudo, uma vez que constitui-se em uma coorte histórica com análise de achados em exames de imagem, estes solicitados pela equipe assistente de acordo com indicações clínicas específicas.

Benefícios:

Potenciais benefícios deste projeto de pesquisa incluem a caracterização objetiva do sinal do halo tomográfico, o que poderá elevar seu valor diagnóstico e orientar decisões diagnósticas e terapêuticas em grupos específicos, quais sejam imunocompetentes ou imunocomprometidos.

Ademais, em âmbito institucional, o projeto poderá fomentar melhoramentos nas ferramentas de busca nos bancos de imagens, alcançando maior robustez a futuras investigações científicas.

Comentários e Considerações sobre a Pesquisa:

Pesquisa clinicamente relevante.

Considerações sobre os Termos de apresentação obrigatória:

Apresenta todos os termos de apresentação obrigatória.

Recomendações:

Cabe ressaltar que, de acordo com o item V da Resolução CNS nº 466 de 2012, "considera-se que toda pesquisa envolvendo seres humanos envolve risco. O dano eventual poderá ser imediato ou tardio, comprometendo o indivíduo ou a coletividade". Ressalte-se ainda o item II.22 da mesma resolução que define como "Risco da pesquisa - possibilidade de danos à dimensão física, psíquica, moral, intelectual, social, cultural ou espiritual do ser humano, em qualquer pesquisa e dela decorrente".

Recomenda-se que sempre sejam apontados os possíveis riscos, ainda que mínimos, tanto no projeto detalhado, bem como na Plataforma Brasil (Aba 4 " Detalhamento do Estudo, item "Riscos") e ainda, recomenda-se descrever as providências e cautelas empregadas para evitar e/ou reduzir danos ou riscos ao participante da pesquisa.

Conclusões ou Pendências e Lista de Inadequações:

Sem pendências.

Endereço: Av. Ipiranga, 6681, prédio 50, sala 703

Bairro: Partenon

CEP: 90.619-900

UF: RS

Município: PORTO ALEGRE

Telefone: (51)3320-3345

Fax: (51)3320-3345

E-mail: cep@puhrs.br

**PONTIFÍCIA UNIVERSIDADE
CATÓLICA DO RIO GRANDE
DO SUL - PUC/RS**



Continuação do Parecer: 2.665.053

Considerações Finais a critério do CEP:

Diante do exposto, o CEP-PUCRS, de acordo com suas atribuições definidas na Resolução CNS n° 466 de 2012 e da Norma Operacional n° 001 de 2013 do CNS, manifesta-se pela aprovação do projeto de pesquisa proposto.

Este parecer foi elaborado baseado nos documentos abaixo relacionados:

| Tipo Documento | Arquivo | Postagem | Autor | Situação |
|---|---|------------------------|-----------------|----------|
| Informações Básicas do Projeto | PB_INFORMAÇÕES_BÁSICAS_DO_PROJETO_1108418.pdf | 16/05/2018 13:28:52 | | Aceito |
| Outros | CartaRespostaCEPGiordano.doc | 16/05/2018 13:28:35 | Bruno Hochegger | Aceito |
| Outros | CartaDiretorTecnicoHSL0805.pdf | 16/05/2018 13:27:26 | Bruno Hochegger | Aceito |
| Outros | ProtocoloCPC.pdf | 25/04/2018 14:02:51 | Bruno Hochegger | Aceito |
| Outros | LinkCV.pdf | 25/04/2018 14:02:15 | Bruno Hochegger | Aceito |
| Outros | Encaminhamentocep.pdf | 25/04/2018 14:01:34 | Bruno Hochegger | Aceito |
| Outros | EncaminhamentoCCientifica.pdf | 25/04/2018 14:01:12 | Bruno Hochegger | Aceito |
| Outros | CheckListProjeto.pdf | 25/04/2018 14:00:24 | Bruno Hochegger | Aceito |
| Outros | ApresentacaoCPC.pdf | 25/04/2018 13:59:56 | Bruno Hochegger | Aceito |
| TCLE / Termos de Assentimento / Justificativa de Ausência | TCUD.pdf | 25/04/2018 13:48:30 | Bruno Hochegger | Aceito |
| Declaração de Instituição e Infraestrutura | Cartachefedoservico.pdf | 25/04/2018 13:48:19 | Bruno Hochegger | Aceito |
| Parecer Anterior | DocumentoUnificado.pdf | 25/04/2018 13:48:07 | Bruno Hochegger | Aceito |
| Parecer Anterior | AprovacaodaComissaoCientifica_1522068763038.pdf | 25/04/2018 13:47:55 | Bruno Hochegger | Aceito |
| Orçamento | orcamento.pdf | 25/04/2018 13:44:48 | Bruno Hochegger | Aceito |
| Projeto Detalhado / Brochura Investigador | ProjetoGiordano2018.pdf | 25/04/2018 13:44:35 | Bruno Hochegger | Aceito |
| Folha de Rosto | FolhaderostoGiordano.pdf | 25/04/2018 13:44:23 | Bruno Hochegger | Aceito |

Endereço: Av. Ipiranga, 6681, prédio 50, sala 703

Bairro: Partenon

CEP: 90.619-900

UF: RS

Município: PORTO ALEGRE

Telefone: (51)3320-3345

Fax: (51)3320-3345

E-mail: cep@pucls.br

PONTIFÍCIA UNIVERSIDADE
CATÓLICA DO RIO GRANDE
DO SUL - PUC/RS



Continuação do Parecer: 2.665.053

Situação do Parecer:

Aprovado

Necessita Apreciação da CONEP:

Não

PORTO ALEGRE, 21 de Maio de 2018

Assinado por:
Paulo Vinicius Sporleder de Souza
(Coordenador)

Endereço: Av.Ipiranga, 6681, prédio 50, sala 703

Bairro: Partenon

CEP: 90.619-900

UF: RS

Município: PORTO ALEGRE

Telefone: (51)3320-3345

Fax: (51)3320-3345

E-mail: cep@puhrs.br

ANEXO B - OUTROS ARTIGOS PRODUZIDOS NO PERÍODO

Uma lista de outros artigos, produzidos também durante o período de doutorado, é apresentada a seguir, observando esta ordem:

1. Computed tomography findings in chronic pulmonary aspergillosis – A systematic review (submetido ao American Journal of Roentgenology);
2. Advances in imaging and automated quantification of pulmonary diseases in non-neoplastic diseases;
3. Solitary lung cavities: CT findings in malignant and non-malignant disease;
4. Computed tomography findings of bronchiectasis in different respiratory phases correlate with pulmonary function test data in adults;
5. Chest CT findings in patients with dysphagia and aspiration: a systematic review;
6. “Pulmonary vein sign” for pulmonary embolism diagnosis in computed tomography angiography.

Computed Tomography Findings In Chronic Pulmonary Aspergillosis – A Systematic Review

Giordano Rafael Tronco Alves¹, Alessandro Comarú Pasqualotto², Marcelo Cardoso Barros³, Edson Marchiori⁴, Luis Carlos Anflor Jr.¹ and Bruno Hochhegger¹

¹ Post-graduation Program in Medicine and Health Sciences, Pontifical Catholic University of Rio Grande do Sul, Brazil

² Department of Clinical Medicine, Federal University of Health Sciences of Porto Alegre, Brazil

³ Department of Radiology, Santa Casa de Misericórdia de Porto Alegre, Brazil

⁴ Department of Radiology, Federal University of Rio de Janeiro

Correspondence to:

Giordano R. T. Alves, MD MSc. Ipiranga Avenue, 6690, Building 60. 90610-000, Porto Alegre-RS, Brazil.
+5555997291990. grtalves@gmail.com

Introduction

Chronic pulmonary aspergillosis (CPA) comprises a group of conditions caused by the prolonged presence of *Aspergillus* species in the respiratory system and it is often diagnosed in patients with previous lung pathologies (1,2).

CPA can present in different forms, including subacute invasive aspergillosis (SAIA), chronic cavitary pulmonary aspergillosis (CCPA), chronic fibrosing pulmonary aspergillosis (CFPA), simple aspergilloma (SA) and *Aspergillus* nodules (AN). Although a superposition of such forms occurs in a number of patients, these subtypes exhibit radiological patterns that may be evident at computed tomography (CT) studies of the lungs (3-5). Data regarding the imaging aspects of CPA are numerous in medical literature, but generally consist of isolated case reports, case series or studies addressing a particular subtype of CPA.

This systematic review focused on the CT findings of CPA and aimed to collate the most relevant evidence available in this topic, including patient demographics, underlying diseases and the most frequent imaging findings.

Results

A number of 17 original investigations in patients with CPA were included, comprising a pooled sample of 459 individuals (Table 1). The majority of patients were male (265, 60.6%), with a mean age of 58.4 years. The most frequent underlying conditions, either pulmonary or systemic, were smoking-related lung disease (including chronic obstructive pulmonary disease, COPD (n=126, 36.0%), previous mycobacterial lung disease including tuberculosis (n=197, 56.2%), previous thoracic surgeries (n=26, 7.4%) and diabetes (n=26, 7.4%). Four studies were not included in this analysis, as they only included otherwise healthy subjects (9, 12), asthmatics with allergic bronchopulmonary aspergillosis (ABPA) (17) or did not specify enough (20).

The most frequent imaging features of CPA included pleural thickening (n=136, 31.1%), one or more lung cavity (n=295, 67.5%), fungus ball / mycetoma (n=144, 32.9%), any form of consolidation (n=164, 37.5%) and pulmonary nodule or mass (n=189, 43.2%). One study was excluded from this analysis for not providing the frequency of each CT abnormality (17).

Table 1. Extracted data from the included studies

| First author (et al.) | Year | N. Patients with CPA | Sex | Mean Age | Underlying Conditions | Imaging Findings |
|-----------------------|------|----------------------|--------|------------|--|---|
| Franquet ⁶ | 2000 | 09 | M (9) | 68 (54-89) | COPD (9) Alcoholism (3) Diabetes (1) Chronic renal disease (1) | Segmental consolidation (6) Pleural thickening (4) Cavity (4) Mycetoma (2) Multiple nodules (3) |
| Kim ⁷ | 2000 | 06 | F (4) | 53 (36-67) | Smoking-related disease (3) Diabetes (3) Previous tuberculosis (3) Alcoholism (1) | Consolidation (5) Cavity (3) Pleural thickening (2) Volume loss (2) Mycetoma (2) |
| Franquet ⁸ | 2002 | 08 | M (7) | 46 (28-67) | Leukemia (6) COPD (1) Liver disease (1) | Bronchial wall thickening (8) Bronchial stenosis (8) Distal atelectasis (5) Tree-in-bud nodules (2) Consolidation (1) Pleural effusion (1) |
| Kang ⁹ | 2002 | 11 | F (6) | 48 (31-72) | None | Nodule or mass (9) Consolidation (2) |
| Denning ¹⁰ | 2003 | 18 | M (13) | 59 (20-77) | Tuberculosis (9) Smoking-related disease (13) | Cavity (18) Pleural thickening (12) Mycetoma (6) Fibrotic changes (5) Infiltrate with or without consolidation (9) Bronchiectasis (2) |
| Nam ¹¹ | 2010 | 43 | M (34) | 60 (45-65) | Previous mycobacterial infection (40) Prior thoracic surgery (9) | Cavity (43) Consolidation (36) Pleural thickening (35) |

| | | | | | | |
|--------------------------|------|----|--------|------------|--|---|
| | | | | | COPD (6) | Mycetoma (21) Bronchiectasis (16) |
| Yoon ¹² | 2011 | 07 | F (6) | 63 (59-75) | None | Nodule or mass (7) Satellite nodules (2) |
| Tashiro ¹³ | 2013 | 04 | M (4) | 62 (51-75) | COPD (3) Previous tuberculosis (2) Diabetes (1) Prior thoracic surgery (1) | Cavity (4) Mycetoma (4) Consolidation (4) Nodules (1) |
| Camara ¹⁴ | 2014 | 44 | M (25) | 65 (54-75) | COPD (15) Bronchiectasis (14) Previous mycobacterial infection (10) | Cavity (40) Consolidation (19) Mycetoma (18) Bronchiectasis (14) Pleural thickening (7) Pleural effusion (5) Centrilobular nodules (8) Tree-in-bud nodules (6) |
| Yzumikawa ¹⁵ | 2014 | 27 | M (20) | 63 (40-80) | Smoking-related disease (16) Bronchiectasis (9) Malnutrition (12) Prior tuberculosis (10) Diabetes (9) Prior thoracic surgery (6) | Cavity (19) Mycetoma (17) Nodules (3) Bronchiectasis (2) |
| Benjelloun ¹⁶ | 2015 | 81 | M (48) | 51 (27-75) | History of tuberculosis (78) Smoking-related disease (18) Diabetes (4) | Pleural thickening (38) Cavity (26) Mycetoma (25) Consolidation (23) |
| Lowes ¹⁷ | 2015 | 22 | N/A | N/A | Early childhood asthma (19) | Bronchiectasis* (22) *Concomitant ABPA Pleural thickening** Upper volume loss** Cavity** Mycetoma** **Value not given |
| Ando ³ | 2016 | 30 | M (28) | 70 (29-86) | Sequelae of tuberculosis (17) Diabetes (8) Prior thoracic surgery (4) | Cavity (30) Mycetoma (21) Consolidation (20) Ground-glass opacities (12) |
| Godet ¹⁸ | 2016 | 36 | M (22) | 58 (46-70) | Previous mycobacterial disease (20) COPD (11) Prior thoracic surgery (6) | Pleural thickening (36) Cavity (32) Mycetoma (20) Tree-in-bud nodules (16) Other nodules (16) Consolidation (24) Atelectasis (22) |
| Kosmidis ¹⁹ | 2016 | 11 | F (6) | 58 (37-73) | Previous mycobacterial disease (8) Smoking-related disease (7) | Cavity (11) Mycetoma (8) Fibrotic changes and volume loss (10) Contralateral nodules (2) |
| Muldoon ⁴ | 2016 | 33 | M (18) | 58 (27-80) | Smoking-related disease (24) | Nodules (33) Solid mass (23) *Cavitating lung lesions with or without aspergilloma were not included |
| Hou ²⁰ | 2017 | 69 | F (41) | 53 (19-74) | Previous lung disease (43) Any immunosuppression (21) | Cavity (65) Nodule (58) Consolidation (3) Pleural thickening (2) |

Table 2. Distribution of imaging findings in patients with CPA

| Imaging Findings | Number of Reports | Prevalence (%) |
|---------------------------------|-------------------|----------------|
| Pulmonary cavity (at least one) | 295 | 67.5 |
| Mycetoma (fungus ball) | 144 | 32.9 |
| Consolidation (any form) | 164 | 37.5 |
| Nodule or mass (at least one) | 189 | 43.2 |
| Pleural thickening | 136 | 31.1 |
| Bronchiectasis | 34 | 7.7 |
| Atelectasis | 27 | 6.2 |
| Fibrotic changes* | 17 | 3.9 |
| Pleural effusion | 6 | 1.4 |

*Probably underestimated due to coexistence with consolidation, pleural thickening and atelectasis.

Discussion

The clinical significance of CPA and its burden on healthcare has been increasingly recognized in the last two decades (5, 16, 21). There is a clear relationship between the development of CPA and the coexistence of one or more pulmonary and systemic pathologies, remarkably previous mycobacterial infection and smoking-related lung diseases, as architectural distortion of the lung is generally present (19, 22).

Patients with CPA may present with different symptoms, based on the subtype of CPA infection and immune status (23). By definition, most forms will affect non-immunocompromised individuals, with the exception of SAIA (formerly known as chronic necrotizing pulmonary aspergillosis), which tends to occur in a mild to moderate state of immunosuppression (5) (Figure 2). A recent study indicated that cough, hemoptysis and chronic sputum as the most prevalent clinical findings in CPA, with an association between hemoptysis and the presence of aspergilloma (20). Indolent constitutional symptoms, including weight loss and low fever, may be present as well (24).

The diagnosis of CPA can be made on the basis of clinical, radiological, serological and histological features. A lung biopsy will often demonstrate chronic inflammatory and fibrotic changes, with or without necrosis, vascular invasion and granulomatous formations (12, 25). It is accepted that the presence of hyphae in pulmonary tissue samples characterizes invasive aspergillosis, and their absence does

not exclude the diagnosis of CPA. Similarly, the detection of *Aspergillus spp.* in the sputum is not diagnostic because the fungus is ubiquitous (26). Denning et al. have proposed six criteria for the diagnosis of CPA (all must be present), including chronic symptoms (>3 months), compatible imaging findings, increased levels of inflammatory markers, positive serological testing or isolation of *Aspergillus spp.* in the pleural cavity or lung, exclusion of other pulmonary pathogens and the absence of significant immunosuppression (10).

The most frequent presentation of CPA is CCPA, which can progress to CFPA if untreated (5) (Figure 3). The notion of these two forms belonging to a common spectrum has previously led to the proposal by Tashiro et al to suggest a unique term (chronic progressive pulmonary aspergillosis) (13). The dominant CT findings are the presence of consolidation, progressing to one or more pulmonary cavities (with or without mycetoma/aspergilloma colonization, crescent sign might be present), pleural thickening and fibrotic changes in the lung parenchyma, ultimately leading to more architectural distortion and volume loss (Figures 1 and 2) (2, 19). These findings do not necessarily follow a temporal order; for example, evidence of progressive or new pleural thickening might indicate CPA and precede the development of aspergilloma (24). There is also growing data linking the massive pleural thickening described in pleuroparenchymal fibroelastosis to *Aspergillus spp.* recurrent infection (27).

The presence of pulmonary nodules in patients with CPA has been recently recognized as a distinct pattern and termed *Aspergillus* nodules (4, 9). These are usually observed in the upper lobes, either as solitary or multiple nodules, varying in size from 5-50 mm (Figure 3). However, because an imaging differential diagnosis with lung cancer and other diseases is often difficult, most cases will still undergo biopsy or resection for appropriate histological characterization (12).

SAIA is the form of chronic invasive aspergillosis, usually affecting mildly immunosuppressed individuals. Consolidation (excavating or not) represents the main finding, corresponding to necrosis, abscess formation, foci of fibrosis and intra-alveolar hemorrhage (6, 7). Due to its invasive character, the identification of *Aspergillus spp.* hyphae in the pulmonary tissue is usually performed, more frequently than in any other form of chronic aspergillosis (5).

Our review study has some limitations. Following the inclusion criteria, it included a limited number of investigations, and combined data from a long list of case reports available in the literature were not included. A small number of the reviewed papers did not provide pieces of information, leading to their exclusion in particular analyses to avoid any calculation bias. The terminology used in some studies could have also been misleading; for example, there can be inter-observer discrepancies when reporting areas of chronic consolidation, fibrotic changes and pleural thickening. Finally, the majority of the articles addressed specific subtypes of CPA, which might affect the interpretation of pooled values. However, as an overlap between those forms is very common, a broader knowledge of the possible presentations of CPA would be advised in daily practice.

In summary, CPA is a challenging and unrecognized condition and it is frequently encountered in association with other very prevalent diseases, such as COPD and diabetes. In general, patients do not exhibit any immunosuppression and the clinical presentation tends to be non-specific and slowly

progressive. The diagnosis can often be delayed because of negative microbiological and histological studies. Whereas the radiological findings are diverse, as well as its subtypes, they may provide radiologists with the opportunity to suggest and foster the diagnostic performance of CPA, particularly when a combination of imaging features is present.

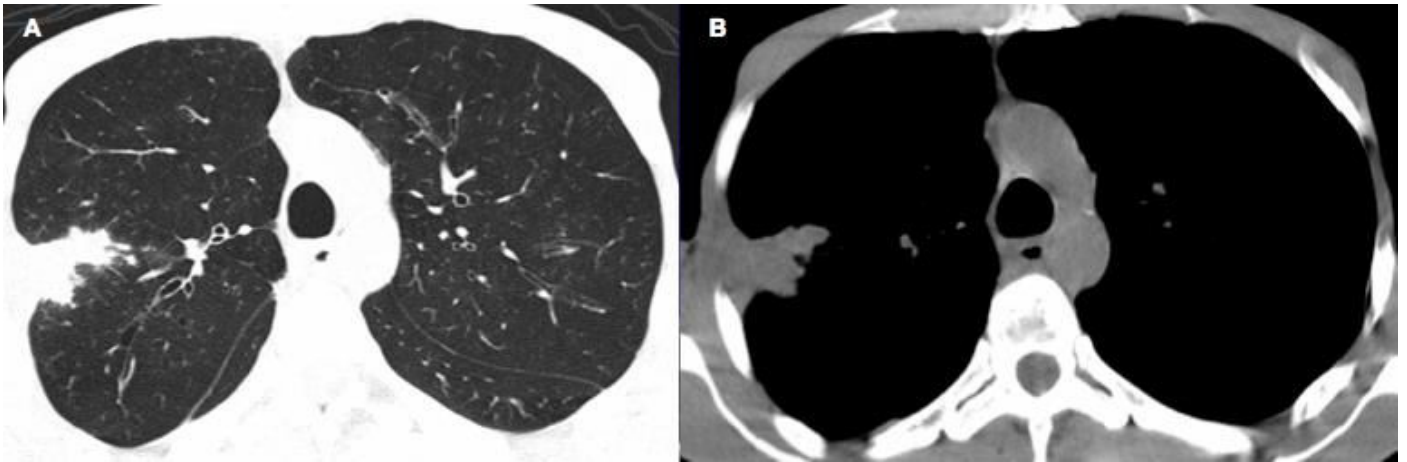


Figure 2. A 46-year-old man diagnosed with chronic pulmonary aspergillosis (subacute invasive form). The patient has been diagnosed with HIV infection for 6 years, with irregular treatment since then. He presented with a 2-month history of constitutional symptoms, including fever, weight loss, cough and dull chest pain. Computed tomography chest scans (lung and mediastinal windows – (A) and (B), respectively) demonstrated a peripheral, irregular solid mass, with tiny perilesional nodules. Post-biopsy histological analysis indicated profuse inflammatory infiltrates, along with cellular debris and septate, dichotomous branching hyphae, suggestive of *Aspergillus spp.*

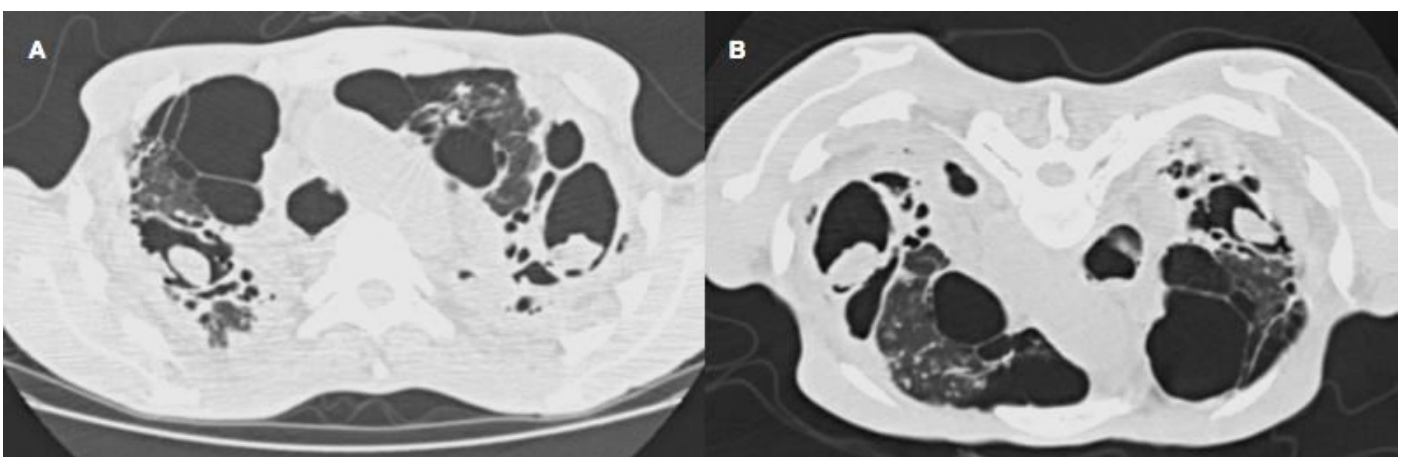



Figure 3. A 78-year-old man diagnosed with chronic pulmonary aspergillosis (chronic cavitary form). The patient had previous history of smoking and mycobacterial infection, and presented with chronic cough (9 months) and recent episodes of hemoptysis. Axial computed tomography scans of the lungs in supine (A) and prone (B) reveal extensive architectural distortion in the upper lobes, with bullae and pulmonary cavities containing rounded soft-tissue material (fungus ball).

References

1. Binder RE, Faling LJ, Pugatch RD, Mahasaen C, Snider GL. Chronic necrotizing pulmonary aspergillosis: a discrete clinical entity. *Medicine (Baltimore)* 1982; 61:109–24.
2. Denning DW. Chronic forms of pulmonary aspergillosis. *Clin Microbiol Infect* 2001; 7(Suppl 2):25–31.
3. Ando T, Tochigi N, Gocho K, Moriya A, Ikushima S, Kumasaka T, et al. Pathophysiological Implication of Computed Tomography Images of Chronic Pulmonary Aspergillosis. *Jpn J Infect Dis.* 2016;69(2):118-26.
4. Muldoon EG, Sharman A, Page I, Bishop P, Denning DW. Aspergillus nodules; another presentation of Chronic Pulmonary Aspergillosis. *BMC Pulm Med.* 2016;16(1):123.
5. Denning DW, Cadranel J, Beigelman-Aubry C, Ader F, Chakrabarti A, Blot S, et al. Chronic pulmonary aspergillosis: rationale and clinical guidelines for diagnosis and management. *Eur Respir J.* 2016;47(1):45-68.
6. Franquet T, Müller NL, Giménez A, Domingo P, Plaza V, Bordes R. Semiinvasive pulmonary aspergillosis in chronic obstructive pulmonary disease: radiologic and pathologic findings in nine patients. *AJR Am J Roentgenol.* 2000;174(1):51-6.
7. Kim SY, Lee KS, Han J, Kim J, Kim TS, Choo SW. Semiinvasive pulmonary aspergillosis: CT and pathologic findings in six patients. *AJR Am J Roentgenol.* 2000;174(3):795-8.
8. Franquet T, Serrano F, Giménez A, Rodríguez-Arias JM, Puzo C. Necrotizing Aspergillosis of large airways: CT findings in eight patients. *J Comput Assist Tomogr.* 2002;26(3):342-5.
9. Kang EY, Kim DH, Woo OH, Choi JA, Oh YW, Kim CH. Pulmonary aspergillosis in immunocompetent hosts without underlying lesions of the lung: radiologic and pathologic findings. *AJR Am J Roentgenol.* 2002;178(6):1395-9.
10. Denning DW, Riniotis K, Dobrashian R, Sambatakou H. Chronic cavitary and fibrosing pulmonary and pleural aspergillosis: case series, proposed nomenclature change, and review. *Clin Infect Dis.* 2003;37 Suppl 3:S265-80.
11. Nam HS, Jeon K, Um SW, Suh GY, Chung MP, Kim H, et al. Clinical characteristics and treatment outcomes of chronic necrotizing pulmonary aspergillosis: a review of 43 cases. *Int J Infect Dis.* 2010;14(6):e479-82.
12. Yoon SH, Park CM, Goo JM, Lee HJ. Pulmonary aspergillosis in immunocompetent patients without air-meniscus sign and underlying lung disease: CT findings and histopathologic features. *Acta Radiol.* 2011;52(7):756-61.
13. Tashiro T, Izumikawa K, Tashiro M, Morinaga Y, Nakamura S, Imamura Y, et al. A case series of chronic necrotizing pulmonary aspergillosis and a new proposal. *Jpn J Infect Dis.* 2013;66(4):312-6.
14. Camara B, Reymond E, Saint-Raymond C, Roth H, Brenier-Pinchart MP, Pinel C, et al. Characteristics and outcomes of chronic pulmonary aspergillosis: a retrospective analysis of a tertiary hospital registry. *Clin Respir J.* 2015;9(1):65-73.

15. Izumikawa K, Tashiro T, Tashiro M, Takazono T, Kosai K, Morinaga Y, et al. Pathogenesis and clinical features of chronic pulmonary aspergillosis - is it possible to distinguish CNPA and CCPA clinically? *J Infect Chemother.* 2014;20(3):208-12.
16. Benjelloun H, Zaghba N, Yassine N, Bakhatar A, Karkouri M, Ridai M, et al. Chronic pulmonary aspergillosis: a frequent and potentially severe disease. *Med Mal Infect.* 2015;45(4):128-32.
17. Lowes D, Chishimba L, Greaves M, Denning DW. Development of chronic pulmonary aspergillosis in adult asthmatics with ABPA. *Respir Med.* 2015;109(12):1509-15.
18. Godet C, Laurent F, Bergeron A, Ingrand P, Beigelman-Aubry C, Camara B, et al. CT Imaging Assessment of Response to Treatment in Chronic Pulmonary Aspergillosis. *Chest.* 2016;150(1):139-47.
19. Kosmidis C, Newton P, Muldoon EG, Denning DW. Chronic fibrosing pulmonary aspergillosis: a cause of 'destroyed lung' syndrome. *Infect Dis (Lond).* 2017;49(4):296-301.
20. Hou X, Zhang H, Kou L, Lv W, Lu J, Li J. Clinical features and diagnosis of chronic pulmonary aspergillosis in Chinese patients. *Medicine (Baltimore).* 2017;96(42):e8315.
21. Denning DW, Pleuvry A, Cole DC. Global burden of chronic pulmonary aspergillosis as a sequel to pulmonary tuberculosis. *Bull World Health Organ.* 2011;89(12):864-72.
22. Smith NL, Denning DW. Underlying conditions in chronic pulmonary aspergillosis including simple aspergilloma. *Eur Respir J.* 2011;37(4):865-72.
23. Kosmidis C, Denning DW. The clinical spectrum of pulmonary aspergillosis. *Thorax.* 2015;70(3):270-7.
24. Desai SR, Hedayati V, Patel K, Hansell DM. Chronic Aspergillosis of the Lungs: Unravelling the Terminology and Radiology. *Eur Radiol.* 2015;25(10):3100-7.
25. Yousem SA. The histological spectrum of chronic necrotizing forms of pulmonary aspergillosis. *Hum Pathol.* 1997;28(6):650-6.
26. Ohba H, Miwa S, Shirai M, Kanai M, Eifuku T, Suda T, Hayakawa H, et al. Clinical characteristics and prognosis of chronic pulmonary aspergillosis. *Respir Med.* 2012;106(5):724-9.
27. Reddy TL, Tominaga M, Hansell DM, von der Thusen J, Rassl D, Parfrey H, et al. Pleuroparenchymal fibroelastosis: a spectrum of histopathological and imaging phenotypes. *Eur Respir J.* 2012;40(2):377-85.

Advances in Imaging and Automated Quantification of Pulmonary Diseases in Non-neoplastic Diseases

Fernanda Balbinot^{1,3,4}  · Álvaro da Costa Batista Guedes⁴ · Douglas Zaione Nascimento⁴ · Juliana Fischman Zampieri⁴ · Giordano Rafael Tronco Alves² · Edson Marchiori² · Adalberto Sperb Rubin⁴ · Bruno Hochhegger⁴

Received: 22 July 2016 / Accepted: 3 September 2016
© Springer Science+Business Media New York 2016

Abstract Histological examination has always been the gold standard for the detection and quantification of lung remodeling. However, this method has some limitations regarding the invasiveness of tissue acquisition. Quantitative imaging methods enable the acquisition of valuable information on lung structure and function without the removal of tissue from the body; thus, they are useful for disease identification and follow-up. This article reviews the various quantitative imaging modalities used currently for the non-invasive study of chronic obstructive pulmonary disease, asthma, and interstitial lung diseases. Some promising computer-aided diagnosis methods are also described.

Keywords Pulmonary disease · Benign disease · Automated quantification · Quantitative method

Introduction

Pulmonary diseases lead to lung functional limitation by causing destruction or remodeling of the parenchyma and/or airway wall. Although histological examination is the gold standard for the assessment of lung remodeling, non-invasive methods enable the investigation of disease pathogenesis and changes over time, as well as the evaluation of new therapeutic interventions [1].

Quantitative imaging of the lung has been proven to be useful for disease identification and follow-up. Valuable information on lung structure can be obtained by quantitative computed tomography (CT) techniques, including high-resolution computed tomography (HRCT) and multidetector computed tomography (MDCT). To overcome the inter- and intraobserver variability inherent to radiologists' interpretation of CT images, the use of computer-aided diagnosis (CAD) systems has been improved since its introduction in the 1980s [2]. Increasing concerns about health risks related

✉ Fernanda Balbinot
balbinotf@gmail.com

Álvaro da Costa Batista Guedes
alv_costa@hotmail.com

Douglas Zaione Nascimento
douglas.zn@bol.com.br

Juliana Fischman Zampieri
ju_zampieri@hotmail.com

Giordano Rafael Tronco Alves
grtalves@gmail.com

Edson Marchiori
edsonmarchiori@gmail.com

Adalberto Sperb Rubin
arubin@terra.com.br

Bruno Hochhegger
brunohochhegger@gmail.com

¹ Federal University of Health Sciences of Porto Alegre, Porto Alegre, Brazil

² Federal University of Rio de Janeiro, Rua Thomaz Cameron, 43, Valparaíso, Petrópolis, RJ 25685120, Brazil

³ Rua Coronel Vicente, 451, Centro, Porto Alegre, RS 90030041, Brazil

⁴ Irmandade Santa Casa de Misericórdia de Porto Alegre, LABIMED - Laboratório de Pesquisas em Imagens Médicas, Rua Prof. Annes Dias, 28, Centro, Porto Alegre, RS 90020090, Brazil

to the ionizing radiation needed to acquire CT images have led to the consideration of alternative methods, such as magnetic resonance imaging (MRI). MRI techniques, such as perfusion and diffusion weighting, allow the acquisition of morphological and functional lung images [3]. The present article reviews the imaging methods and CAD systems available for the quantification of pulmonary changes in chronic obstructive pulmonary disease (COPD), asthma, and interstitial lung diseases (ILDs).

Chronic Obstructive Pulmonary Disease

COPD is characterized by irreversible airflow limitation, as demonstrated by a post-bronchodilator forced expiratory volume in the first second/forced vital capacity (FEV_1/FVC) $<70\%$ [4]. Airflow limitation in COPD is caused by a combination of factors, such as parenchymal lung destruction (emphysema) and loss or narrowing of small airways [5]. Because of its implications for the patient's response to therapeutic intervention, efforts have been made to evaluate the relative contributions of these two pathological processes to airflow limitation [6]. CT is currently the most widely available and precise imaging method for the characterization of COPD, although imaging techniques that do not require ionizing radiation are preferred for longitudinal monitoring.

Computed Tomography

Emphysema

Emphysema is characterized by abnormal, permanent enlargement of air spaces distal to the terminal bronchioles,

accompanied by the destruction of their walls [7]. On CT, emphysema appears as a set of areas with low attenuation values similar to those of air (Fig. 1). Currently, the reference standard for evaluation of the extent of disease on CT images is visual examination. This method, however, is subject to high degrees of inter- and intraobserver variability, and demands significant amounts of time and financial resources. Automated quantification of emphysema, on the other hand, provides objectivity and reproducibility [8].

On CT, the emphysematous lung is represented by image voxels with densities <-950 Hounsfield units (HU) (Fig. 2) [9]. The identification of all voxels with densities below this threshold is a process referred as density masking. The predetermined threshold can vary, however, depending on CT acquisition parameters, such as section thickness and reconstruction algorithm. Madani et al. [10] found that a threshold of -960 to -970 HU was suitable for the quantification of emphysema in continuous-volume MDCT datasets. Another approach—the percentile technique—consists of choosing a point on the percentile scale where the cumulative percentage of lung voxels is less than the cut-off value, and determining the corresponding attenuation value at that point. The 15th percentile has been proven to serve as a measure of lung destruction [1].

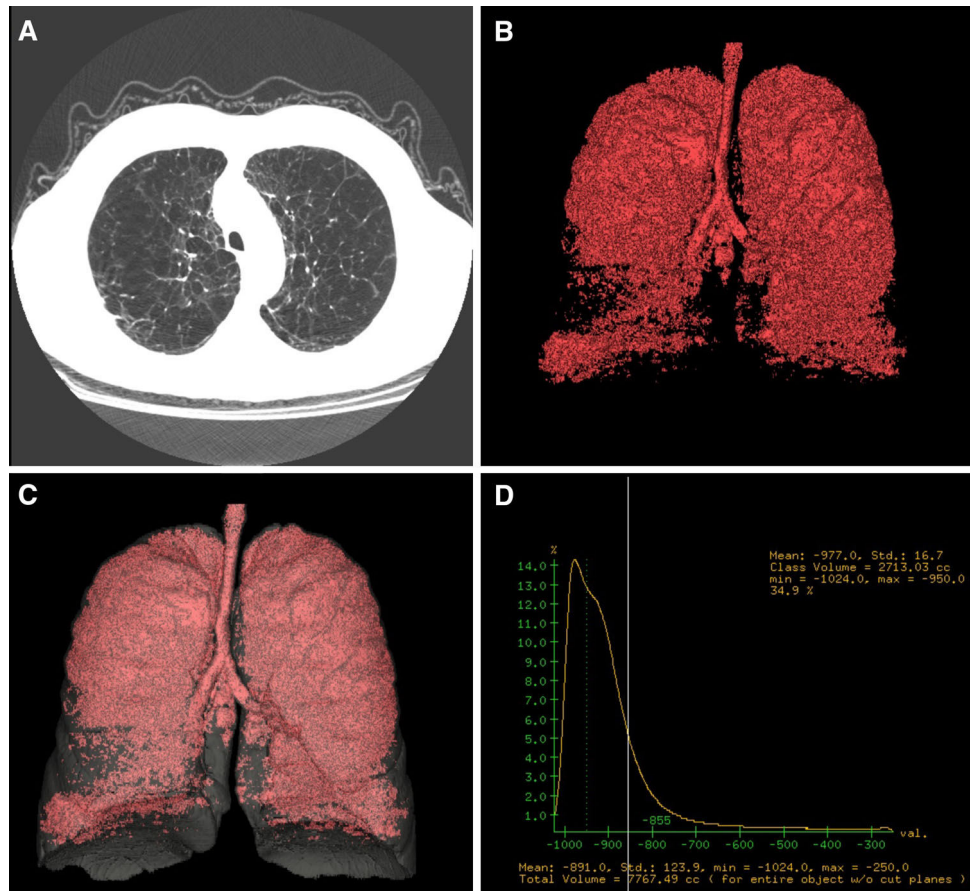
Numerous studies have assessed the usefulness of densitometric analysis in predicting clinically significant metrics, such as lung function. Although previous studies have shown that the extent of emphysema is not always correlated with the severity of airflow limitation [11, 12], the degree of emphysema measured by CT was found more recently to be correlated with levels of dyspnea, FEV_1 , diffusing capacity of carbon monoxide, frequency of



Fig. 1 45-year-old woman with alpha-1 antitrypsin deficiency. **a** Coronal CT image demonstrating extensive areas of low attenuation and bronchial wall thickening, mainly in the lower lobes. **b** Three-dimensional CT reconstruction demonstrating emphysematous areas

(in red). **c** Three-dimensional CT reconstruction of total lung volume, overlaid with emphysematous areas (in red). Automated quantification revealed a total lung volume of 5.5 L and an emphysema index of 32.8 %, using a threshold of -950 HU

Fig. 2 65-year-old male smoker with dyspnea. **a** Axial CT image demonstrating extensive areas of emphysema. **b** Three-dimensional CT reconstruction demonstrating emphysematous areas (*in red*). **c** Three-dimensional CT reconstruction of total lung volume, overlaid with emphysematous areas (*in red*). Automated quantification revealed a total lung volume of 7.5 L, an estimated normal lung index of 52 %, and an emphysema index of 34.9 %, using a threshold of -950 HU



COPD exacerbations, the BODE index [composed of the body mass index (B), degree of airflow obstruction (O), level of functional dyspnea (D), and exercise capacity (E)], and quality of life scores [13]. Moreover, quantitative CT has been considered for the monitoring of emphysema progression and response to therapy [14].

However, the quantification of emphysema by automated methods has some limitations that cannot be ignored. First, quantification using density measures relies on a single threshold and independent voxel information. In addition, the level of inspiration during image acquisition, noise, scanner model, and reconstruction filter are all possible interfering variables [15–18]. Finally, another major limitation is the relative inability of these methods to provide information about the distribution of emphysematous changes, which differs according to emphysema subtype and should be taken into consideration to determine the appropriate therapeutic intervention [19].

In an attempt to overcome these problems, texture-based quantification of emphysema has been developed. Texture analysis involves the selection of a discrete region of interest in the lung and the assessment of several parameters in this constrained region, such as density and patterns of changes therein [1]. The simplest textural approach

involves the identification of discrete and isolated zones of emphysema, and quantification of zones that are connected or clustered together [20].

Several CAD systems using texture analysis have been proposed to automate quantitative analysis and avoid intra- and inter-reader variability. The texture-based adaptive multiple feature method (AMFM), for example, uses mathematical formulations of the bright/dark pattern within the lung field to establish feature sets, which include measures such as mean lung density, kurtosis, skewness, entropy, run-length encoding, and stochastic fractal dimensions [7]. Uppaluri et al. [21] showed that the AMFM was more accurate than mean lung density for the discrimination of regional normal and emphysematous tissues. However, both methods correlated poorly with pulmonary function test results in the normal and emphysema groups.

Airway Measures

Small airway changes are considered to be among the earliest signs of COPD, preceding the development of emphysema [5]. The examination of air trapping on expiratory CT images is becoming quite popular for the assessment of small airway disease [22]. Air trapping,

which appears on these images as areas with less-than-normal increases in attenuation, is the retention of air distal to an obstruction (Fig. 3) [23]. The magnitude of change in lung attenuation after expiration is quantified using densitometric parameters, such as the difference between inspiratory and expiratory CT scans in the proportion of lung volume with a particular attenuation value (usually -856 HU), or the expiratory–inspiratory attenuation ratio (the ratio of mean lung attenuation on expiratory CT to that on inspiratory CT) [24].

Because pulmonary emphysema also corresponds to areas of reduced lung attenuation and is in itself a cause of air trapping, it acts as a confounding factor in the quantification of air trapping. In an effort to solve this problem, Matsuoka et al. [24] determined the attenuation threshold value for the detection and quantification of air trapping using paired inspiratory and expiratory volumetric MDCT images. The densitometric parameter of relative volume change using the threshold of -856 HU in impaired lungs was correlated closely with airway dysfunction in COPD, regardless of the degree of emphysema.

Several studies have shown that indexes derived from attenuation values on expiratory or paired expiratory and inspiratory CT images reflect airway obstruction in COPD. Lee et al. [2] demonstrated that expiratory lung density was correlated with the BODE index, and that CT and physiological measures of air trapping were correlated. Akira et al. [25] found that expiratory CT features were associated with pulmonary function in subjects with severe obstruction alone. Both studies showed that air trapping detection is enhanced when assessed on expiratory images, compared with inspiratory images.

One drawback of the use of expiratory CT is that it exposes the subject to extra radiation associated with a second CT examination. The radiation dose influences the signal-to-noise ratio: the noise level increases with decreasing dose [26]. Increased noise reduces the contrast

between the airway wall and surrounding tissue, thereby reducing measurement accuracy. In addition to radiation exposure, the need for two CT acquisitions constitutes a disadvantage of the technique because expiration is difficult to obtain in patients with COPD. Quantification using expiratory CT also provides an assessment only of the consequences of pathological airway changes, and thus cannot be compared with pathological measures [27].

Magnetic Resonance Imaging

A substantial amount of research in lung imaging has focused on the development and application of inhaled and intravenous contrast agents to improve data collection [1]. The development of inhaled hyperpolarized helium-3 (^3He) and xenon-129 (^{129}Xe) contrast agents has overcome the low proton density issues inherent to lung tissues, which have limited image acquisition by conventional MRI [28]. In this approach, imaging typically takes place with the subject in breath-hold, 10–15 s after inhalation of a discrete volume of hyperpolarized xenon or helium gas. To date, hyperpolarized ^3He has been used widely in clinical research, as the gas remains in the airways without further interaction with the human body [29]. Hyperpolarized ^3He diffuses freely in the air at a rate of $0.88\text{ cm}^2/\text{s}$ until the diffusive movement is restricted by the alveolar boundaries. This restriction of movement is measurable by MRI and is known as the apparent diffusion coefficient (ADC), which is a direct representation of small airway size [30, 31] and is correlated closely with histology [32]. A high ADC indicates that the alveolar walls are further apart—due to alveolar destruction or acinar expansion—which is an early sign of emphysema [29]. The ADC was found to be more sensitive than spirometry and CT to mild emphysema in ex-smokers, and was related to symptoms and exercise limitation in these patients [33]. Importantly, the ADC has been shown to be sensitive to age [34–36],



Fig. 3 40-year-old woman with severe persistent asthma. **a** Airway wall thickness (WT) measurement from an axial CT image. **b** Coronal CT image and **c** three-dimensional CT reconstruction demonstrating air trapping areas

disease-related changes [37–39], and gravity-dependent compression of the lung [40].

More recently, MRI with ^{129}Xe has shed new light on lung function [41]. As xenon is lipid soluble, it has the additional advantage of being freely diffusible across the alveolar–capillary membrane, after which it is removed by capillary blood flow. This phenomenon allows the measurement of alveolar surface and alveolar blood-barrier thickness, which makes this technique a good option for the assessment of ventilation and perfusion [42].

Although MRI, particularly that performed with hyperpolarized gases, offers exciting possibilities for the measurement of alveolar dimensions, it currently cannot surpass HRCT in terms of speed, image contrast and content, and spatial resolution. In addition, a main disadvantage of MRI is that the contrast is exogenous and non-renewable. To overcome some of these limitations, other MRI techniques, such as the use of fluorine, ultrashort-echo-time pulse sequences, and oxygen-enhanced imaging, have been developed. These techniques may ultimately improve the treatment of patients with COPD.

Asthma

Asthma is characterized by chronic airway inflammation, which leads to airway remodeling and airway wall thickening [43]. Airway thickening involves the whole bronchial tree and results from mucosal infiltration by inflammatory cells; deposition of connective tissue on the extracellular matrix; and increases in muscle mass, mucus glands, and vessel area [44]. The severity of asthma is correlated with the degree of wall thickening, duration of the disease, and level of airflow obstruction [45–47]. The involvement of small airways, in particular, is largely responsible for irreversible airflow obstruction and increased airway responsiveness [48].

Airway dimensions in asthmatic patients have been assessed quantitatively by CT, which enables indirect measurement of airway remodeling using the total airway area, wall area, luminal area, and wall thickness of cross-sectional airways. Although HRCT may be used to assess structural changes in the asthmatic lung, MDCT is thought to be a better technique because it enables three-dimensional (3D) reconstruction of the bronchial tree for the measurement of more peripheral airways and segment-by-segment comparison among individuals [1]. Recently, Aysola et al. [45] used MDCT to demonstrate that airway walls are thicker in individuals with severe asthma than in those with mild or no asthma. The authors also demonstrated that thickening of airway walls is correlated positively with pathological measures of remodeling and the degree of airflow obstruction.

The analysis of smaller (luminal diameter < 1–2 mm) airway dimensions is beyond the spatial resolution limits of CT. Thus, some investigators have turned their attention to densitometric measurement on expiratory CT images. Measures of air trapping were shown to be correlated with clinical symptoms and response to therapy in asthmatic patients [49–52]. Busacker et al. [50] investigated whether air trapping was predictive of a more severe asthma phenotype. They defined air trapping as <–850 HU attenuation on expiratory CT images, and considered involvement of >9.66 % of the whole lung volume to be significant. They concluded that patients with the air trapping phenotype were more likely to have histories of asthma-related hospitalization and mechanical ventilation. They also noted some risk factors of this phenotype, such as a history of pneumonia, neutrophilic inflammation, and atopy.

Recently, the use of dynamic oxygen-enhanced MRI was compared with the use of quantitative CT for the assessment of clinical stage and pulmonary function change due to treatment in patients with asthma [53]. Correlations of dynamic oxygen-enhanced MRI with all parameters derived from pulmonary function tests—pre-therapeutic FEV₁/FVC, FEV₁, and the forced expiratory flow at 25–75 % of FVC (FEF_{25–75} %)—were significantly better than those of quantitative CT. However, as inspiratory–expiratory CT was not tested, the potential of quantitative CT may have been underestimated.

Interstitial Lung Diseases

ILD encompasses more than 200 entities, including adult respiratory distress syndrome, sarcoidosis, non-specific interstitial pneumonia, and interstitial pulmonary fibrosis (IPF) [54]. HRCT is the current method of choice for ILD assessment. Several CAD tools have been developed for application to HRCT data. They involve texture-based voxel/pixel classification [55, 56], the assessment of first-order features based on density masks or histogram analysis [57, 58], and even sophisticated classification techniques such as continuous learning with physician-in-the-loop [59] or integrated methods [60, 61]. Although several CAD CT analytical methods have been proven to be useful for the assessment of disease severity and IPF progression, the NL % [which is defined as the percentage of the normally attenuated lung volume as defined from –950 to –701 HU (NL) to the volume of the whole lung (WL)] is significantly more useful than the percentages of predicted FVC and predicted diffusing capacity of the lungs for carbon monoxide for this purpose [62].

CAD schemes enable not only the quantification of disease extent, but also estimation of the contribution of each specific abnormality—ground-glass opacity,

reticulation, and honeycombing—to disease progression (Figs. 4, 5) [63]. Maldonado et al. [64] explored the use of Computer-Aided Lung Informatics for Pathology Evaluation and Rating (CALIPER) to assess baseline and follow-up HRCT images in patients with IPF. They found that the volume of reticular densities, total volume of interstitial abnormalities, and percent total of interstitial abnormalities were predictive of survival after a median follow-up period

of 2.4 years. However, the authors noted that misclassification of abnormalities with similar density but different morphologies may occur with CALIPER.

Traditionally, technical limitations of CT scanners required that HRCT imaging protocols involve the acquisition of non-contiguous thin slices (1 mm) every 10–20 mm, which limited the ability to cover the entire lung parenchyma volume and restricted anatomic

Fig. 4 54-year-old woman with idiopathic pulmonary fibrosis.

a Axial CT image demonstrating areas of ground-glass opacity, septal thickening, and honeycombing bilaterally in the cortical zones of the lower lobes. **b** Coronal CT image depicting the prevalence of these findings in the lower lobes. **c** Three-dimensional CT reconstruction of the total lung volume. **d** Three-dimensional CT reconstruction of interstitial lung disease volumes. Automated quantification revealed a total lung volume of 3.2 L, an estimated normal lung index of 32 %, and an interstitial lung disease index of 22 %

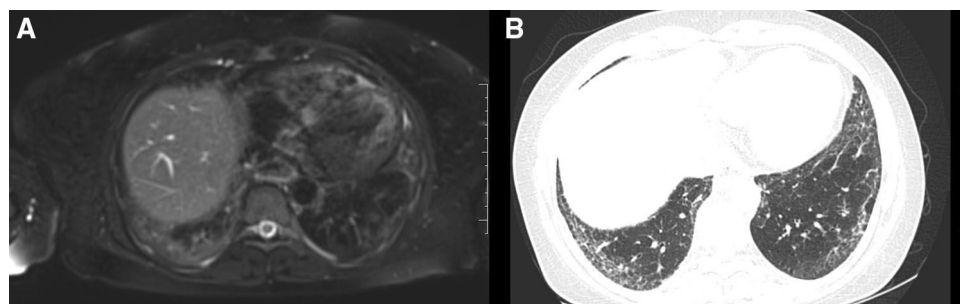
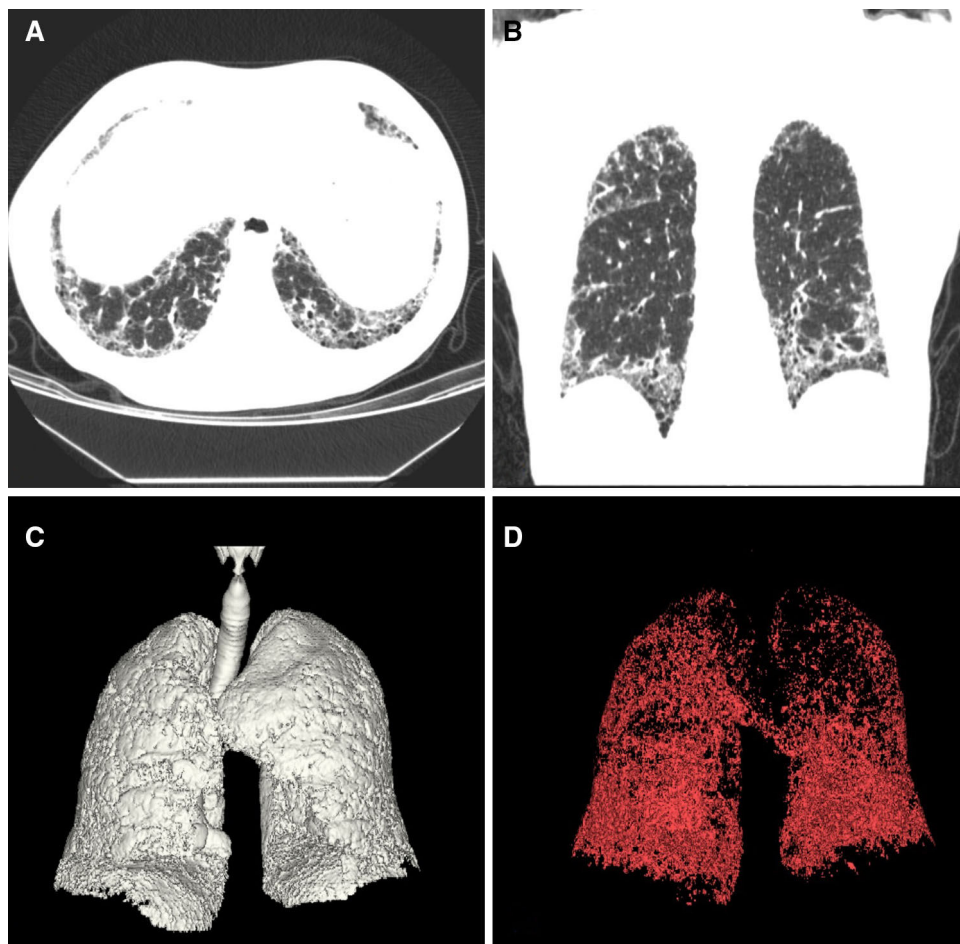


Fig. 5 42-year-old man with scleroderma. **a** Axial CT image demonstrating extensive areas of ground-glass opacity and septal thickening bilaterally in the cortical zones of the lower lobes. **b** Axial

T2-weighted MR image demonstrating extensive areas of hyperintensity unilaterally in the cortical zone of the right lower lobe, suggesting the presence of a non-inflammatory lesion at this site

comparability in follow-up studies [65]. MDCT has enabled the performance of isotropic high-resolution 3D scans of the entire chest in a single breath-hold. Some CAD systems have been developed for application to MDCT image data, which enables the volumetric quantification of disease extent [56, 60, 61]. Recently, Colombi et al. [58] found that values of the 40th and the 80th percentiles on MDCT attenuation frequency histograms were promising parameters for the monitoring of disease extent in patients with IPF. The 40th percentile appears to reflect the change in the overall extent of lung abnormalities, notably the ground-glass pattern, and the 80th percentile was found to reveal the course of reticular opacities.

Although CT is the method of choice for the evaluation of patients with suspected or known ILD, some studies have assessed the use of alternative imaging methods, such as MRI, for disease characterization and follow-up. Buzan et al. [66] evaluated the use of lung T2 mapping for the quantitative characterization and differentiation of normal tissue, ground-glass opacity, reticulation, and honeycombing in patients with stable usual interstitial pneumonia or non-specific interstitial pneumonia. They found significant differences in T2 relaxation between normal and pathological areas, and among ground-glass opacities, reticulation, and honeycombing. These findings indicate that T2 relaxation in lung remodeling can reflect the amount of fibrosis burden and may allow for the monitoring of progression and response to therapy in ILD. The ability of MRI to depict pulmonary abnormalities suggestive of pneumonia was compared with that of HRCT in patients with neutropenia [66]. The sensitivity of MR images for the detection of pneumonia was 95 %, the specificity was 88 %, and the positive and negative predictive values were 95 and 88 %, respectively. After proper adjustment, the description of lesion location and distribution did not differ significantly between modalities. Ground-glass opacities were detected by CT in 14 patients and by MRI in the same 14 patients as well as 2 others. Of these two cases additionally detected by MRI, one was misdiagnosed as a result of blurring artifacts; in the other case, CT performed 3 days later showed a ground-glass area in the location depicted previously on MRI. These findings suggest that MRI has greater sensitivity than CT in this context. Few published studies have directly compared pulmonary CT and MRI for the assessment of ILD; thus, this topic requires further investigation.

Conclusion

CT remains the method of choice for quantitative assessment of the lung. However, other imaging modalities and CAD systems are being developed and improved to enable

the best quantitative studies of lung anatomy and function. When properly controlled, these methods can produce reliable and valuable data for the analysis of lung structure, which can be used to study the pathogenesis of diseases and the effects of therapeutic interventions.

Compliance with Ethical Standards

Conflict of Interest All authors declare that they have no conflict of interest.

References

1. Washko GR, Parraga G, Coxson HO (2012) Quantitative pulmonary imaging using computed tomography and magnetic resonance imaging. *Respirology* 17:432–444
2. Lee YK, Oh YM, Lee JH et al (2008) Quantitative assessment of emphysema, air trapping, and airway thickening on computed tomography. *Lung* 186:157–165
3. Henzler T, Schmid-Bindert G, Schoenberg SO et al (2010) Diffusion and perfusion MRI of the lung and mediastinum. *Eur J Radiol* 76:329–336
4. Pauwels RA, Buist AS, Calverley PM et al (2001) Global Strategy for the diagnosis, management, and prevention of chronic obstructive pulmonary disease. NHLBI/WHO global initiative for chronic obstructive lung disease (GOLD) workshop summary. *Am J Respir Crit Care Med* 163:1256–1276
5. McDonough JE, Yuan R, Suzuki M et al (2011) Small-airway obstruction and emphysema in chronic obstructive pulmonary disease. *N Engl J Med* 365:1567–1575
6. Tho NV, Ryuji Y, Ogawa E et al (2015) Relative contributions of emphysema and airway remodelling to airflow limitation in COPD: consistent results from two cohorts. *Respirology* 20:594–601
7. Hoffman EA, Reinhardt JM, Sonka M et al (2003) Characterization of the interstitial lung diseases via density-based and texture-based analysis of computed tomography images of lung structure and function. *Acad Radiol* 10:1104–1118
8. Ginsburg SB, Lynch DA, Bowler RP et al (2012) Automated texture-based quantification of centrilobular nodularity and centrilobular emphysema in chest CT images. *Acad Radiol* 19:1241–1251
9. Milne S, King GG (2014) Advanced imaging in COPD: insights into pulmonary pathophysiology. *J Thorac Dis* 6:1570–1585
10. Madani A, Zanen J, de Maertelaer V et al (2006) Pulmonary emphysema: objective quantification at multi-detector row CT—comparison with macroscopic and microscopic morphometry. *Radiology* 238:1036–1043
11. Gelb AF, Schein M, Kuei J et al (1993) Limited contribution of emphysema in advanced chronic obstructive pulmonary disease. *Am Rev Respir Dis* 147:1157–1161
12. Hogg JC, Wright JL, Wiggs BR et al (1994) Lung structure and function in cigarette smokers. *Thorax* 49:473–478
13. Martinez CH, Chen YH, Westgate PM et al (2012) Relationship between quantitative CT metrics and health status and BODE in chronic obstructive pulmonary disease. *Thorax* 67:399–406
14. Coxson HO, Dirksen A, Edwards LD et al (2013) The presence and progression of emphysema in COPD as determined by CT scanning and biomarker expression: a prospective analysis from the ECLIPSE study. *Lancet Respir Med* 1:129–136
15. Boedeker KL, McNitt-Gray MF, Rogers SR et al (2004) Emphysema: effect of reconstruction algorithm on CT imaging measures. *Radiology* 232:295–301

16. Stoel BC, Bakker ME, Stolk J et al (2004) Comparison of the sensitivities of 5 different computed tomography scanners for the assessment of the progression of pulmonary emphysema: a phantom study. *Invest Radiol* 39:1–7
17. Sieren JP, Newell JD, Judy PF et al (2012) Reference standard and statistical model for intersite and temporal comparisons of CT attenuation in a multicenter quantitative lung study. *Med Phys* 39:5757–5767
18. Bakker ME, Stolk J, Putter H, Shaker SB et al (2005) Variability in densitometric assessment of pulmonary emphysema with computed tomography. *Invest Radiol* 40:777–783
19. Fishman A, Martinez F, Naunheim K et al (2003) National Emphysema Treatment Trial Research Group. A randomized trial comparing lung-volume-reduction surgery with medical therapy for severe emphysema. *N Engl J Med* 348:2059–2073
20. Mishima M, Hirai T, Itoh H et al (1999) Complexity of terminal airspace geometry assessed by lung computed tomography in normal subjects and patients with chronic obstructive pulmonary disease. *Proc Natl Acad Sci USA* 96:8829–8834
21. Uppaluri R, Mitsa T, Sonka M et al (1997) Quantification of pulmonary emphysema from lung computed tomography images. *Am J Respir Crit Care Med* 156:248–254
22. Coxson HO, Lam S (2009) Quantitative assessment of the airway wall using computed tomography and optical coherence tomography. *Proc Am Thorac Soc* 6:439–443
23. Hansell DM, Bankier AA, MacMahon H et al (2008) Fleischner society: glossary of terms for thoracic imaging. *Radiology* 246:697–722
24. Matsuoka S, Kurihara Y, Yagihashi K et al (2008) Quantitative assessment of air trapping in chronic obstructive pulmonary disease using inspiratory and expiratory volumetric MDCT. *AJR Am J Roentgenol* 190:762–769
25. Akira M, Toyokawa K, Inoue Y et al (2009) Quantitative CT in chronic obstructive pulmonary disease: inspiratory and expiratory assessment. *AJR Am J Roentgenol* 192:267–272
26. Madani A, De Maertelaer V, Zanen J et al (2007) Pulmonary emphysema: radiation dose and section thickness at multidetector CT quantification—comparison with macroscopic and microscopic morphometry. *Radiology* 243:250–257
27. Hackx M, Bankier AA, Gevenois PA (2012) Chronic obstructive pulmonary disease: CT quantification of airways disease. *Radiology* 265:34–48
28. Fain S, Schiebler ML, McCormack DG et al (2010) Imaging of lung function using hyperpolarized helium-3 magnetic resonance imaging: review of current and emerging translational methods and applications. *J Magn Reson Imaging* 32:1398–1408
29. van Beek EJR, Hoffman EA (2008) Functional imaging: CT and MRI. *Clin Chest Med* 29:195–216
30. de Lange EE, Mugler JP, Brookeman JR et al (1999) Lung air spaces: MR imaging evaluation with hyperpolarized ^3He gas. *Radiology* 210:851–857
31. Kauczor HU, Ebert M, Kreitner KF et al (1997) Imaging of the lungs using ^3He MRI: preliminary clinical experience in 18 patients with and without lung disease. *J Magn Reson Imaging* 7:538–543
32. Woods JC, Choong CK, Yablonskiy DA et al (2006) Hyperpolarized ^3He diffusion MRI and histology in pulmonary emphysema. *Magn Reson Med* 56:1293–1300
33. Kirby M, Owrangi A, Svenningsen S et al (2013) On the role of abnormal DL(CO) in ex-smokers without airflow limitation: symptoms, exercise capacity and hyperpolarised helium-3 MRI. *Thorax* 68:752–759
34. Fain SB, Altes TA, Panth SR et al (2005) Detection of age-dependent changes in healthy adult lungs with diffusion-weighted ^3He MRI. *Acad Radiol* 12:1385–1393
35. Altes TA, Mata J, de Lange EE et al (2006) Assessment of lung development using hyperpolarized helium-3 diffusion MR imaging. *J Magn Reson Imaging* 24:1277–1283
36. Parraga G, Mathew L, Etamad-Rezai R et al (2008) Hyperpolarized ^3He magnetic resonance imaging of ventilation defects in healthy elderly volunteers: initial findings at 3.0. Tesla *Acad Radiol* 15:776–785
37. Salerno M, de Lange EE, Altes TA et al (2002) Emphysema: hyperpolarized helium 3 diffusion MR imaging of the lungs compared with spirometric indexes—initial experience. *Radiology* 222:252–260
38. Swift AJ, Wild JM, FICHELE S et al (2005) Emphysematous changes and normal variation in smokers and COPD patients using diffusion ^3He MRI. *Eur J Radiol* 54:352–358
39. van Beek EJ, Dahmen AM, Stavngaard T et al (2009) Hyperpolarised $^3\text{-He}$ MRI vs HRCT in COPD and normal volunteers—PHIL trial. *Eur Respir J* 34:1311–1321
40. FICHELE S, Woodhouse N, Said Z et al (2004) MRI of Helium-3 Gas in healthy lungs: posture related variations of alveolar size. *J Magn Reson Imaging* 20:331–335
41. Patz S, Muradyan I, Hrovat MI et al (2011) Diffusion of hyperpolarized ^{129}Xe in the lung: simplified model of ^{129}Xe septal uptake and experimental results. *New J Phys* 13:015009
42. Patz S, Muradian I, Hrovat MI et al (2008) Human pulmonary imaging and spectroscopy with hyperpolarized $^{129}\text{-Xe}$ at 0.2T. *Radiology* 15:713–727
43. Niimi A, Matsumoto H, Takemura M et al (2004) Clinical assessment of airway remodeling in asthma: utility of computed tomography. *Clin Rev Allergy Immunol* 27:45–58
44. Bousquet J, Chanez P, Lacoste JY et al (1992) Asthma: a disease remodeling the airways. *Allergy* 47:3–11
45. Aysola RS, Hoffman EA, Gierada D et al (2008) Airway remodeling measured by multidetector CT is increased in severe asthma and correlates with pathology. *Chest* 134:1183–1191
46. Niimi A, Matsumoto H, Amitani R et al (2004) Effect of short-term treatment with inhaled corticosteroid on airway wall thickening in asthma. *Am J Med* 116:725–731
47. Kasahara K, Shiba K, Ozawa T et al (2002) Correlation between the bronchial subepithelial layer and whole airway wall thickness in patients with asthma. *Thorax* 57:242–246
48. Gono H, Fujimoto K, Kawakami S et al (2003) Evaluation of airway wall thickness and air trapping by HRCT in asymptomatic asthma. *Eur Respir J* 22:965–971
49. Busacker A, Newell JD Jr, Keefe T et al (2009) A multivariate analysis of risk factors for the air-trapping asthmatic phenotype as measured by quantitative CT analysis. *Chest* 135:48–56
50. Zeidler MR, Kleerup EC, Goldin JG et al (2006) Montelukast improves regional air-trapping due to small airways obstruction in asthma. *Eur Respir J* 27:307–315
51. Lee E, Seo JB, Lee HJ et al (2015) Quantitative assessment of global and regional air trappings using non-rigid registration and regional specific volume change of inspiratory/expiratory CT scans: studies on healthy volunteers and asthmatics. *Korean J Radiol* 16:632–640
52. Ohno Y, Nishio M, Koyama H et al (2014) Asthma: comparison of dynamic oxygen-enhanced MR imaging and quantitative thin-section CT for evaluation of clinical treatment. *Radiology* 273:907–916
53. Ryu JH, Colby TV, Hartman TE et al (2001) Smoking-related interstitial lung diseases: a concise review. *Eur Resp J* 17:122–132
54. Yoon RG, Seo JB, Kim N et al (2013) Quantitative assessment of change in regional disease patterns on serial HRCT of fibrotic interstitial pneumonia with texture-based automated quantification system. *Eur Radiol* 23:692–701

55. Korfiatis PD, Karahaliou AN, Kazantzi AD et al (2010) Texture-based identification and characterization of interstitial pneumonia patterns in lung multidetector CT. *IEEE Trans Inf Technol Biomed* 14:675–680
56. Hartley PG, Galvin JR, Hunninghake GW et al (1994) High-resolution CT-derived measures of lung density are valid indexes of interstitial lung disease. *J Appl Physiol* 76:271–277
57. Colombi D, Dinkel J, Weinheimer O et al (2015) Visual vs fully automatic histogram-based assessment of idiopathic pulmonary fibrosis (IPF) progression using sequential multidetector computed tomography (MDCT). *PLoS One* 10:e0130653
58. Shyu CR, Brodley CE, Kak AC et al (1999) Assert: a physician-in-the-loop content-based retrieval system for HRCT image databases. *Comput Vis Image Underst* 75:111–132
59. Zavaletta VA, Bartholmai BJ, Robb RA (2007) High resolution multidetector CT-aided tissue analysis and quantification of lung fibrosis. *Acad Radiol* 14:772–787
60. Xu Y, van Beek EJ, Hwanjo Y et al (2006) Computer-aided classification of interstitial lung diseases via MDCT: 3D adaptive multiple feature method (3D AMFM). *Acad Radiol* 13:969–978
61. Ohkubo H, Kanemitsu Y, Uemura T et al (2016) Normal lung quantification in usual interstitial pneumonia pattern: the impact of threshold-based volumetric ct analysis for the staging of idiopathic pulmonary fibrosis. *PLoS One*. doi:[10.1371/journal.pone.0152505](https://doi.org/10.1371/journal.pone.0152505)
62. Gruden JF, Panse PM, Leslie KO et al (2013) UIP diagnosed at surgical lung biopsy, 2000–2009: HRCT patterns and proposed classification system. *AJR Am J Roentgenol* 200:W458–W467
63. Maldonado F, Moua T, Rajagopalan S et al (2014) Automated quantification of radiological patterns predicts survival in idiopathic pulmonary fibrosis. *Eur Respir J* 43:204–212
64. Uchiyama Y, Katsuragawa S, Abe H et al (2003) Quantitative computerized analysis of diffuse lung disease in high-resolution computed tomography. *Med Phys* 30:2440–2454
65. Buzan MTA, Eichinger M, Kreuter M et al (2015) T2 mapping of CT remodelling patterns in interstitial lung disease. *Eur Radiol* 25:3167–3174
66. Eibel R, Herzog P, Dietrich O et al (2006) Pulmonary abnormalities in immunocompromised patients: comparative detection with parallel acquisition MR imaging and thin-section helical CT. *Radiology* 241:880–891



Solitary lung cavities: CT findings in malignant and non-malignant disease



C.S. Nin^a, V.V.S. de Souza^a, G.R.T. Alves^{b,*}, R.H. do Amaral^a, K.L. Irion^c,
E. Marchiori^b, B. Hochegger^b

^a Federal University of Health Sciences of Porto Alegre, Brazil

^b Post-graduation Program in Medicine (Radiology), Federal University of Rio de Janeiro, Brazil

^c Radiology Department Liverpool Heart and Chest Hospital, UK

ARTICLE INFORMATION

Article history:

Received 13 July 2015

Received in revised form

6 April 2016

Accepted 8 April 2016

AIM: To assess the computed tomography (CT) findings of solitary cavitory lesions which could potentially aid in differentiating malignant from non-malignant lung disease.

MATERIALS AND METHODS: A retrospective study of patients diagnosed with a solitary lung cavity at two university hospitals, who underwent multidetector CT examinations of the chest between 2012 and 2014, was performed. Lesions were evaluated for maximum diameter, maximum wall thickness, and associated findings. Statistical analyses were then conducted and a receiver operating characteristic (ROC) curve was calculated to select the most accurate cut-off value for malignant and non-malignant lesions.

RESULTS: CT and clinical records from 96 patients were reviewed. The most frequent aetiologies of non-malignant and malignant lung cavities were mycobacterial infection sequelae (50%, 33/66) and primary lung carcinoma (94%, 28/30), respectively. Significant differences ($p < 0.05$) were found between malignant and non-malignant cases when comparing the averages of maximum wall thickness (15.2 and 7.8 mm, respectively) and maximum diameter of lesions (51 and 35 mm, respectively). The presence of either perilesional consolidation or centrilobular nodules favoured the diagnosis of non-malignant conditions ($p < 0.05$). Maximum wall thicknesses thresholds of ≤ 7 or ≥ 24 mm were the most accurate in suggesting non-malignant and malignant aetiologies, respectively.

CONCLUSION: Malignant and non-malignant solitary lung cavities differ significantly at CT. Non-malignant lesions tend to exhibit thinner walls, but more perilesional consolidation and centrilobular nodules than malignant lesions. The results reveal that maximum wall thicknesses of ≤ 7 and ≥ 24 mm are indicative of non-malignant and malignant disease, respectively.

© 2016 The Royal College of Radiologists. Published by Elsevier Ltd. All rights reserved.

Introduction

A cavity is a gas-filled space that appears on imaging examinations as an area of lucency or low attenuation. Pulmonary cavities can occur within areas of pulmonary consolidation, masses, or nodules, and usually result from the drainage of necrotic lesions via the bronchial tree.¹

* Guarantor and correspondent: G.R.T. Alves, Federal University of Rio de Janeiro, Post-graduation Program in Medicine (Radiology), Professor Rodolpho Paulo Rocco Street, 255, Rio de Janeiro, 21941-913, Brazil. Tel.: +55 55 97291990.

E-mail address: grtalves@gmail.com (G.R.T. Alves).

Although large, thick-walled lesions can be identified in simple chest radiography (CXR) examinations, a number of smaller cavities (or those with thinner walls) may remain unnoticed until a more accurate radiological assessment is performed. Similarly, the wide range of possible aetiologies for solitary lung cavities detected at CXR often prompts the need for further imaging investigation.

Multidetector computed tomography (CT) of the chest is the current technique of choice for evaluating lung cavities, as it provides precise information on size, shape, location of lesions, and other characteristics that may not be evident on CXRs.^{2,3} Based on such features, in combination with an appropriate clinical and laboratory background, radiologists are able to narrow the list of possible diagnoses, such as lung cancer, mycobacterial infection, or even rarer conditions (e.g., pulmonary mycoses and vasculitides)^{1–5}; however, few data exist regarding an objective assessment of cavitory lesions at thoracic CT.

The aim of the present study was to determine the most accurate CT findings of solitary lung cavities that would help differentiate malignant from non-malignant conditions.

Materials and methods

Patients

Using the picture archiving and communication systems (PACSs, PixViwer; Pixon, Florianópolis, Brazil) of two university hospitals located in Brazil's southernmost state (Rio Grande do Sul), patients with cavitory lung lesions who had undergone thoracic CT between June 2012 and April 2014 were identified retrospectively. The searched was initially performed using the terms "cavity" and "cavitory lesion" in the report text field. A third-year radiology resident subsequently confirmed the presence of a solitary lung cavity within the examinations and recorded the demographical data. The local ethics review board approved this study, and

it is registered under the reference ISCMPA-25152713.0.0000.5335. Due to its retrospective and anonymised nature, informed consent forms were waived.

Additional information regarding patient data, such as laboratory results, histological reports, and immune status, were retrieved from the electronic medical records (Philips Tasy; Wheb Sistemas, Blumenau, Brazil). The criteria for immunosuppression included corticotherapy or chemotherapy regimens within 4 weeks preceding CT, any history of organ transplant, and patients diagnosed with acquired immunodeficiency syndrome (AIDS). Definitive diagnoses were achieved by histological study, bacilloscopy, or clinical and radiological follow-up. A diagnosis of tuberculosis was made when patients presented with suggestive symptoms, demonstrated response to treatment, and had cultures from respiratory secretions that were positive for *Mycobacterium tuberculosis* and/or histology of the cavity indicated this diagnosis. Lung abscesses were defined by the presence of a compatible clinical history and resolution of both clinical and radiological findings after antimicrobial therapy, and/or postoperative histological analysis. The diagnosis of sequelae from previous mycobacterial infections was established when (1) records of pharmacological treatment completion were present; (2) patients remained asymptomatic for at least 2 years after therapy; and (3) at least two negative results for *M. tuberculosis* culture were demonstrated.

CT assessment and parameters

All examinations were performed using two 64-multidetector CT systems (LightSpeed VCT; GE Healthcare, Milwaukee, WI, USA). The acquisition protocol was: 0.625 mm section collimation, 0.625 mm reconstruction, 0.4 second gantry rotation, 7.5 mm/s table speed, 120 kV tube voltage, 200 mA tube current, and a 40–50-cm field of view.

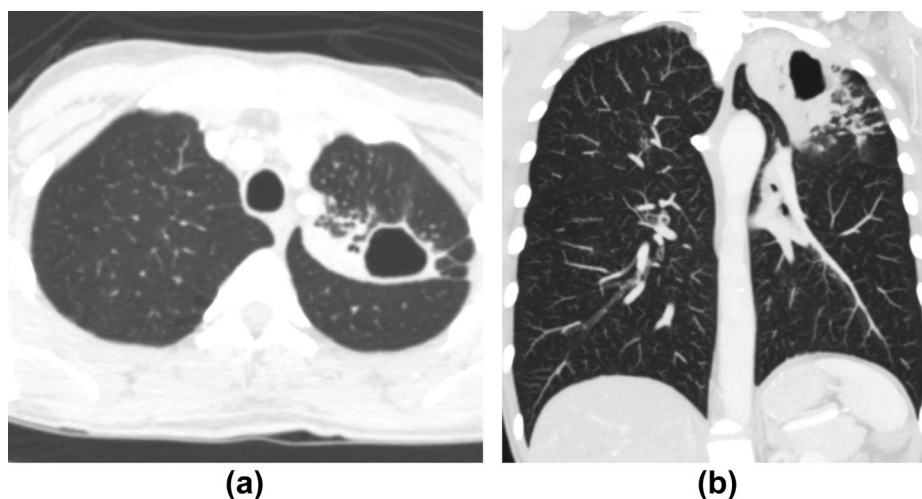


Figure 1 A 50-year-old man with active tuberculosis. (a) Axial CT image demonstrates a thin-walled cavitory lesion in the left upper lobe of the lung. (b) Coronal CT reformatted image evidences perilesional centrilobular nodules. The culture from bronchoalveolar lavage was positive for *M. tuberculosis*.

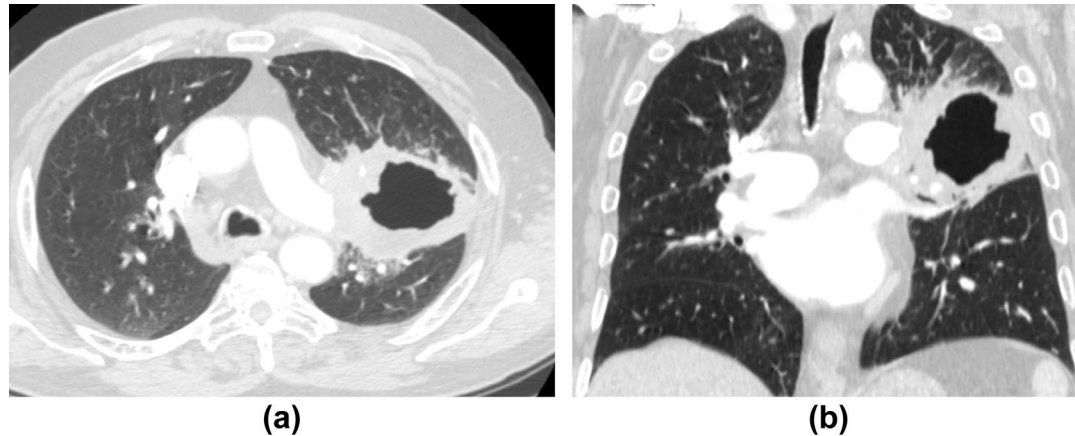


Figure 2 A 75-year-old man with primary lung cancer. (a) Axial CT image reveals a thick-walled cavitary lesion in the left upper lobe of the lung. (b) Coronal CT reformatted image demonstrates the absence of perilesional findings. Histological analysis following lung biopsy confirmed the diagnosis of squamous cell carcinoma.

Two thoracic radiologists, with 5 and 8 years of experience in chest imaging, reviewed the scans consensually using the same workstation (Advantage Workstation 4.4; GE Healthcare). Disagreements between readers were presented to a senior radiologist with more than 20 years of experience in thoracic imaging, who provided the final answer. The radiologists were blinded to both clinical and histological information. For each examination, lesion size (maximum diameter), maximum wall thickness of the cavity (both measured on axial images), and associated findings, regardless of their location or extent, were noted.

Images were volumetrically acquired and evaluated on both pulmonary and mediastinal windows, using high-resolution and soft kernels, respectively. Measurements were further performed in the axial plane only on a pulmonary window, as the aim was to increase the reproducibility of the results and use a readily applicable technique. Consolidation was defined as a homogeneous increase in lung attenuation obscuring the margins of adjacent vessels and airway walls,¹ and centrilobular nodules were considered as nodular opacities occupying the centre of a normal secondary pulmonary lobule, following the recommendations of the Nomenclature Committee of the Fleischner Society.¹

Table 1
Patient, lesion, and diagnostic characteristics (n=96).

| | |
|-----------------------------------|----------|
| Patient characteristics | |
| Sex (male) | 59 (61) |
| Age (years) | 55±17 |
| Immunosuppressed | 20 (21) |
| Lesion characteristics | |
| Wall thickness (mm) ^a | 10.1±6.7 |
| Malignant | 15.2±7.4 |
| Non-malignant | 7.8±4.8 |
| Diameter (mm) ^a | 40±23 |
| Malignant | 51±28 |
| Non-malignant | 35±21 |
| Diagnostic characteristics | |
| Malignant | 30 (31) |
| Primary | 28 (94) |
| Metastasis | 2 (6) |
| Non-malignant | 66 (69) |
| Mycobacterial infection sequelae | 33 (50) |
| Active pulmonary tuberculosis | 24 (36) |
| Abscess | 8 (12) |
| Aspergillosis | 1 (2) |
| Diagnostic confirmation | |
| Malignant | 30 (31) |
| Histological | 30 (100) |
| Non-malignant | 66 (69) |
| Histological | 30 (45) |
| Clinical/radiological | 15 (23) |
| Bacilloscopy | 21 (32) |

Data are presented as $n \pm$ standard deviation (SD) or n (%).

^a $p < 0.05$ (malignant versus non-malignant).

Statistical analysis

Study data tabulation and subsequent analyses were performed using the Statistical Package for the Social Sciences (SPSS, version 20.0; IBM, Armonk, NY, USA). For comparison purposes, patients were divided into two groups, according to their final diagnosis, in malignant and non-malignant aetiologies of the solitary pulmonary cavities. The variables of the groups were analysed using independent-sample Student's *t*-test, when numerical and normally distributed, and using the Chi-square test when categorical or expressed in proportions. Tests were run bilaterally, assuming significance if $p < 0.05$. After preliminary analysis of the results, receiver operating characteristic (ROC) curves were devised to determine the most accurate cut-off points for differentiating malignant and non-malignant lesions by using the maximum wall thickness of cavities.

Results

Images and medical records of 96 patients who were identified with solitary pulmonary cavities at CT were reviewed, with a mean age of 55±17 years (61% male). Sixty-six cavitary lesions were diagnosed as non-malignant

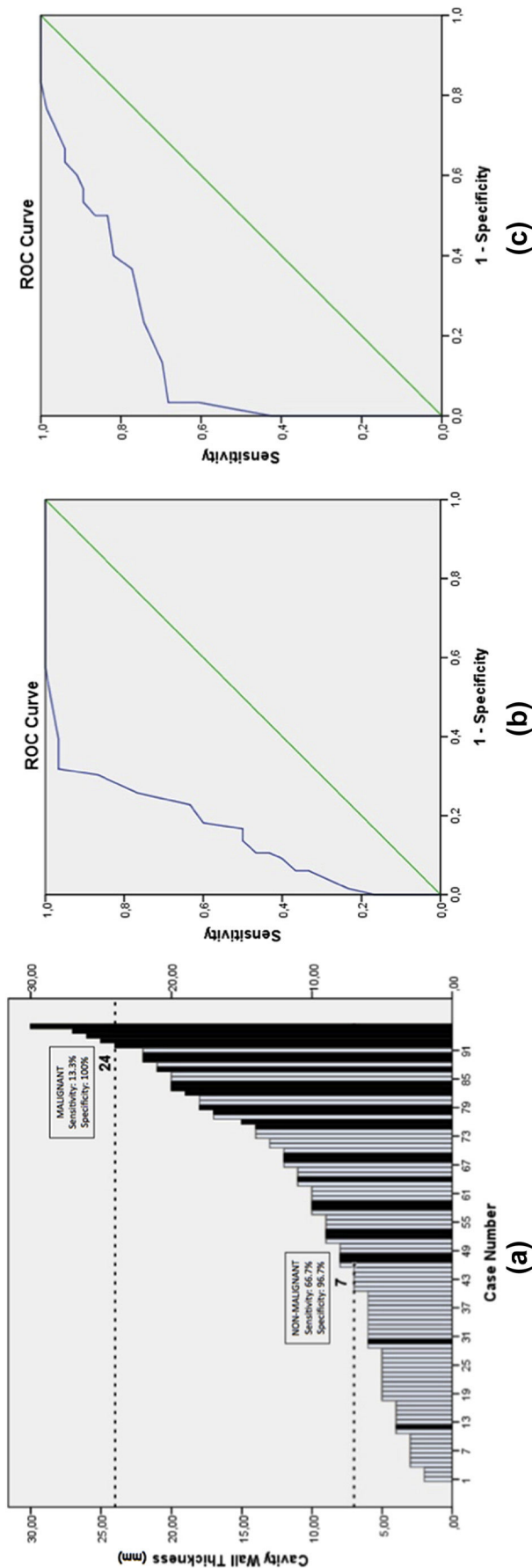


Figure 3 (a) Histogram demonstrating the maximum wall thickness thresholds that best correlate with malignant and non-malignant lesions: 24 mm was considered 100% specific, 13.3% sensitive for malignant aetiologies (b, area under curve, AUC=0.298), whereas 7 mm achieved a specificity of 96.7% and a 66.7% sensitivity (AUC=0.379) for non-malignant lesions (c).

(69%) and 30 (31%) as malignant. Among the non-malignant diagnoses, 33 (50%) consisted of mycobacterial infection sequelae, 24 (36%) of active pulmonary tuberculosis (Fig 1), eight (12%) of lung abscess, and one (2%) of aspergillosis. In the group of malignant aetiologies for solitary lung cavities, 28 (94%) had a final diagnosis of primary lung cancer (Fig 2), and two (6%) were diagnosed as having metastatic disease (Table 1). The immune status did not influence malignancy rates (31% versus 30% prevalence of lung cancers in immunocompetent and immunosuppressed patients, respectively; $p>0.05$) Histological confirmation was obtained in all cases of the malignant group. For non-malignant aetiologies, 30 (45%) were confirmed at histology, 21 (32%) at bacilloscopy, and 15 (23%) using clinical and radiological findings.

Twenty patients (21%) were classified as being immunosuppressed. Among these, 14 were diagnosed with a non-malignant condition (12 with active tuberculosis and two with mycobacterial infection sequelae), and six with malignant conditions (six cases of primary lung cancer). It is noteworthy that the prevalence of active tuberculosis was four-times higher among immunosuppressed than in immunocompetent individuals (60%, 12/20 versus 15%, 12/76; $p<0.05$).

The averages of maximum lesion diameter differed significantly between the malignant and non-malignant groups (51 ± 28 versus 35 ± 21 mm; $p<0.05$). The averages of maximum wall thickness in the malignant and benign lesions were also significantly different (15.2 ± 7.4 versus 7.8 ± 4.8 mm; $p<0.05$). Fig 3 demonstrates the maximum wall thickness thresholds that best correlated with malignant and non-malignant lesions: 24 mm was considered 100% specific and 13.3% sensitive for malignant aetiologies, whereas 7 mm achieved a specificity of 96.7% and a sensitivity of 66.7% for non-malignant lesions.

Among the associated findings, perilesional centrilobular nodules were seen on the CT images in 27 cases, all of which had a non-malignant aetiology ($p<0.05$). Perilesional consolidations were present in 42 cases, 31 (74%) of which were benign lesions (Table 2, $p<0.05$). No other associated features were found to be statistically significant.

Discussion

Pulmonary cavities are often encountered in chest imaging examinations, and their differential diagnosis

Table 2
Associated CT findings in patients with solitary lung cavities.

| Associated findings | |
|---|----------|
| Perilesional centrilobular nodules ^a | n=27 |
| Malignant | 0 (0) |
| Non-malignant | 27 (100) |
| Perilesional consolidation ^a | n=42 |
| Malignant | 11 (26) |
| Non-malignant | 31 (74) |

Data are presented as n (%).

^a $p<0.05$ (malignant versus non-malignant).

includes diverse malignant and non-malignant diseases, caused by multiple processes of acquired or congenital origin.^{6,7} Various pathogenic mechanisms underlie the formation of cavitory lesions: inadequate local blood supply creating central necrosis, infarction from occlusion of regional nutritional vessels, and blockage of a bronchus resulting in necrosis distal to the obstruction.^{8,9}

Many reports have suggested that primary lung abscess, bronchogenic carcinoma, and post-primary tuberculosis are the most common causes of lung cavitation, followed by metastatic tumours, fungal disease, lymphoma, rheumatoid nodules, and granulomatous vasculitides.^{9,10} In adults, the two main causes of cavitory pulmonary lesions are malignancy and infection. In the present cohort, possibly because of geographical and epidemiological aspects, tuberculosis-related lesions were the most prevalent (33 residual and 24 cases of active disease).¹²

Different clinical and radiological parameters may be helpful in assessing solitary pulmonary cavities, such as the duration of symptoms, the lesion's inner aspect (smooth or irregular), and its location. When addressed individually, a considerable overlap between malignant and non-malignant aetiologies tends to occur. Previous authors have described that a combination of solitary cavities with thicker walls and irregular inner contours favoured the diagnosis of primary or metastatic lung cancer.^{8–11} Woodring *et al.*^{4,5} reported that most nodules with a maximum wall thickness >15 mm on CXRs are likely to be malignant in nature, whereas most of those with a maximum wall thickness of ≤4 mm indicate a benign condition. Similarly, other authors had suggested the cut-off points of 15 and 3 mm, respectively.³ Although other studies have conducted similar investigations on CT series of patients that exhibited pulmonary cavities,^{9,10} there is still a lack of defined CT thresholds that effectively aid the evaluation of such lesions at CT. Although the majority of solitary cavities still undergo additional testing (i.e., histological or laboratory sampling), comprehensive CT characterization would avoid unnecessary investigations on benign lesions, as well as eliciting more robust interventions in suspicious lesions.

The results of the present study indicate that maximum wall thickness is among the best criteria for differentiating malignant and non-malignant causes of solitary pulmonary cavities, and that the most reliable limits are 24 and 7 mm, respectively. Not surprisingly, these values contrast with previous thresholds, mainly because of the better spatial resolution and post-acquisition tools provided by CT. The presence of perilesional centrilobular nodules and

perilesional consolidations were found to support this differentiation. Although similar descriptions have not been reported thus far, this finding is secondary to the predominantly infective nature of the non-malignant aetiologies of the solitary lung cavities.

Some limitations of the present study should be noted. First, its retrospective nature prevents the authors from correcting occasional inaccuracies in the databases. Second, the relatively small sample rendered the performance of an analysis of covariance and other desirable statistical tests unfeasible. Third, data were obtained from two tertiary-care centres, in which the populations are likely to differ from the general population in some aspects (e.g., prevalence of immunosuppression etc.).

In summary, chest CT imaging is a valuable tool for the characterization of solitary lung cavities. The maximum wall thickness and the presence of centrilobular nodules or perilesional consolidations are the best criteria in distinguishing malignant and non-malignant underlying conditions. At CT, the most appropriate cut-off values that indicate malignancy and benignity are ≥24 and ≤7 mm, respectively.

References

1. Hansell DM, Bankier AA, MacMahon H, *et al.* Fleischner Society: glossary of terms for thoracic imaging. *Radiology* 2008;**246**:697–722.
2. Gadkowski LB, Stout JE. Cavitory pulmonary disease. *Clin Microbiol Rev* 2008;**21**:305–33.
3. Ryu JH, Swensen SJ. Cystic and cavitory lung diseases: focal and diffuse. *Mayo Clin Proc* 2003;**78**:744–52.
4. Woodring JH, Fried AM, Chuang VP, *et al.* Solitary cavities of the lung: diagnostic implications of cavity wall thickness. *AJR Am J Roentgenol* 1980;**135**:1269–71.
5. Woodring JH, Fried AM. Significance of wall thickness in solitary cavities of the lung: a follow-up study. *AJR Am J Roentgenol* 1983;**140**:473–4.
6. Kim NR, Han J. Pathologic review of cystic and cavitory lung diseases. *Korean J Pathol* 2012;**46**:407–14.
7. Erasmus JJ, Connolly JE, McAdams HP, *et al.* Solitary pulmonary nodules: part I. Morphologic evaluation for differentiation of benign and malignant lesions. *RadioGraphics* 2000;**20**:43–58.
8. Gurney JW. Determining the likelihood of malignancy in solitary pulmonary nodules with Bayesian analysis. *Radiology* 1993;**186**:405–13.
9. Vourtsi A, Gouliamos A, Mouloupoulos L, *et al.* CT appearance of solitary and multiple cystic and cavitory lung lesions. *Eur Radiol* 2001;**11**:612–22.
10. Li B-G, Ma D-Q, Xian Z-Y, *et al.* The value of multislice spiral CT features of cavitory walls in differentiating between peripheral lung cancer cavities and single pulmonary tuberculous thick-walled cavities. *Br J Radiol* 2012;**85**:147–52.
11. Yang Y-W, Kang YA, Lee SH, *et al.* Aetiologies and predictors of pulmonary cavities in South Korea. *Int J Tuberc Lung Dis* 2007;**11**:457–62.
12. Conde MB, Melo FA, Marques AM, *et al.* III Brazilian Thoracic Association Guidelines on tuberculosis. *J Bras Pneumol* 2009;**35**:1018–48.

Computed Tomography Findings of Bronchiectasis in Different Respiratory Phases Correlate with Pulmonary Function Test Data in Adults

Ricardo Holderbaum do Amaral¹ · Carlos S. Nin¹ · Vinicius V. S. de Souza¹ ·
Giordano R. T. Alves¹ · Edson Marchiori¹ · Klaus Irion¹ · Gustavo S. P. Meirelles¹ ·
Bruno Hochhegger¹

Received: 29 December 2016 / Accepted: 9 March 2017
© Springer Science+Business Media New York 2017

Abstract

Objective To investigate bronchiectasis variations in different computed tomography (CT) respiratory phases, and their correlation with pulmonary function test (PFT) data, in adults.

Methods Retrospective data analysis from 63 patients with bronchiectasis according to CT criteria selected from the institution database and for whom PFT data were also available. Bronchiectasis diameter was measured on inspiratory and expiratory phases. Its area and matched airway–vessel ratios in both phases were also calculated. Finally, PFT results were compared with radiological measurements.

Results Bronchiectatic airways were larger on inspiration than on expiration (mean cross-sectional area, 69.44 vs. 40.84 mm²; $p < 0.05$) as were airway–vessel ratios (2.1 vs. 1.4; $p < 0.05$). Cystic bronchiectasis cases showed the least variation in cross-sectional area (48%). Mean predicted values of forced expiratory volume in 1 s (FEV1) and forced vital capacity (FVC) were 81.5 and 77.2%, respectively, in the group in which bronchiectasis could not be identified on expiratory images, and 58.3 and 56.0%, respectively, in the other group ($p < 0.05$). Variation in bronchiectasis area was associated with poorer lung function ($r = 0.32$).

Conclusion Bronchiectasis detection, diameter, and area varied significantly according to CT respiratory phase, with

non-reducible bronchiectasis showing greater lung function impairment.

Keywords Computed tomography · Bronchiectasis · Pulmonary function test · Pulmonary disease · Thorax

Abbreviations

CT Computed tomography
PFT Pulmonary function test
FEV1 Forced expiratory volume in 1 s
FVC Forced vital capacity

Introduction

Bronchiectasis is defined as irreversible localized or diffuse dilation of the airways, usually arising from chronic bronchial inflammation or infection [1, 2]. It is a fairly common progressive respiratory disorder, characterized by high morbidity and reduced quality of life, due mainly to recurrent chest infection and related complications [3]. The pathophysiology of bronchiectasis development is rather complex; the airways dilate in response to an inflammatory reaction, causing damage to the airway walls, which ultimately advances to muscle and cartilage loss [4]. In addition, elevated mucosal activity and impaired mucociliary clearance are contributive factors leading to the chronic obstructive character of bronchiectasis [3].

Computed tomography (CT) plays a central role in the assessment of bronchiectasis [1, 5–11]. Routine high-resolution CT protocols include the acquisition of inspiratory and expiratory images during maximum and minimum voluntary breath holds [12, 13]. While end-inspiratory scans are useful for the evaluation of structural changes, such as bronchial wall thickening, consolidations, and

✉ Ricardo Holderbaum do Amaral
rh.doamaral@gmail.com

¹ LABIMED - Medical Imaging Research Laboratory of Federal University of Health Sciences of Porto Alegre and Santa Casa de Misericórdia de Porto Alegre Hospitals, 295 Professor Annes Dias St., Centro Histórico, Porto Alegre, Rio Grande Do Sul 90020-090, Brazil

bronchiectasis, end-expiratory images are crucial for the detection of air trapping, which is often an early finding in the spectrum of small airway diseases [13–15].

Various efforts have been made to decrease CT radiation exposure in patients with conditions that require multiple follow-up CT examinations, including the development of ultra-low-dose protocols and the acquisition of only expiratory images to monitor airway disease using volumetric analysis [12]. Nevertheless, significant variations have been described in quantifications related to the expiratory CT phase [16].

Parenchymal impairment and airway loss can be evaluated consistently with pulmonary function tests (PFTs) [17–20], but evidence of correlation between CT measurements of bronchiectasis in different pulmonary phases and lung function is limited. We aimed to investigate the variation in the tomographic characteristics of bronchiectasis on end-inspiratory and end-expiratory images in adults, and to evaluate their correlations with PFT findings.

Materials and Methods

With the approval of our institutional ethics review board, we conducted this retrospective study by searching the term “bronchiectasis” in radiology reports from our Radiology Department’s picture archiving and communication system. All chest CT examinations conducted between June 2012 and January 2015 were included in the search. One hundred and ten cases for which end-inspiratory and end-expiratory images were available were initially enrolled.

Twenty-four cases were excluded because no PFT was performed within 3 months of the date of CT acquisition. Other exclusion criteria were tomographic signs of acute infection ($n=10$), unsatisfactory expiratory effort [as defined by previous studies [21] as the absence of anterior bowing of the posterior tracheal wall ($n=7$)], and patient age <18 years ($n=6$).

CT Measurements

Images were acquired using a 64-multidetector CT scanner (LightSpeed VCT; GE Healthcare, Milwaukee, WI, USA). The acquisition protocol included 0.625-mm slice collimation, 0.625-mm reconstruction, 0.4-s gantry rotation interval, 7.5-mm/s table speed, 120 kV, and 200 mA. For end-expiratory CT, the tube current was fixed at 50 mAs. Each study comprised one volumetric end-inspiratory and one end-expiratory scan. All patients received standard instructions for voluntary breath holding before the examination.

Two thoracic radiologists with 5 and 8 years of experience, respectively, who were blinded to clinical information reviewed the scans together at an GE Advantage

workstation (AW 4.4; CA, USA) and collected study data consensually. The diagnosis of bronchiectasis was based on the Fleischner Society’s CT criteria, defined by an increased bronchial diameter compared with the accompanying pulmonary artery (signet ring sign), lack of tapering of bronchi, and identification of bronchi within 1 cm of the pleural surface [8].

Bronchiectasis was then classified according to morphological appearance as cylindrical, varicose, or cystic. Cylindrical bronchiectasis was defined by a uniformly dilated bronchus. The varicose type was characterized by irregularly shaped and variably sized bronchiectasis, with deformities due to local constrictions. The cystic type was defined by dilation that increased progressively toward the lung periphery, with a ballooning appearance [1].

All bronchiectatic changes were measured on inspiratory images that were true transverse sections including the airway wall (external diameter), with selection of a point 2.0 cm distal to the bronchial bifurcation for the assessment, using multiplanar reconstruction. The measurements were repeated at the same level using the identical technique on corresponding expiratory images. Matched airway–vessel ratios were calculated on both inspiratory and expiratory images, by dividing the airway diameter by the accompanying artery diameter measured at the same level [16].

Paired expiratory images were evaluated to assess the maintenance of bronchiectasis criteria. Subjects were grouped according to whether they fulfilled the criteria in both phases. In patients with bronchiectasis at more than one site, the site showing greater reduction on end-expiratory images was selected for analysis. End-expiratory CT images were also used to register the occurrence of air trapping.

Pulmonary Function Tests

Spirometry (Erich Jaeger Laboratories, Friedberg, Germany) was performed in all patients according to the American Thoracic Society requirements [18]. FEV1 and FVC were expressed as predicted percentage values. Inspiratory and expiratory images data were used to examine the correlation of PFT results with bronchiectasis area variability and bronchiectasis criteria maintenance on expiration.

Statistical Analysis

SPSS software (version 14.0 for Windows; SPSS Inc., Chicago, IL, USA) was used for all statistical analyses, with a significance level of $p < 0.05$. Pearson’s product-moment correlation coefficient was used to compare the variation among bronchiectatic areas on CT images with PFT results.

Table 1 Baseline characteristics of the study sample

| Characteristic | Value |
|---|-------------|
| Mean age (years) | 53.2 |
| Disease extension | |
| Unilobar | 34/63 (54%) |
| Multilobar | 29/63 (46%) |
| Bronchiectasis mean area (mm ²) | |
| Inspiration | 69.44 |
| Expiration | 40.84 |

Table 2 Main diagnoses

| Main diagnosis | n (%) |
|-----------------------------------|-----------|
| Idiopathic | 24 (38) |
| Tuberculosis-related | 13 (20.6) |
| Asthma | 6 (9.5) |
| COPD | 5 (7.9) |
| Interstitial lung disease | 4 (6.3) |
| Lung cancer | 2 (3.2) |
| Lung transplant | 2 (3.2) |
| Aspiration | 2 (3.2) |
| Mediastinal cancer (post-actinic) | 2 (3.2) |
| Cystic fibrosis | 1 (1.6) |
| Mycobacteria (non-tuberculosis) | 1 (1.6) |
| Sarcoidosis | 1 (1.6) |
| Total | 63 (100) |

COPD chronic obstructive pulmonary disease

Results

The analysis included data from 63 patients [$n=23$ (36.5%) males] aged 18–80 (mean, 53.2 ± 17.1) years. The baseline characteristics of the study sample are shown in Table 1. The most common diagnoses were tuberculosis sequelae and primary bronchiectasis (Table 2).

A total of 126 matched airway–vessel pairs were measured on inspiratory and expiratory CT images. Affected airways were larger on inspiration than on expiration (mean cross-sectional area, 69.44 vs. 40.84 mm²; $p < 0.05$; Figs. 1, 2, 3). Airway–vessel ratios were also higher in the end-inspiratory phase (2.1 vs. 1.4; $p < 0.05$; Fig. 2). If analyzed in the end-expiratory, 62% of bronchiectasis cases diagnosed by end-inspiratory examination did not meet CT criteria for diagnosis.

Cylindric bronchiectasis was present in 71% of cases, whereas the varicose and cystic forms were found in 17 and 12% of cases, respectively. Less variation in cross-sectional area was observed for cystic bronchiectasis (48%) than for the cylindric (54%) and varicose (59%) types, but this difference was not significant. Air trapping and multiple lobe disease were present in 59 and 54% of cases, respectively. The presence of either finding did not differ according to bronchiectatic area variation on end-inspiratory versus end-expiratory images.

Significant differences in pulmonary function were observed between patients whose bronchiectasis did and did not persist in the end-expiratory phase, as defined by the persistence or not of its diagnostic criteria on the expiratory scan. The first group, of persistent bronchiectasis, had a FEV1 of 58.3 versus 81.5% on the second group ($p < 0.05$).

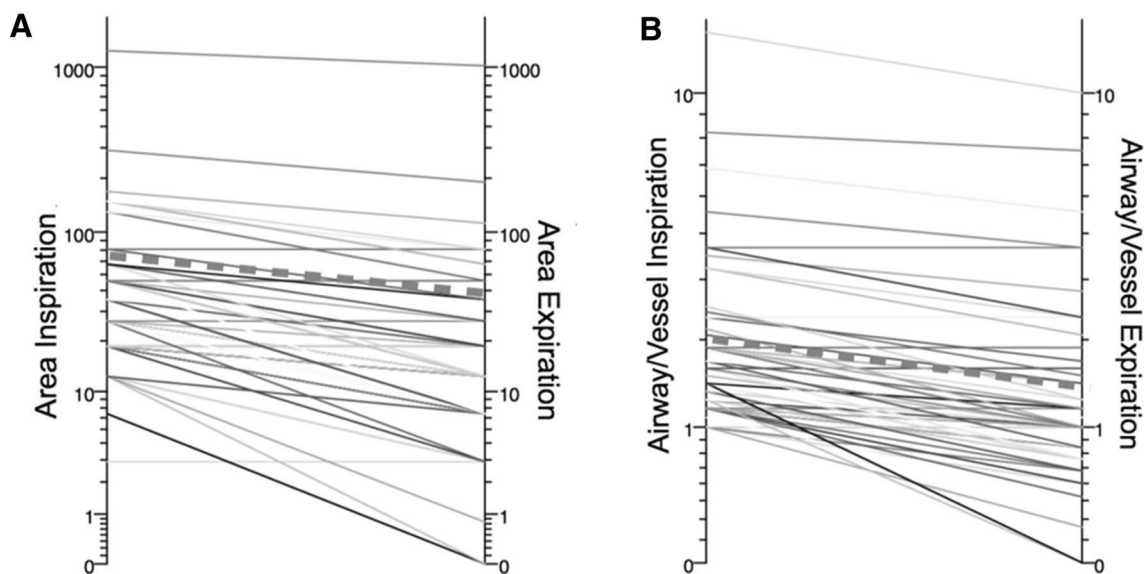


Fig. 1 Bronchiectasis areas (A) and airway–vessel ratios (B) on inspiration and expiration (logarithmic scale). Dashed lines indicate tendency

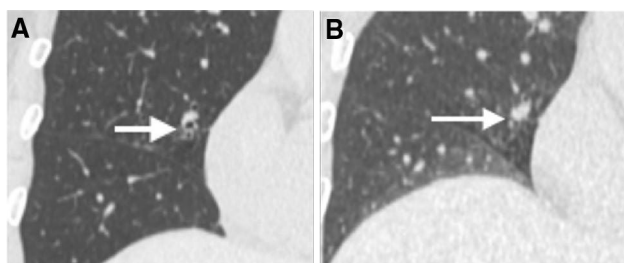


Fig. 2 Fifty-three-year-old woman with asthma. Inspiratory (A) and expiratory (B) coronal views demonstrate loss of the signet ring sign and, consequently, bronchiectasis diagnostic criteria (arrows).

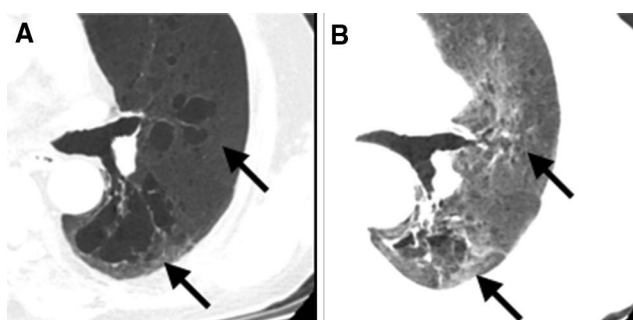


Fig. 3 Twenty-six-year-old man with cystic fibrosis. Inspiratory (A) and expiratory (B) axial views of minimum-intensity projection reconstructions, demonstrating unequivocal bronchiectasis size reduction (arrows)

Additionally, FVC was 56.0% in the first group compared to 77.2% in the latter ($p < 0.05$). Correlation analysis also demonstrated that bronchiectatic area variation on CT was related to poorer pulmonary function ($r = 0.32$).

Discussion

Studies examining whether end-expiratory CT is sufficient to diagnose diseased airways in children have produced discrepant results. Mott et al. [16] found that airways were more dilated on end-inspiratory images than on end-expiratory images, and concluded that expiratory scans were less sensitive for the detection of bronchiectasis, as they led to the underestimation of disease extension in a pediatric population with cystic fibrosis. Conversely, Loeve et al. [12] reported that bronchiectasis scores matched closely, with good agreement between end-inspiratory and end-expiratory CT images for the Brody-II total score and measures of bronchiectasis, airway wall thickening, mucus plugging, and pulmonary opacity in children with cystic fibrosis. In our study, bronchiectasis dimensions and airway–vessel ratios were larger on end-inspiratory images. In

addition, the majority of bronchiectasis cases diagnosed by end-inspiratory examination did not fulfill the CT criteria in the end-expiratory phase. This difference may relate to the examination of data from a more general population, which was not restricted to patients with cystic fibrosis, as in previous studies. Another difference among studies is the mean age of patients (12.6 years in Loeve et al. [12]), which might have influenced the understanding of breath-hold instructions. We believe that adults can better understand and comply with these instructions.

Reid [22] found that the varicose form of bronchiectasis was most common (62%), followed by the cylindric (27%) and cystic (11%) forms. In our study, cylindric bronchiectasis was most prevalent, followed by the varicose and cystic types. This discrepancy may be explained by differences between study populations, as the patients investigated by Reid [22] underwent lobectomy due to bronchiectasis, which is usually indicated for advanced cases, in which varicose and cystic features are more frequent.

We observed that air trapping was present in the majority of cases. This feature is often accompanied by other abnormal findings on high-resolution CT. In a previous study, 64% of 50 subjects with normal pulmonary function had some degree of air trapping [23]. Similarly, we found no significant difference in bronchiectasis reduction between patients with and without air trapping, likely due to the high prevalence of this feature in healthy individuals.

Our results show that poorer pulmonary function was associated with the fulfillment of diagnostic criteria for bronchiectasis on end-expiratory CT. This finding suggests that both end-inspiratory and end-expiratory scans should be acquired routinely, given that the former alone cannot predict bronchiectasis variation, and use of the latter alone might lead examiners to miss a large number of bronchiectatic areas.

One limitation of our study is the heterogeneity of the sample, which could limit the reproducibility of our results. In addition, the assessment of bronchiectasis can be affected by several variables; even with the use of high-resolution protocols, the low dose applied for expiratory scans could influence the measurements. The reduction of radiation dose increases the variability in airway change assessment, notably in smaller airways; this effect is more pronounced at doses ≤ 20 mAs [24].

Conclusions

Bronchiectasis presence, diameter, and area varied according to respiratory phase on CT scans. Our results demonstrate that low-dose end-expiratory scans are not sufficient for the evaluation of bronchiectasis. Moreover, persistent bronchiectasis on end-expiratory CT is associated with

poorer pulmonary function. These findings can have important implications for the future comprehension of the dynamic characteristics of bronchiectasis as markers of pulmonary function impairment.

Compliance with Ethical Standards

Conflict of interest The authors declare no conflict of interest.

Ethical Approval All procedures performed in this study were in accordance with the ethical standards of the institutional and national research committee and with the 1964 Helsinki declaration and its later amendments or comparable ethical standards.

Informed Consent Informed consent was waived according to the institution ethics committee resolution.

References

- Barker AF (2002) Bronchiectasis. *N Engl J Med* 346:1383–1393
- King P, Holdsworth S, Freezer N, Holmes P (2006) Bronchiectasis. *Intern Med J* 36(11):729–37
- Milliron B, Henry TS, Veeraraghavan S, Little BP (2015) Bronchiectasis: mechanisms and imaging clues of associated common and uncommon diseases. *Radiographics* 35(4):1011–30
- Cole PJ (1986) Inflammation: a two-edged sword—the model of bronchiectasis. *Eur J Respir Dis Suppl* 147:6–15
- Pasteur MC, Bilton D, Hill AT, British Thoracic Society Bronchiectasis non-CF Guideline Group (2010) British Thoracic Society guideline for non-CF bronchiectasis. *Thorax* 65(Suppl. 1):i1–i58
- Diederich S, Roos N, Thomas M, Peters PE (1996) Diagnostic imaging in bronchiectasis: value of CT and HRCT. *Radiologe* 36:550–559 (in German)
- Hansell DM (1998) Bronchiectasis. *Radiol Clin North Am* 36:107–128
- Hansell DM, Bankier AA, MacMahon H, McLoud TC, Müller NL, Remy J (2008) Fleischner Society: glossary of terms for thoracic imaging. *Radiology* 246(3):697–722. doi:10.1148/radiol.2462070712
- Lynch DA, Newell JD, Tschomper BA et al (1993) Uncomplicated asthma in adults: comparison of CT appearance of the lungs in asthmatic and healthy subjects. *Radiology* 188:829–833
- Dodd JD, Souza CA, Muller NL (2006) Conventional high-resolution CT versus helical high-resolution MDCT in the detection of bronchiectasis. *AJR Am J Roentgenol* 187:414–420
- Grenier P, Maurice F, Musset D et al (1986) Bronchiectasis: assessment by thin-section CT. *Radiology* 161:95–99
- Loeve M, Lequin MH, deBruijne et al (2009) Cystic fibrosis: are volumetric ultra-low-dose expiratory CT scans sufficient for monitoring related lung disease? *Radiology* 253:223–229
- Tiddens HA, de Jong PA (2006) Update on the application of chest computed tomography scanning to cystic fibrosis. *Curr Opin Pulm Med* 12:433–439
- Martinez TM, Llapur CJ, Williams TH et al (2005) High-resolution computed tomography imaging of airway disease in infants with cystic fibrosis. *Am J Respir Crit Care Med* 172:1133–1138
- Bonnel AS, Song SM, Kesavaraju K et al (2004) Quantitative air-trapping analysis in children with mild cystic fibrosis lung disease. *Pediatr Pulmonol* 38:396–405
- Mott LS, Graniel KG, Park J et al (2013) Assessment of early bronchiectasis in young children with cystic fibrosis is dependent on lung volume. *Chest* 144:1193–1198
- Johns DP, Walters JA, Walters EH (2014) Diagnosis and early detection of COPD using spirometry. *J Thorac Dis* 6(11):1557–1569
- Miller MR, Crapo R, Hankinson J et al (2005) Standardisation of spirometry. *ATS/ERS task force: standardisation of lung function testing. Eur Respir J* 26:319–338
- da Silva LCC, Rubin AS, da Silva LMC, Fernandes JC (2005) Spirometry in medical practice. *Rev AMRIGS* 49(3):183–194
- Timmins SC, Diba C, Farrow CE et al (2012) The relationship between airflow obstruction, emphysema extent, and small airways function in COPD. *Chest* 142:312–319
- Chung JH, Kanne JP, Gilman MD (2011) CT of diffuse tracheal disease. *AJR Am J Roentgenol* 196:W240–W246. doi:10.2214/AJR.09.4146
- Reid LM (1950) Reduction in bronchial subdivision in bronchiectasis. *Thorax* 5(3):233–247
- Tanaka N, Matsumoto T, Miura G et al (2003) Air trapping at CT: high prevalence in asymptomatic subjects with normal pulmonary function. *Radiology* 227:776–785
- de Jong PA, Long FR, Nakano Y et al (2006 Oct) Computed tomography dose and variability of airway dimension measurements: how low can we go? *Pediatr Radiol* 36(10):1043–1047



Chest CT findings in patients with dysphagia and aspiration: a systematic review

Betina Scheeren¹, Erissandra Gomes², Giordano Alves³, Edson Marchiori³, Bruno Hochhegger¹

1. Programa de Pós-Graduação em Medicina, Universidade Federal de Ciências da Saúde de Porto Alegre, Porto Alegre (RS) Brasil.
2. Universidade Federal do Rio Grande do Sul, Porto Alegre (RS) Brasil.
3. Universidade Federal do Rio de Janeiro, Rio de Janeiro (RJ) Brasil.

Submitted: 31 August 2016.

Accepted: 4 May 2017.

Study carried out at the Universidade Federal de Ciências da Saúde de Porto Alegre, Universidade Federal do Rio Grande do Sul, Porto Alegre (RS) e Universidade Federal do Rio de Janeiro, Rio de Janeiro (RJ) Brasil.

ABSTRACT

The objective of this systematic review was to characterize chest CT findings in patients with dysphagia and pulmonary aspiration, identifying the characteristics and the methods used. The studies were selected from among those indexed in the Brazilian Virtual Library of Health, LILACS, *Índice Bibliográfico Español de Ciencias de la Salud*, Medline, Cochrane Library, SciELO, and PubMed databases. The search was carried out between June and July of 2016. Five articles were included and reviewed, all of them carried out in the last five years, published in English, and coming from different countries. The sample size in the selected studies ranged from 43 to 56 patients, with a predominance of adult and elderly subjects. The tomographic findings in patients with dysphagia-related aspiration were varied, including bronchiectasis, bronchial wall thickening, pulmonary nodules, consolidations, pleural effusion, ground-glass attenuation, atelectasis, septal thickening, fibrosis, and air trapping. Evidence suggests that chest CT findings in patients with aspiration are diverse. In this review, it was not possible to establish a consensus that could characterize a pattern of pulmonary aspiration in patients with dysphagia, further studies of the topic being needed.

Keywords: Respiratory aspiration; Tomography, X-ray computed; Lung.

INTRODUCTION

The epidemiology of aspiration syndromes is not well described in the literature because of the lack of specificity and sensitivity markers; however, the literature indicates that 5-15% of the cases of community-acquired pneumonia are due to aspiration.⁽¹⁾ Lung injury caused by aspiration of saliva or food particles can often result from dysphagia.^(2,3) Dysphagia can be of neurogenic, mechanical, or psychogenic origin and manifests itself through a series of signs and symptoms, such as cough, choking, and pharyngeal globus, being a major risk factor for malnutrition, dehydration, and aspiration pneumonia.⁽⁴⁻⁶⁾

Evaluation of dysphagia involves clinical evaluation and speech pathology assessment, as well as ancillary tests, such as videofluoroscopic swallowing study (VFSS) and fiberoptic endoscopic evaluation of swallowing (FEES), which serve to aid in the diagnosis of swallowing disorders, such as aspiration.⁽⁷⁻⁹⁾ In contrast, chest CT is used to evaluate pulmonary lesions, being of great importance in the diagnosis of aspiration disorders, since pulmonary symptoms can be the first manifestation of aspiration.⁽¹⁰⁾

Imaging findings of aspiration are numerous and usually nonspecific, pulmonary infection being the most serious complication of aspiration.^(10,11) Therefore, knowledge about the different types of pulmonary aspiration is important for drawing correlations between the clinical information and the main CT findings, including diffuse aspiration bronchiolitis, aspiration pneumonitis, aspiration

pneumonia, foreign body aspiration, and exogenous lipid pneumonia.⁽¹¹⁾ By specifically detailing the imaging findings of aspiration pneumonia, segmental or lobar airspace consolidation can be observed, which may or may not be associated with pleural effusion.⁽¹¹⁾

Knowledge about the CT findings of aspiration is essential for establishing the diagnosis of aspiration disorders and for attempting to prevent lung injury. Here, we aimed to perform a systematic literature review of chest CT findings that characterize pulmonary aspiration in patients with dysphagia, identifying the characteristics and the methods used.

METHODS

Research strategies

This systematic review followed the recommendations of the latest version of the Cochrane Handbook for Systematic Reviews of Interventions,⁽¹²⁾ which involve formulating the research question, finding and selecting scientific articles, and critically assessing the selected articles. The research question used was: "What chest CT image findings are diagnostic markers of aspiration in patients with dysphagia?" The review was developed by three researchers, two of whom searched for articles independently and blindly and one of whom was assigned as a reviewer, being consulted in cases of uncertainty so as to establish agreement. All of the researchers involved—two speech-language pathologists and one

Correspondence to:

Betina Scheeren. Rua Teixeira Mendes, 187, apto. 301, Chácara das Pedras, CEP 90050-170, Porto Alegre, RS, Brasil.
Tel.: 55 51 9725-8226. E-mail: betinascheeren@hotmail.com
Financial support: None.

radiologist who works in thoracic radiology—have over 10 years of clinical and practical experience in the study area. Studies were selected by using the following search terms: “*pneumonia aspirativa*” and “aspiration pneumonia”; “*aspiração*” and “aspiration”; “*pulmonar*” and “pulmonary”; and “*tomografia computadorizada*” and “computed tomography”. These search terms were obtained from DeCS and MeSH and were used to search the Brazilian Virtual Library of Health, LILACS, *Índice Bibliográfico Español de Ciencias de la Salud*, Medline, Cochrane Library, SciELO, and PubMed online databases. The search was carried out between June and July of 2016, on the basis of the intersection of the chosen search terms.

Selection criterion

Studies in humans, written in English, Portuguese, or Spanish, regardless of the publication year, and whose title, abstract, or body of text contained any of the search terms chosen for this review were selected. Studies mentioning aspiration of food particles into the upper digestive tract and chest CT were included. Repeated studies were excluded, as were studies whose abstracts or full texts were not found in the databases consulted, review articles, dissertations, theses, case studies, and studies in which the underlying disease was tuberculosis. No search filters were applied. The article selection process is described as a flowchart in Figure 1, as recommended in the PRISMA statement.⁽¹³⁾

Data analysis

After the abstracts of the studies found were selected, the full texts of the articles were retrieved. After full text reading, the following data were extracted: names of the authors; year of publication; country where the study was conducted; study design; study subjects;

sample size; diagnostic tests used; underlying disease; and chest CT findings, which were defined in accordance with the glossary of terms for thoracic imaging from the Fleischner Society.⁽¹⁴⁾

RESULTS

Five articles were selected for inclusion in the present systematic review, all of them carried out in the last 5 years, published in English, and coming from different countries (Italy, USA, Japan, China, and Brazil; Table 1). Sample sizes in the studies ranged from 43 to 56 patients, the predominant population being adults (19-59 years) and elderly subjects (≥ 60 years).

Most of the studies evaluated in this review had a retrospective, cross-sectional design.⁽¹⁵⁻¹⁸⁾ The sample characteristics varied. The patients studied had laryngeal cancer,⁽¹⁵⁾ acute pneumonia associated with dysphagia,⁽¹⁶⁾ or chronic aspiration,^(17,18) and a study of healthy subjects assessed the presence or absence of aspiration.⁽¹⁹⁾ The diagnostic tests used in the studies were VFSS,^(15,16,18) FEES,^(15,19) bronchoscopy,⁽¹⁷⁾ HRCT,⁽¹⁵⁾ and conventional CT.⁽¹⁶⁻¹⁹⁾

The CT findings in patients with dysphagia-related aspiration were varied, including emphysema,⁽¹⁵⁾ bronchiectasis,^(15,16,19) bronchial wall thickening,^(15,16,18,19) nodules,^(15,16,18) tree-in-bud pattern,^(15,19) consolidation,⁽¹⁵⁻¹⁸⁾ pleural effusion,⁽¹⁵⁻¹⁷⁾ ground-glass attenuation,^(15,16,18) septal thickening,^(15,16) cavitory lesions,⁽¹⁵⁾ lymph nodes,⁽¹⁵⁾ atelectasis,⁽¹⁶⁻¹⁸⁾ bronchiolectasis,^(18,19) fibrosis,⁽¹⁹⁾ and air trapping.^(18,19) One of the studies demonstrated a higher frequency of findings in the right lung,⁽¹⁷⁾ and two found changes that were more prevalent in lower lung zones.^(16,18) In the study by Simonelli et al.,⁽¹⁵⁾ it was not possible to describe the proportion of findings, because they

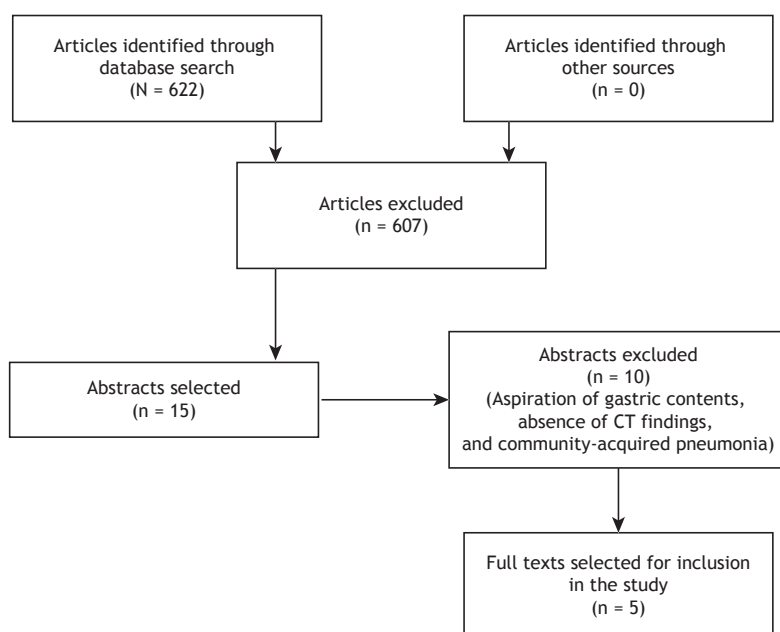


Figure 1. Article selection flowchart of the present systematic review.

Table 1. Characteristics of the selected articles.

| Study | Year | Country | Population | Study design | Sample size and characteristics | Diagnostic tests used | Chest CT findings |
|----------------------------------|------|---------|------------|--------------|--|----------------------------------|--|
| Simonelli et al. ⁽¹⁵⁾ | 2010 | Italy | A/G | RS | 45 patients after partial laryngectomy (mean age = 67 years; 92.2% men) and 45 controls (patients with COPD and normal swallowing) | FEES, VFSS, and HRCT | Emphysema; bronchiectasis; bronchial wall thickening; pulmonary nodules or cysts; tree-in-bud pattern; consolidation; pleural effusion; septal thickening; cavitory lesions; and lymph nodes |
| Komiya et al. ⁽¹⁶⁾ | 2013 | Japan | G | RS | 53 patients admitted to the hospital with pneumonia and dysphagia (mean age = 84 years; 66% of men) | VFSS and conventional CT | Centrilobular nodules (74%); ground-glass attenuation (74%); peribronchovascular thickening (42%); airspace consolidation (34%); atelectasis (17%); septal thickening (13%); pleural effusion (13%); and traction bronchiectasis (2%) |
| Lin et al. ⁽¹⁷⁾ | 2014 | China | A/G | RS | 43 patients with aspiration (G = 17; A = 26; mean age = 56 years; 70% of men) | Bronchoscopy and conventional CT | ^a Consolidation (93%/92%); atelectasis (14%/23%); high-density airway lesion (29%/4%); pleural effusion (0%/8%); foreign body – food particles – (21%/35%): left lung (35%/31%) and right lung (65%/69%) |
| Butler et al. ⁽¹⁹⁾ | 2014 | USA | G | PS | 50 healthy patients divided into 2 groups: aspirators (n = 25; mean age = 77 years; 15 women) and non-aspirators (n = 25; mean age = 76 years; 16 men) | FEES and conventional CT | ^b Bronchiectasis (2%/8%); bronchiolectasis (10%/6%); bronchial wall thickening (22%/12%); parenchymal band (8%/4%); fibrosis (16%/16%); air trapping (20%/26%); intraluminal airway debris (6%/8%); and tree-in-bud pattern (6%/4%) p > 0.05 for all |
| Scheeren et al. ⁽¹⁸⁾ | 2016 | Brazil | A/G | RS | 56 patients divided into 2 groups: non-aspirators and aspirators (n = 28 in each group; mean age = 65 years; 29 men) | VFSS and conventional CT | ^b Bronchial wall thickening (54%/53%)*; bronchiolectasis (15%/0%)**; centrilobular nodules (16%/4%)**; ground-glass attenuation (4%/0%)**; atelectasis (18%/2%)**; consolidation (6%/0%)**; and air trapping (54%/53%)* *p = 0.208; **p < 0.001 |

A: adult; G: geriatric; RS: retrospective study; FEES: fiberoptic endoscopic evaluation of swallowing; VFSS: videofluoroscopic swallowing study; and PS: prospective study. ^aG patients/A patients. ^bAspirators/non-aspirators.

were reported by degree of aspiration. It is of note that, in two studies, aspirators and non-aspirators were compared.^(18,19)

DISCUSSION

The selection, reading, and analysis of articles revealed that there have been few studies attempting to define a pattern of chest CT findings related to dysphagia-related pulmonary aspiration. The five articles selected in the present review were published in the last 5 years, which may explain the recent concern over early

identification of patients with dysphagia who aspirate and over strategies that may intervene in the etiology. One study found a significant correlation between the degree of dysphagia and the relative risk of pneumonia, demonstrating that patients with tracheal aspiration are ten times more likely to develop pneumonia than individuals with normal swallowing.⁽²⁰⁾

The most serious complication associated with aspiration in patients with dysphagia is pulmonary infection.⁽¹⁰⁾ Studies indicate aspiration pneumonia as a cause of community-acquired pneumonia.^(21,22) It is important to note that, in addition to the respiratory

complication, the swallowing disorder is a risk factor for malnutrition and functional decline.⁽²³⁾ Aspiration pneumonia is the leading cause of death in patients with dysphagia, a condition that affects 300,000-600,000 people per year in the USA.⁽¹⁾

Simonelli et al.⁽¹⁵⁾ addressed the relationship between dysphagia and aspiration in laryngectomized patients, compared with a control group of patients with COPD, and found no significant differences in radiological findings between the groups. It is currently known that patients with COPD have dysphagia symptoms related to airway protection because of changes in the breathing pattern and in the coordination of swallowing and breathing, leading to a greater likelihood of developing pneumonia.⁽²⁴⁾ It should be noted here that, of the 116 patients selected for the study,⁽¹⁵⁾ only 45 had aspiration by VFSS and then underwent chest CT scans to assess the radiological manifestations of aspiration. In the two groups, the findings with the highest incidence rates were bronchial wall thickness, bronchiectasis, nodules, emphysema, consolidation, and septal thickening, with rates varying according to the degree of aspiration in the study group.

In the study by Komiya et al.,⁽¹⁶⁾ the pulmonary CT findings were described in patients with an acute condition, that is, presenting with pneumonia at hospital admission, and dysphagia was confirmed by VFSS. The most frequent chest CT findings were airspace consolidation, ground-glass attenuation, centrilobular nodules, and peribronchovascular thickening. Pulmonary opacities predominated in lower or diffuse areas of the lung and were distributed posteriorly. The authors did not enroll a control group (without dysphagia/aspiration). In the study,⁽¹⁶⁾ there was a predominance of elderly patients (geriatric population), among whom the risk of aspiration of oropharyngeal secretions and food particles is increased.⁽²⁵⁾ There is evidence in the literature that the frequency of dysphagia is higher in the elderly, and aspiration is an important etiologic factor leading to pneumonia in this population.⁽²⁶⁾

One of the studies analyzed in the present review did not use ancillary tests to assess swallowing or detect dysphagia; the presence of acute aspiration of large food particles was identified solely by bronchoscopy.⁽¹⁷⁾ The most prevalent chest CT findings in the study were consolidation, atelectasis, and high-density airway lesion, predominantly in the right lung and lower lobe.⁽¹⁷⁾

In the study by Butler et al.⁽¹⁹⁾ aspiration status was prospectively evaluated by administering liquid boluses, and other bolus consistencies were not used, which could result in an increased number of pulmonary imaging findings. In addition, the authors did not use VFSS, which is considered the gold standard for detecting aspiration, choosing to use FEES. FEES is an exam that is performed with a nasal endoscope and allows direct observation and evaluation of laryngopharyngeal structures, as well as of swallowing; however, aspiration can only be observed after the swallow, through visualization of the presence of dyed food particles in the trachea.⁽²⁷⁾ The authors did not find significant differences in the radiological pattern between the case and control groups, the findings being bronchiectasis, bronchiolectasis, bronchial wall thickening, air trapping, and fibrosis.⁽¹⁹⁾

The most recent study addressing pulmonary findings in patients with chronic aspiration⁽¹⁸⁾ included patients with and without aspiration diagnosed by VFSS who underwent chest CT. A comparison of the two groups revealed that the patients with aspiration had a higher frequency of changes such as atelectasis, centrilobular nodules, bronchiolectasis, consolidation, and ground-glass attenuation. Bronchial wall thickening and air trapping were the most prevalent findings in both groups; however, no significant differences were demonstrated. In addition, the authors reported that the findings were more prevalently distributed in lower lung zones. Figures 2 and 3 exemplify some of the CT findings described.

One of the limitations of the present systematic review was the lack of articles published on the subject,

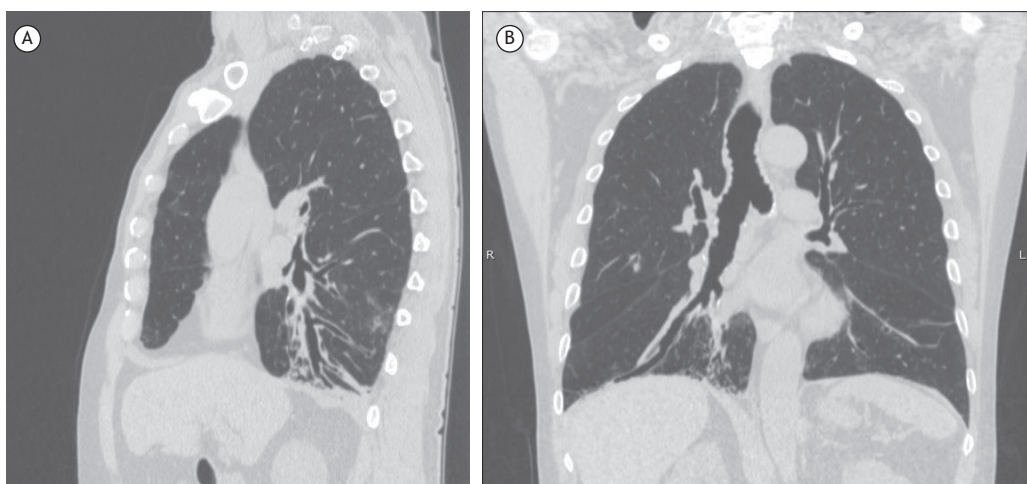


Figure 2. In A, sagittal chest CT scan demonstrating bronchiolectasis, atelectasis, and areas of ground-glass opacity in the lower lobes. In B, coronal chest CT scan demonstrating better visualization of bronchiolectasis in the right lower lobe.

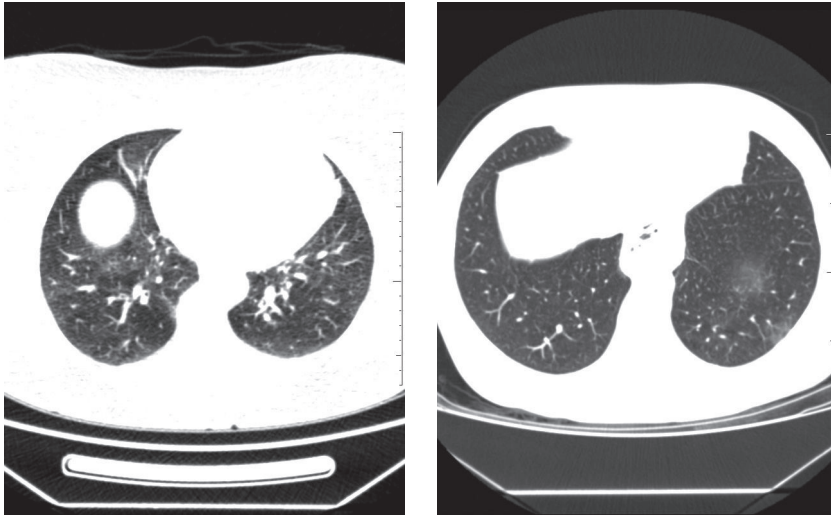


Figure 3. Axial chest CT scans showing areas of ground-glass attenuation in the left lower lobe.

as well as the varied sample characteristics. In this review, it was not possible to establish a consensus that could characterize a pattern of pulmonary aspiration in patients with dysphagia, and further studies on the subject are needed. Evidence suggests





that chest CT findings in patients with aspiration are diverse; however, the articles mentioning the location of pulmonary findings detected that the findings were more prevalently distributed in the right lung and in lower lung zones.

REFERENCES

- Marik PE. Aspiration pneumonia and aspiration pneumonia. *N Engl J Med.* 2001;344(9):665-71. <https://doi.org/10.1056/NEJM200103013440908>
- Makharia GK, Seith A, Sharma SK, Sinha A, Goswami P, Aggarwal A, et al. Structural and functional abnormalities in lungs in patients with achalasia. *Neurogastroenterol Motil.* 2009;21(6):603-8, e20.
- Oue K, Mukaisho K, Higo T, Araki Y, Nishikawa M, Hattori T, et al. Histological examination of the relationship between respiratory disorders and repetitive microaspiration using a rat gastro-duodenal contents reflux model. *Exp Anim.* 2011;60(2):141-50. <https://doi.org/10.1538/expanim.60.141>
- Matsuo K, Palmer JB. Anatomy and physiology of feeding and swallowing: normal and abnormal. *Phys Med Rehabil Clin N Am.* 2008;19(4):691-707, vii. <https://doi.org/10.1016/j.pmr.2008.06.001>
- Karkos PD, Papouliakos S, Karkos CD, Theochari EG. Current evaluation of the dysphagic patient. *Hippokratia.* 2009;13(3):141-6.
- Carucci LR, Turner MA. Dysphagia revisited: common and unusual causes. *Radiographics.* 2015;35(1):105-22. <https://doi.org/10.1148/rg.351130150>
- Martin-Harris B, Jones B. The videofluorographic swallowing study. *Phys Med Rehabil Clin N Am.* 2008;19(4):769-85, viii. <https://doi.org/10.1016/j.pmr.2008.06.004>
- Kelly AM, Drinnan MJ, Leslie P. Assessing penetration and aspiration: how do videofluoroscopy and fiberoptic endoscopic evaluation of swallowing compare? *Laryngoscope.* 2007;117(10):1723-7. <https://doi.org/10.1097/MLG.0b013e318123ee6a>
- Bours GJ, Speyer R, Lemmens J, Limburg M, de Wit R. Bedside screening tests vs. videofluoroscopy or fibreoptic endoscopic evaluation of swallowing to detect dysphagia in patients with neurological disorders: systematic review. *J Adv Nurs.* 2009;65(3):477-93. <https://doi.org/10.1111/j.1365-2648.2008.04915.x>
- Franquet T, Giménez A, Rosón N, Torrubia S, Sabaté JM, Pérez C. Aspiration diseases: findings, pitfalls, and differential diagnosis. *Radiographics.* 2000;20(3):673-85. <https://doi.org/10.1148/radiographics.20.3.g00ma01673>
- Prather AD, Smith TR, Poletto DM, Tavora F, Chung JH, Nallamshetty L, et al. Aspiration-related lung diseases. *J Thorac Imaging.* 2014;29(5):304-9. <https://doi.org/10.1097/RTI.0000000000000092>
- Higgins JPT, Green S, editors. *Cochrane Handbook for Systematic Reviews of Interventions* Version 5.1.0 [updated 2011 Mar]. The Cochrane Collaboration; 2011. Available from: <http://www.cochrane-handbook.org>
- Moher D, Liberati A, Tetzlaff J, Altman DG; PRISMA Group. Preferred reporting items for systematic reviews and meta-analyses: the PRISMA statement. *Int J Surg.* 2010;8(5):336-41. Erratum in: *Int J Surg.* 2010;8(8):658. <https://doi.org/10.1016/j.ijsu.2010.02.007>
- Hansell DM, Bankier AA, MacMahon H, McLoud TC, Müller NL, Remy J. Fleischner Society: glossary of terms for thoracic imaging. *Radiology.* 2008;246(3):697-722. <https://doi.org/10.1148/radiol.2462070712>
- Simonelli M, Ruoppolo G, de Vincentis M, Di Mario M, Calcagno P, Vitiello C, et al. Swallowing ability and chronic aspiration after supracricoid partial laryngectomy. *Otolaryngol Head Neck Surg.* 2010;142(6):873-8. <https://doi.org/10.1016/j.otohns.2010.01.035>
- Komiya K, Ishii H, Umeki K, Kawamura T, Okada F, Okabe E, et al. Computed tomography findings of aspiration pneumonia in 53 patients. *Geriatr Gerontol Int.* 2013;13(3):580-5. <https://doi.org/10.1111/j.1447-0594.2012.00940.x>
- Lin L, Lv L, Wang Y, Zha X, Tang F, Liu X. The clinical features of foreign body aspiration into the lower airway in geriatric patients. *Clin Interv Aging.* 2014;9:1613-8.
- Scheeren B, Marchiori E, Pereira J, Meirelles G, Alves G, Hochhegger B. Pulmonary computed tomography findings in patients with chronic aspiration detected by videofluoroscopic swallowing study. *Br J Radiol.* 2016;(1063):20160004. <https://doi.org/10.1259/bjr.20160004>
- Butler SG, Clark H, Baginski SG, Todd JT, Lintzenich C, Leng X. Computed tomography pulmonary findings in healthy older adult aspirators versus nonaspirators. *Laryngoscope.* 2014;124(2):494-7. <https://doi.org/10.1002/lary.24284>
- Pikus L, Levine MS, Yang YX, Rubesin SE, Katzka DA, Laufer I, et al. Videofluoroscopic studies of swallowing dysfunction and the relative risk of pneumonia. *AJR Am J Roentgenol.* 2003;180(6):1613-6. <https://doi.org/10.2214/ajr.180.6.1801613>
- Torres A, Serra-Batlles J, Ferrer A, Jiménez P, Celis R, Cobo E, et al. Severe community-acquired pneumonia. Epidemiology and prognostic factors. *Am Rev Respir Dis.* 1991;144(2):312-8. <https://doi.org/10.1164/ajrccm/144.2.312>
- Moine P, Vercken JB, Chevret S, Chastang C, Gajdos P. Severe community-acquired pneumonia. Etiology, epidemiology, and prognosis factors. French Study Group for Community-Acquired Pneumonia in the Intensive Care Unit. *Chest.* 1994;105(5):1487-95. <https://doi.org/10.1378/chest.105.5.1487>

23. Serra-Prat M, Palomera M, Gomez C, Sar-Shalom D, Saiz A, Montoya JG, et al. Oropharyngeal dysphagia as a risk factor for malnutrition and lower respiratory tract infection in independently living older persons: a population-based prospective study. *Age Ageing*. 2012;41(3):376-81. <https://doi.org/10.1093/ageing/afs006>
24. Chaves Rde D, Carvalho CR, Cukier A, Stelmach R, Andrade CR. Symptoms of dysphagia in patients with COPD. *J Bras Pneumol*. 2011;37(2):176-83.
25. Augusto DK, Miranda LF, Cruz CE, Pedroso ER. Comparative study of elderly inpatients clinically diagnosed with community-acquired pneumonia, with or without radiological confirmation. *J Bras Pneumol*. 2007;33(3):270-4. <https://doi.org/10.1590/S1806-37132007000300007>
26. Marik PE, Kaplan D. Aspiration pneumonia and dysphagia in the elderly. *Chest*. 2003;124(1):328-36. <https://doi.org/10.1378/chest.124.1.328>
27. Leder SB, Murray JT. Fiberoptic endoscopic evaluation of swallowing. *Phys Med Rehabil Clin N Am*. 2008;19(4):787-801, viii-ix. <https://doi.org/10.1016/j.pmr.2008.05.003>

“Pulmonary Vein Sign” for Pulmonary Embolism Diagnosis in Computed Tomography Angiography

Luciana Volpon Soares Souza¹ · Matheus Zanon^{2,3}  · Arthur Soares Souza¹  · Klaus Irion⁴  · Diana Penha⁴ · Giordano Rafael Tronco Alves⁵ · Edson Marchiori⁵  · Bruno Hochhegger^{2,3}

Received: 21 May 2017 / Accepted: 11 September 2017
© Springer Science+Business Media, LLC 2017

Abstract

Purposes Considering that pulmonary arterial obstruction decreases venous flow, we hypothesized that filling defects in pulmonary veins can be identified in areas adjacent to pulmonary embolism (PE). This sign was named the “pulmonary vein sign” (PVS), and we evaluated its prevalence and performance for PE diagnosis in computed tomography pulmonary angiography (CTPA).

Methods This retrospective study enrolled consecutive patients with clinical suspicion of PE who underwent CTPA scan. The PVS was defined by the following criteria: (a) presence of a homogeneous filling defect of at least 2 cm in a pulmonary vein; (b) attenuation of the left atrium > 160 Hounsfield units. Using the cases that presented PE on CTPA as reference, sensitivity, specificity, and positive and negative predictive values were calculated for PVS.

Results In total, 119 patients (73 female; mean age, 62 years) were included in this study. PE was diagnosed in 44 (35.8%) patients. The PVS was present in 16 out of 44 patients with PE. Sensitivity was 36.36% (95% confidence interval (CI) 22.83–52.26%); specificity, 98.67% (95% CI 91.79–99.93%); positive predictive value, 94.12% (95% CI 69.24–99.69%); negative predictive value, 72.55% (95% CI 62.67–80.70%). The Kappa index for the PVS was good (0.801; 95% CI 0.645–0.957). PVS was correlated with lobar and segmental pulmonary embolism ($p < 0.01$).

Conclusion Despite a low sensitivity, presence of the pulmonary vein sign was highly specific for PE, with a good agreement between readers. This sign could contribute for PE diagnosis on CTPA studies.

Keywords Pulmonary embolism · Computed tomography pulmonary angiography · Pulmonary vein sign

✉ Matheus Zanon
mhgzanon@hotmail.com

Luciana Volpon Soares Souza
luvolpon@gmail.com

Arthur Soares Souza
asouzajr@gmail.com

Klaus Irion
klaus.irion@btinternet.com

Diana Penha
dianapenha@gmail.com

Giordano Rafael Tronco Alves
grtalves@gmail.com

Edson Marchiori
edmarchiori@gmail.com

Bruno Hochhegger
brunohochhegger@gmail.com

¹ Rio Preto Radiodiagnostic Institute - Rua Cila, 3033, Sao Jose Do Rio Preto 15015-800, Brazil

² LABIMED – Medical Imaging Research Lab, Department of Radiology, Pavilhão Pereira Filho Hospital, Irmandade Santa Casa de Misericórdia of Porto Alegre - Av. Independência, 75, Porto Alegre 90020-160, Brazil

³ Department of Diagnostic Methods, Federal University of Health Sciences of Porto Alegre - R. Sarmiento Leite, 245, Porto Alegre 90050-170, Brazil

⁴ Department of Radiology, Liverpool Heart and Chest Hospital, NHS Foundation Trust - Thomas Drive, Broadgreen, Liverpool L143PE, UK

⁵ Department of Radiology, Federal University of Rio de Janeiro Medical School - Av. Carlos Chagas Filho, 373, Rio De Janeiro 21941-902, Brazil

Introduction

Pulmonary embolism (PE) is a relatively common medical emergency. Characterized by partial or total obstruction of pulmonary arteries usually due to a thrombus, PE results in a sudden reduction or cessation of perfusion in the corresponding zone [1]. The most common clinical presentations are shortness of breath and chest pain, but cough, fever, hemoptysis, and syncope can occur [2]. As these symptoms are non-specific, imaging plays a fundamental role in the diagnosis of PE [3].

Computed tomographic pulmonary angiography (CTPA) is one of the most accurate imaging modalities for PE diagnosis [4, 5]. The diagnostic criteria for acute PE include an arterial occlusion with failure to enhance the entire lumen due to a filling defect, and the artery could be enlarged compared to adjacent patent vessels. Some ancillary signs have been used for indirect diagnosis of PE [6, 7]. These include regional oligemia (Westermarck sign); peripheral, pleural-based, wedge-shaped area of increased opacity (Hampton hump); and prominence of the central pulmonary artery (Fleischner sign) [8]. Determination of the diagnostic value of these ancillary signs may permit more reliable diagnoses when emboli are suboptimally visualized, or they can suggest the diagnosis when PE is not suspected.

The main hemodynamic consequence of PE is an acute mechanical reduction of the pulmonary vascular cross-sectional area, which results in sudden increase in pulmonary vascular resistance and pulmonary arterial pressure, intensifying right ventricular work [9, 10]. In addition, all PE cases show an ipsilateral reduction in venous drainage [9, 10]. Based on the theory that the pulmonary arterial obstruction decreases venous flow, our hypothesis is that we can identify filling defects in the pulmonary veins in areas adjacent to the PE. This sign was named the “pulmonary vein sign” (PVS). The aim of this study was to evaluate the prevalence and performance of this sign to diagnose PE in CTPA.

Materials and Methods

Patient Selection

This study was performed with the approval of our Institutional Review Board (ISCOMPA Committee, IRB00002509), and informed consent was waived. We retrospectively analyzed CTPA scans performed between March 2012 and February 2013 of patients who presented in our emergency department with clinical suspicion of PE. All examinations were completed within 48 h of clinical

presentation. Subjects were excluded if there were any contraindications for CTPA, such as chronic renal failure or allergy to iodine medium.

Computed Tomography Protocol

Computed tomography angiography was performed using a multidetector scanner (64-slice LightSpeed VCT XT scanner, GE Healthcare Technologies, Waukesha, Wisconsin, United States of America). Lungs were scanned from the base to the apex in the caudocephalic direction using the following parameters: using the following scan parameters: 225 mAs, 120 kV, 0.5 mm collimation, rotation time of 0.75 s with a 3.5 cm/s table movement per gantry rotation. Administration of contrast material was performed using an automatic power injector (CT Injector, Ulrich Medical, Ulm-Jungingen, Germany) at a flow rate of 4.5 mL/s. All patients received 1 mL of Omnipaque 350 mg/mL per kilogram body weight (Amersham Health, Cork, Ireland). Administration of each bolus was followed immediately by a 60 mL saline flush. The helical acquisition was initiated after the start of the bolus administration of contrast medium, which was determined by a region of interest (ROI) with a threshold of 130 HU in the left atrium. (Smart Prep; GE Medical Systems). We routinely use this protocol to increase the contrast fill in subsegmental vessels.

Imaging Evaluation

Image interpretation was performed by two radiologists specifically trained in thoracic imaging, with 10 and 9 years of experience. After these two radiologists had conducted independent analyses, they reviewed the images together with a third senior chest radiologist with more than 20 years of experience to reach final consensus. Findings were analyzed according to the Fleischner Society's Glossary of Terms [11].

For acute PE diagnosis, the following criteria had to be included: (a) arterial occlusion with failure to enhance the entire lumen due to a large filling defect, and artery could be enlarged compared to adjacent patent vessels; (b) partial filling defect surrounded by contrast material, producing the “polo mint” sign on images acquired perpendicular to the long axis of a vessel and the “railway track” sign on longitudinal images of the vessel; (c) a peripheral intraluminal filling defect that forms acute angles with the arterial wall.

The PVS was defined by the following criteria: (a) presence of a homogeneous filling defect in the least 2 cm of a pulmonary vein; and (b) attenuation of the left atrium > 160 HU. We hypothesized that this filling defect would be a consequence of a decreased venous flow due to

pulmonary arterial obstruction. Likewise, we have settled this threshold for attenuation of the left atrium for a better visualization of pulmonary veins.

Statistical Analysis

All results were analyzed using commercial software (SPSS ver. 20, SPSS Inc., Chicago, IL, USA; Excel 2010, Microsoft Corporation, Redmond, WA, USA). Two-tailed p values < 0.05 were considered to indicate statistical significance. Based on the CT images, prevalences were obtained for all radiological findings. Using the cases that presented PE on CTPA as reference, sensitivity, specificity, and positive and negative predictive values were calculated for the PVS. Values for likelihood ratios for a positive test were calculated as the sensitivity, divided by 1 minus the specificity; and likelihood ratios for a negative test were calculated as 1 minus the sensitivity, divided by the specificity [12, 13]. Agreement between radiologists was assessed using kappa statistics. Interpretation was conducted based on the following parameters: kappa < 0.20 , poor agreement; kappa = 0.21–0.40, fair agreement; kappa = 0.41–0.60, moderate agreement; kappa = 0.61–0.80, good agreement; kappa = 0.81–1.00, very good agreement [14]. Fisher's exact test was used to assess any associations between the PVS and other parenchymal findings. 95% confidence intervals (CI) were calculated for the proportions, according to Wilson score interval with continuity correction [15].

Results

The study protocol included 119 patients (female, $n = 73$ (61.34%); mean age, 62 years; age range, 11–88 years). Median total CTPA scanning time was about 7.40 min (SD ± 1.45 min) for the entire chest, varying according to the covered volume. The time interval for repositioning the patient from bed to the magnet and back has not been assessed. All findings were of sufficient quality for conclusive interpretation.

Pulmonary embolism was diagnosed in 44 (35.8%) patients. Among these patients, considering the possibility of emboli in different levels in the same subject, 10.92% ($n = 13$) had emboli in the pulmonary trunk, 11.76% ($n = 14$) in lobar arteries, 20.17% ($n = 24$) in the segmental level, and 6.72% ($n = 8$) were subsegmental PE (Table 1).

The PVS was present in 16 out of 44 patients with PE. Figure 1 depicts an example of the PVS associated with PE in the right lower lobe. Sensitivity was 36.36% (95% confidence interval (CI) 22.83–52.26%); specificity, 98.67% (95% CI 91.79–99.93%); positive predictive value,

Table 1 Pulmonary embolism prevalence and the “pulmonary vein sign” performance in 119 patients

| Parameters | n (%) | 95% CI |
|-------------------------|------------|-------------|
| Prevalence | 44 (36.97) | – |
| Location | | |
| Main | 13 (10.92) | – |
| Lobar | 14 (11.76) | – |
| Segmental | 24 (20.17) | – |
| Subsegmental | 8 (6.72) | – |
| “Vein sign” performance | | |
| Sensitivity | 36.36% | 22.83–52.26 |
| Specificity | 98.67% | 91.79–99.93 |
| PPV | 94.12% | 69.24–99.69 |
| NPV | 72.55% | 62.67–80.70 |
| LR+ | 27.27 | 3.74–198.66 |
| LR– | 0.64 | 0.52–0.81 |
| Kappa index | 0.80 | 0.64–0.96 |

CI confidence interval, LR+ positive likelihood ratio, LR– negative likelihood ratio, NPV negative predictive value, PPV positive predictive value

94.12% (95% CI 69.24–99.69%); negative predictive value, 72.55% (95% CI 62.67–80.70%). Positive likelihood ratio was 27.27 (95% CI 3.74–198.66), and negative likelihood ratio was 0.64 (95% CI: 0.52–0.81). The Kappa index for the pulmonary vein sign between the two radiologists was good (0.801; 95% CI 0.645–0.957).

There was a statically significant association between the PVS and PE location at lobar and segmental levels ($p < 0.01$). Among the 44 patients with PE, six had localized (unilobar) embolisms and this location was not correlated with the PVS ($p = 0.21$). There was a statistically significant association between unilateral PE and the PVS ($p < 0.05$).

Prevalences of other pulmonary findings are presented in Table 2. Pulmonary nodule, bronchial thickening, and linear brands were the most common additional pulmonary findings (prevalences, 37.5, 22, and 20%, respectively). None of the correlations between these features and PE was statistically significant.

Discussion

In this study, we have tried to demonstrate an association between the PVS in CTPA scans and pulmonary embolism. Although this sign had not been reported previously in literature, other authors have studied the diagnostic performance of other ancillary CT signs of PE [8, 16]. Worsley et al. described classic signs for PE, such as Westermark, Fleischner, and Hampton hump signs, presenting sensitivities ranging from 8 to 22%, and

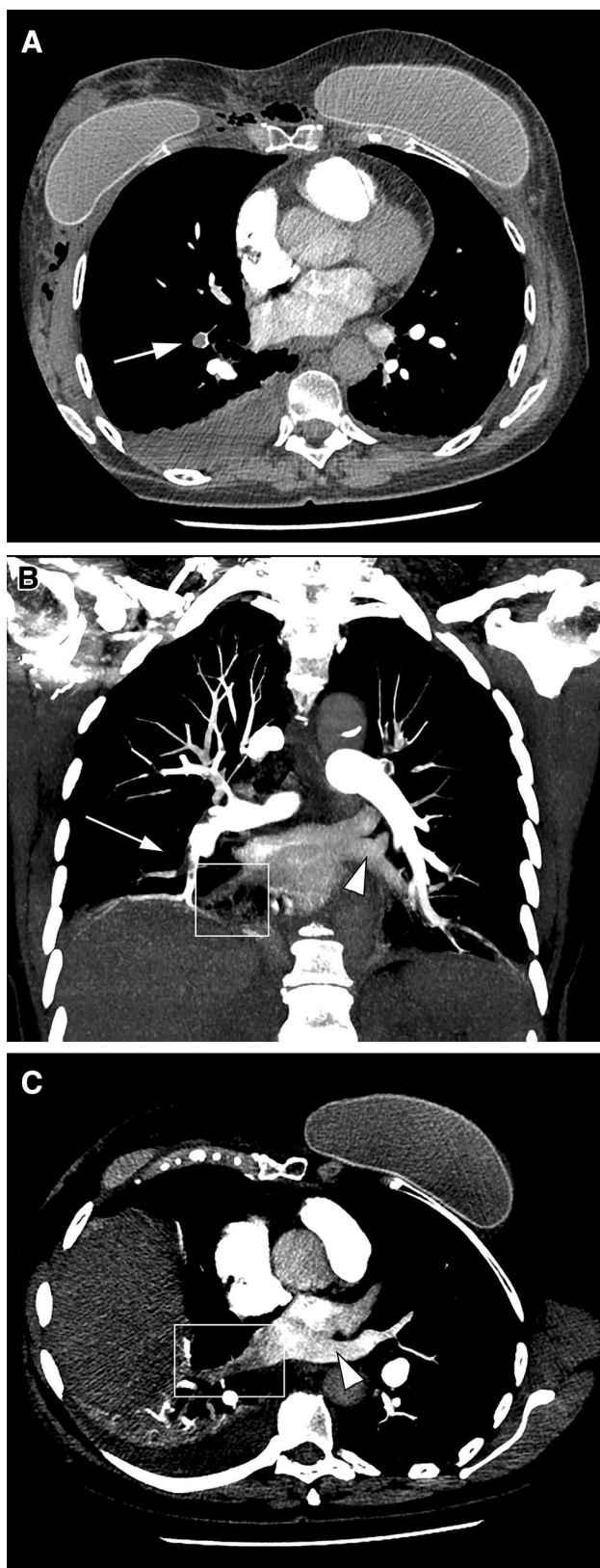


Fig. 1 Images from a 46-year-old woman on the seventh post-operative day after bilateral breast augmentation surgery, with history of mastectomy due to breast cancer. Patient presented at the emergency department with sudden chest pain and dyspnea. Axial (a) and coronal (b) computed tomography images demonstrating a filling defect on a segmental pulmonary artery of the right lower lobe (white arrow). A filling defect greater than 2 cm is also noted in the adjacent pulmonary vein on the coronal (b) and oblique (c) CT reconstructions (white square), characterizing the “pulmonary vein sign.” Comparatively, the other pulmonary veins are normally filled with contrast media (white arrowhead)

specificities ranging from 80 to 96% [8]. However, this study evaluated these signs at chest radiographies for patients that PE was angiographically confirmed. Despite methodological differences, our study demonstrated comparable low sensitivity (36.4%) and high specificity (98.7%) for the PVS. Additionally, we demonstrated a PE prevalence (36.97%) similar to several previous CTPA series [16–21].

There was a statistically significant correlation for the PVS and lobar and segmental pulmonary emboli but not for clots in the pulmonary trunk neither for subsegmental PE. This could be due to the small sample size and low prevalence of subsegmental PE (6.72%). However, some physiopathology mechanisms might be also accountable for this association. Usually initial pulmonary hemodynamic changes due to PE occurs from a reflex mechanism that causes vasoconstriction of small pulmonary arteries, increasing pulmonary arteriolar resistance [22]. When PE is massive or repetitive, mechanical blockage of the pulmonary vascular bed might result in sustained pulmonary hypertension [22]. This mechanism could also affect the PVS, which could be transient with small PEs. In a recent study by Koike et al. [23] that used dual-energy CT to assess lung perfusion in PE, the authors have found that difference in perfusion blood volume of the lung between patients with and those without PE tend to be larger in the early phase than in the late phase (respectively, 14 vs. 40 s from the start of injection of contrast media). This result might have reflected the reduction of pulmonary perfusion from the pulmonary artery and an enhanced role of systemic collaterals in patients with PE. This could also interfere in the PVS, as an increase in perfusion blood volume of the lung due to systemic collateral flow during late acquisition images could also increase venous flow, modifying PVS presentation.

Despite frequent additional pulmonary findings, no statistically significant correlation was found with pulmonary embolism. In a study by Coche et al. that tried to determine the value of lung parenchymal and pleural findings in patients with clinical suspicion of PE, a statistically significant difference was found only for wedge-shaped consolidations and linear bands [16]. Although we have not analyzed consolidations

Table 2 Prevalence of other pulmonary findings

| Imaging findings | Prevalence <i>n</i> (%) | Unilateral <i>n</i> (%) | Bilateral <i>n</i> (%) |
|----------------------|-------------------------|-------------------------|------------------------|
| Consolidation | 12 (10.0) | 8 (66.7) | 4 (33.3) |
| Pleural effusion | 15 (12.6) | 3 (20.0) | 12 (80.0) |
| Pulmonary fibrosis | 8 (6.7) | 0 | 8 (100) |
| Atelectasis | 12 (10.0) | 2 (16.7) | 10 (83.3) |
| Linear bands | 24 (20.0) | 9 (37.5) | 15 (62.5) |
| Lung mass | 6 (5.0) | 0 | 6 (100) |
| Bronchial thickening | 26 (22.0) | 0 | 26 (100) |
| Bronchiectasis | 2 (1.6) | 2 (100) | 0 |
| Pulmonary nodule | 45 (37.8) | 5 (11.1) | 40 (88.9) |

None of the correlations between these features and PE was statistically significant

according to their morphology likewise, these findings were not associated with PE in our series.

Some limitations of this study include a small sample size. Further prospective studies should also try to evaluate any correlation between the PVS and clinical indicators of pulmonary embolism, such as the Wells score and/or mortality risk. In addition, estimating a mean time between the PE event and the sign presentation could be helpful to further characterize this finding. We have analyzed the PVS in patients with acute PE. Further studies could investigate this finding in chronic PE and/or non-thrombotic embolism. Some patients included in our sample presented structural abnormalities in the lungs, such as pulmonary fibrosis and lung masses, what could affect pulmonary circulation, influencing on the accuracy of the PVS. The PVS should also be investigated in situations of decreased venous flow, such as left heart dysfunction and pulmonary veno-occlusive disease, which probably affect this sign prevalence and accuracy.

In summary, despite a low sensitivity, presence of the “pulmonary vein sign” was highly specific for PE, with a good agreement between readers. This sign could contribute for PE diagnosis on CTPA studies.

Compliance With Ethical Standards

Conflict of interest The authors declare that they have no conflict of interest.

Ethical Approval All procedures performed in studies involving human participants were in accordance with the ethical standards of the institutional and/or national research committee and with the 1964 Helsinki declaration and its later amendments or comparable ethical standards.

References

1. McCaig LF, Nawar EW (2006) National hospital ambulatory medical care survey: 2004 emergency department summary. *Adv Data* 372:1–29
2. Pollack CV, Schreiber D, Goldhaber SZ et al (2011) Clinical characteristics, management, and outcomes of patients diagnosed with acute pulmonary embolism in the emergency department: initial report of EMPEROR (multicenter emergency medicine pulmonary embolism in the real world registry). *J Am Coll Cardiol* 57:700–706
3. Roy PM, Meyer G, Vielle B et al (2006) Appropriateness of diagnostic management and outcomes of suspected pulmonary embolism. *Ann Intern Med* 144:157–164
4. Schoepf U, Holzkecht N, Helmberger TK et al (2002) Subsegmental pulmonary emboli: improved detection with thin-collimation multi-detector row spiral CT. *Radiology* 222:483–490
5. Stein PD, Fowler SE, Goodman LR et al (2006) Multidetector computed tomography for acute pulmonary embolism. *N Engl J Med* 354:2317–2327
6. Coche EE, Muller NL, Kim K et al (1998) Acute pulmonary embolism: ancillary findings at spiral CT. *Radiology* 207:753–758
7. Marchiori E, Zanetti G, Escuissato DL et al (2012) Reversed halo sign: high-resolution CT scan findings in 79 patients. *Chest* 141:1260–1266
8. Worsley DF, Alavi A, Aronchick JM et al (1993) Chest radiographic findings in patients with acute pulmonary embolism: observations from the PIOPED study. *Radiology* 189:133–136
9. Riedel M, Rudolph W (1989) Hemodynamics and gas exchange in acute lung embolism. *Herz* 14:109–114
10. Feihl F (1991) Hemodynamics and gas exchange in pulmonary embolism: physiopathology and treatment. *Schweiz Med Wochenschr* 121:1645–1653
11. Hansell DM, Bankier AA, MacMahon H et al (2008) Fleischner society: glossary of terms for thoracic imaging. *Radiology* 246:697–722
12. Lijmer JG, Mol BW, Heisterkamp S et al (1999) Empirical evidence of design-related bias in studies of diagnostic tests. *JAMA* 282:1061–1066
13. Jaeschke R, Guyatt GH, Sackett DL (1994) Users' guides to the medical literature. III. How to use an article about a diagnostic test. B. What are the results and will they help me in caring for my patients? the evidence-based medicine working group. *JAMA* 271:703–707
14. Landis JR, Koch GG (1977) The measurement of observer agreement for categorical data. *Biometrics* 33:159–174
15. Newcombe RG (1998) Interval estimation for the difference between independent proportions: comparison of eleven methods. *Stat Med* 17:873–890
16. Coche EE, Müller NL, Kim KI et al (1998) Acute pulmonary embolism: ancillary findings at spiral CT. *Radiology* 207:753–758

17. Revel MP, Sanchez O, Couchon S et al (2012) Diagnostic accuracy of magnetic resonance imaging for an acute pulmonary embolism: results of the 'IRM-EP' study. *J Thromb Haemost* 10:743–750
18. Revel MP, Sanchez O, Lefort C et al (2013) Diagnostic accuracy of unenhanced, contrast-enhanced perfusion and angiographic MRI sequences for pulmonary embolism diagnosis: results of independent sequence readings. *Eur Radiol* 23:2374–2382
19. Weir ID, Drescher F, Cousin D et al (2010) Trends in use and yield of chest computed tomography with angiography for diagnosis of pulmonary embolism in a Connecticut hospital emergency department. *Conn Med* 74:5–9
20. Pasin L, Zanon M, Moreira J et al (2017) Magnetic Resonance Imaging of Pulmonary Embolism: diagnostic Accuracy of Unenhanced MR and Influence in Mortality Rates. *Lung* 195:193–199
21. Donohoo J, Mayo-Smith W, Pezzullo J, Egglin T (2008) Utilization patterns and diagnostic yield of 3421 consecutive multidetector row computed tomography pulmonary angiograms in a busy emergency department. *J Comput Assist Tomogr* 32:421–425
22. Parmley LF Jr, North RL, Ott BS (1962) Hemodynamic alterations of acute pulmonary thromboembolism. *Circ Res* 11:450–465
23. Koike H, Sueyoshi E, Sakamoto I, Uetani M (2017) Clinical significance of late phase of lung perfusion blood volume (lung perfusion blood volume) quantified by dual-energy computed tomography in patients with pulmonary thromboembolism. *J Thorac Imaging* 32:43–49



Pontifícia Universidade Católica do Rio Grande do Sul
Pró-Reitoria de Graduação
Av. Ipiranga, 6681 - Prédio 1 - 3º. andar
Porto Alegre - RS - Brasil
Fone: (51) 3320-3500 - Fax: (51) 3339-1564
E-mail: prograd@pucrs.br
Site: www.pucrs.br